A *Hubble Space Telescope* Imaging Survey of Nearby Active Galactic Nuclei

Matthew A. Malkan, Varoujan Gorjian, Raymond Tam
University of California, Los Angeles

Accepted for publication in the July 1998, Vol. 117 # 1, issue of the *Astrophysical Journal Supplement Series*

A *Hubble Space Telescope*[1] Imaging Survey of Nearby Active Galactic Nuclei

Matthew A. Malkan, Varoujan Gorjian, and Raymond Tam
Department of Physics & Astronomy, University of California, Los Angeles, CA 90095-1562
malkan@astro.ucla.edu, vg@astro.ucla.edu, utam@physics.ucla.edu

ABSTRACT

We have obtained WFPC2 images of 256 of the nearest ($z \leq 0.035$) Seyfert 1, Seyfert 2, and starburst galaxies. Our 500-second broadband (F606W) exposures reveal much fine-scale structure in the centers of these galaxies, including dust lanes and patches, bars, rings, wisps and filaments, and tidal features such as warps and tails. Most of this fine structure cannot be detected in ground based images. We have assigned qualitative classifications for these morphological features, a Hubble type for the inner region of each galaxy, and also measured quantitative information such as 0.18 and 0.92 arcsecond aperture magnitudes, position angles and ellipticities where possible.

There is little direct evidence for unusually high rates of interaction in the Seyfert galaxies. Slightly less than 10% of all the galaxies show tidal features or multiple nuclei. The incidence of inner starburst rings is about 10% in both classes of Seyfert galaxies. In contrast, galaxies with H II region emission line spectra appear substantially more irregular and clumpy, because of their much higher rates of current star formation per unit of galactic mass.

The presence of an unresolved central continuum source in our *HST* images is a virtually perfect indicator of a Seyfert 1 nucleus as seen by

[1]Based on observations made with the NASA/ESA *Hubble Space Telescope*, obtained at the Space Telescope Science Institute, which is operated by the Association of Universities for research in Astronomy, Inc., under NASA contract NAS 5-26555.

ground-based spectroscopy. Fifty-two percent (52%) of these Seyfert 1 point sources are saturated in our images; we use their wings to estimate magnitudes ranging from 15.8 to 18.5. The converse is not universally true, however, as over a third of Seyferts with direct spectroscopic evidence for broad Balmer wings show no nuclear point source. These 34 resolved Seyfert 1's have fainter nonstellar nuclei, which appear to be more extinguished by dust absorption. Like the Seyfert 2's, they have central surface brightnesses consistent with those expected for the bulges of normal galaxies.

The rates for the occurrences of bars in Seyfert 1's and 2's and non-Seyferts are the same. We found one significant morphological difference between the host galaxies of Seyfert 1 and Seyfert 2 nuclei. The Seyfert 2 galaxies are significantly more likely to show nuclear dust absorption, especially in lanes and patches which are irregular or reach close to the nucleus. A few simple tests show that the difference cannot be explained by different average redshifts or selection techniques. It is confirmed by our galaxy morphology classifications, which show that Seyfert 1 nuclei reside in earlier type galaxies than Seyfert 2 nuclei. If, as we believe, this is an intrinsic difference in host galaxy properties, it would undermine one of the postulates of the strong unification hypothesis for Seyfert galaxies, that they merely appear different due to the orientation of their central engine. The excess galactic dust we see in Seyfert 2's may cause substantial absorption which obscures their hypothesized broad-emission-line regions and central nonstellar continua. This galactic dust could produce much of the absorption in Seyfert 2 nuclei which had instead been attributed to a thick dusty accretion torus forming the outer part of the central engine.

Subject headings: Galaxies — galaxies: active — galaxies: nuclei — galaxies: Seyfert — galaxies : starburst

1. Introduction

Several causal connections have been proposed between an active galactic nucleus (AGN) and the host galaxy in which it resides. The principal ways in which the latter could affect the former are through influencing a) the formation of a nonstellar central engine; b) its fueling; and c) obscuring it from our view, (which can alter the central engine's appearance even if it is not physically affected.)

It is widely believed that active galactic nuclei (AGNs) are powered by non-spherical accretion onto massive black holes. This is partly because this model has the lowest fuel supply requirements: an AGN's luminosity is proportional to its mass accretion rate, which would be about 0.01 $M_{\odot}$year^{-1} for a bright Seyfert nucleus. It is not known how this rate of fuel supply can be brought from the host galaxy down to several thousand Schwarzschild radii (of order 10^{17} cm for a "typical" Seyfert galaxy black hole mass of 10^{8} $M_{\odot}$(Malkan 1983)) at which point viscous processes are supposed to drive the final accretion onto the black hole. One speculation is that a close interaction with another galaxy can distort the galactic potential and disturb the orbits of gas clouds sufficiently to carry a significant mass of fuel into the galaxy's center (Shlosman et al. 1989, 1990, Hernquist and Mihos 1996). More indirect scenarios are also possible, in which a tidal galaxy interaction stimulates a burst of star formation which in turn stimulates nonstellar nuclear activity. A further possibility is that special conditions in isolated galaxies may trigger the feeding of fuel to an active nucleus, such as a bar instability. (Schwartz 1981; Shlosman, Frank, & Begelman 1990; Mulchaey and Regan 1997)

However, direct observational evidence that galaxy encounters stimulate the luminosity of an AGN has been ambiguous (Adams 1977, Petrosian 1983, Kennicutt and Keel 1984, Dahari 1985a, 1985b, Bushouse 1986, Fuentes-Williams and Stocke 1988). One difficulty is that the most dramatic morphological indications of the encounter may have subsided by the time that the newly injected fuel reaches the nucleus. In any case, the weak correlation between galaxy interactions and Seyfert activity is stronger for type 2 Seyferts than for type 1's.

Conversely, the presence of an AGN could alter the appearance of the central regions of its host galaxy, principally by its injection of substantial energy, both radiative and mechanical, over many millions of years. A further question is whether the particular type of active nucleus, Seyfert 1 or 2, is related to any property of the host galaxy.

We have therefore used the superior spatial imaging resolution of the post-repair *Hubble Space Telescope* to make a snapshot survey of nearby active galaxies to investigate the morphological implications of different theories on the formation and fueling of AGN.

2. Snapshot Survey

In our survey program 256 images have been obtained of the cores of active galaxies selected from the "Catalog of Quasars and Active Nuclei" by Véron-Cetty and Véron (1987), hereafter VCV. The criteria for choosing a galaxy from the VCV to be in our sample was that they have a $z \leq 0.035$ and not be duplicated by other cycle 4 *HST* observing programs. These requirements resulted in a total of 311 galaxies. The actual choice of the subset of 256 galaxies discussed here was random, since they resulted from the ef-

forts of the *HST* scheduling program to fill in dead time by slewing to a nearby object for a relatively fast exposure. This resulted in "snapshots" of 91 galaxies with nuclear optical spectra classified as "Seyfert 1," 114 galaxies classified as "Seyfert 2", and 51 galaxies classified as "HII's." Although some of these galaxies have since been reclassified either as intermediate Seyferts like 1.5 or 1.8, or have been switched from Sy 1's to Sy 2's upon closer spectroscopic examination. For our statistics we have used the most recent spectroscopic classifications from the NASA Extragalactic Database[2] noted in tables 1, 2, and 3.

Some "Active Galaxies" in the VCV are actually starbursts which are simply included due to their very strong emission lines and are denoted as "HII". The line ratios are consistent with photoionization from young stars rather than a nonstellar central engine (which emits a far larger proportion of high-energy photons). Thus, these nuclei are radically different from Seyfert 1's, and are probably different from Seyfert 2's. We nonetheless included them in the target list to provide a comparison with the Seyferts.

Since the targets we have imaged constitute more than a third of all of the nearest Seyfert galaxies currently known, they are broadly representative of this observational class. Two biases are likely to be present because they were present in the original searches which produced many of the entries in the VCV. The first is that the optical discovery techniques used to find most of these galaxies were biased against reddened, dusty active galaxies, which are prominent in the far-infrared (e.g., Spinoglio and Malkan 1989, Rush et al. 1993). The second bias is that the median redshift of the Seyfert 1's (0.024) is somewhat larger than that of the Seyfert 2's (0.017). Since the more prominent Seyfert 1 nuclei are easier to detect, they are relatively more numerous at larger distances, where our WFPC2 images provide a somewhat poorer linear resolution. To compensate for the effect of the different median z's, we also did our statistical comparisons for a modified subset of Sy 1's cut off at z=0.030, which then has a median z close to the median z of the Sy 2's.

The images were taken using the F606W filter because of its very high throughput (Burrows 1994). This filter includes both the standard WFPC2 V and R bands, and has a mean wavelength of 5940Åand a FWHM of 1500Å. We chose 500 seconds as our exposure time in a compromise between the maximum exposure time per orbit and the minimum amount of overhead time. The galaxy centers were usually well centered on the planetary camera CCD of WFPC2, which has a plate scale of 0.″046 per pixel and a field of view of $37'' \times 37''$. Some of the images did not fall on the planetary camera chip and fell on the wide field chip. Each wide field CCD has a plate scale of 0.″1 per pixel and a field of view of $1.3' \times 1.3'$.

3. Data Reduction. The Atlas

Flat field calibration, bias removal, and other initial data reduction steps were performed at the Space Telescope Science Institute. We performed cosmic ray removal using standard routines from the IRAF [3] software

[2]The NASA/IPAC Extragalactic Database (NED) is operated by the Jet Propulsion Laboratory, California Institute of Technology, under contract with the National Aeronautics and Space Administration

[3]IRAF (Image Reduction and Analysis Facility) is distributed by the National Optical Astronomy Observa-

package. Unfortunately, the images have such severe cosmic ray contamination that automated packages have difficulty in removing all the cosmic rays. This is especially a problem for glancing hits on the CCD which leave extended narrow trails.

Hence the problem was to remove cosmic rays from 256 images in an efficient manner. Doing this by hand was not practical due to the numbers involved. The solution was to pick a threshold level which would remove most of the cosmic ray contamination without removing any real features. This threshold level was determined experimentally by picking multiple galaxies and running the task *cosmicrays* with many different values and seeing which threshold value eliminated the most cosmic rays without affecting any real features. The final value that we arrived at was one where the cosmic ray would be eliminated if its flux ratio was 80% of the mean neighboring pixel flux. This value would leave some residual cosmic ray contamination but would not affect real galaxy data. We therefore chose to err on the side of caution: it is better to leave in a cosmic ray trail rather than remove real structures.

It must be noted here that although there is heavy contamination, the cosmic rays are easily separable from real features within the image, since the cosmic rays leave either a point or a line in the image. These points are distinguishable from unresolved astronomical point sources because they do not have the PSF surrounding the cosmic ray hit. Extended hits make linear streaks, tightly confined to a few pixels, and thus are also easily identifiable in contrast to real structures which have more two-dimensional profiles.

We did not attempt to subtract the sky background from these images, because it was difficult to determine accurately, and relatively insignificant in any case. The difficulty arises because in most of the images, the galaxy is more extended than the PC chip, so that little or no true sky was measured. Fortunately, the expected sky brightness is so faint–23rd magnitude per square arcsecond–that it hardly effects any of our measurements or conclusions.

In Figures 1,2,3 we have reproduced the central 200×200 pixels of each image (with a few 400×400 pixel reproductions of larger galaxies), centered on the centroid of the galaxy nucleus. In only a few cases (those marked with an asterisk) is the image from one of the Wide Field chips (with a plate scale of 0.″1 per pixel.) All other images are from the Planetary Camera CCD (with a plate scale of 0.″046 per pixel.) This magnification emphasizes nuclear features that are not detectable with ground-based seeing limitations. The grey scales are logarithmic, with full black set to the brightest pixel values in the center of the galaxy. In most of the Seyfert 1 images, which have saturated nuclei, this is around 3600 Data Numbers (see Table 1). In the other galaxies, the brightest pixel typically has 1000 to 2000 counts. Inevitably, a substantial amount of information is lost in this reproduction process.

4. Morphological Classes and Estimation of Central Magnitudes

We have assigned morphological classes based on our images of the inner regions of each galaxy in Tables 3, 4, and 5 on the usual Hubble tuning fork system E/S0/Sa,Sab,Sb etc. In most cases (75%) our classification

tories, which are operated by the Association for Research in Astronomy, Inc., under cooperative agreement with the National Science Foundation.

agrees with the one given in the Third Reference Catalog (RC3) (Corwin et al. 1994) to within one full class (i.e., from Sb to Sc). Our morphological classes for the Sy 2's are on average the same as that from the RC3, but our Sy 1 classifications have, on average, a slight tendency to be later than the RC3 (by less than a subclass i.e., , less than the difference between Sa and Sab).

We have also derived azimuthally-averaged surface brightness profiles of the centers of these galaxies to further help classify them. Fifty-two percent, 92% and 100% of the Seyfert 1, Seyfert 2 and non-Seyfert galaxies have unsaturated centers. For these we have used the *apphot* routines in IRAF to measure magnitudes within circular diameters of 4 pixels (0.″18) and 20 pixels (0.″92). The first aperture includes about 85% of the light of a point source measured by the *HST* Planetary Camera; the second aperture is selected to be comparable to the seeing in good ground-based images. The magnitude in the inner diameter, 0.″18, and the magnitude in the outer diameter, 0.″9, get slightly dimmer with higher z, but this trend is marginal (Figure 4). Kotilainen et al. (1993) reported 3- and 6-arcsecond aperture photometry of 5 galaxies for which we have unsaturated images. We confirmed that there is no systematic difference between the V magnitudes they measure and those we obtained from our data, with a scatter of 0.1 to 0.2 magnitudes. Their 3-arcsecond aperture magnitudes however, tend to be about 0.1 magnitudes fainter than ours, which we attribute to their ground-based seeing spilling nuclear light out of this small aperture.

For most of the Seyfert 2 galaxies (in which there is no evidence for a nuclear point source component), our measurements refer primarily to the bulge light. The large-aperture magnitudes of nuclei yield a median central surface brightness of 16.4[4]/magsq with a standard deviation of 2.0. Byun et al. (1996) studied early type galaxies using deconvolved PC1, F555W images. The central surface brightness magnitudes they measured were for the area within a break radius (r_b) which was usually about twice the size of our outer magnitude of r=0.″46. For comparison we chose their galaxies which have relatively flat central brightness laws ($\gamma \leq 0.3$) so that the brightness does not rise much inside r_b. The average μ for these galaxies was 16.9 $\pm$1.7, consistent with our sample of Sy 2 galaxies.

Phillips et al. (1996) used deconvolved PC1 images of 9 early-type disk galaxies to estimate an average surface brightness at 555nm of 16.6 /magsq in annuli from 0.″2 to 0.″5. The average surface brightness of our Sy 2 galaxies is consistent with their value but not with the central brightness of late-type spirals. The centers of spirals of type Sc and later (which are disk dominated rather than bulge dominated) are nearly 2 magnitudes fainter. However our average Seyfert galaxy centers are bulge-dominated, as expected from the very small proportion of Hubble types later than Sc.

For the Seyfert 1 images with saturated nuclei, we developed an indirect method for estimating the flux from the central point source presumed to be present in the unresolved Seyfert 1 nucleus. Although the values for radii less than a few pixels are artificially

[4]Magnitudes are given in the monochromatic-F_λ Space Telescope system (Holtzman et al. 1995). Our F606W magnitudes correspond to V magnitudes 0.1 to 0.2 magnitudes brighter. (i.e. Subtract 0.1-0.2 magnitudes from the tabulated values to estimate V magnitudes.))

pinned at around 3600 DN due to saturation, these profiles are accurate and linear at radii larger than 4 to 9 pixels.

We compared the inner portions of these galaxy profiles with those obtained for 5 similarly bright (also saturated) stars from the same PC frames (Table 6). Their estimated total magnitudes were "bootstrapped" by comparison with the profiles and magnitudes of 4 field stars with unsaturated images also listed in Table 4. By matching the logarithmically plotted profiles over the range of r = 4 to 9 pixels we were able to estimate the TOTAL flux from a central point source. Our estimates given in Table 1 are slightly too large because we did not attempt to subtract the pedestal of galactic bulge emission, since that correction was small and rather uncertain. Figure 5 shows some examples of this inner-profile matching procedure. In the good cases (bright central point source), the uncertainty, as estimated by the scatter between estimates from different stars, is $\pm$ 0.25 magnitudes.

5. Measuring the Nuclear Point Source in Seyfert 1's

Previous imaging studies have shown that nearly all Seyfert 1 nuclei emit a featureless continuum and its ubiquitous time variability indicates that it arises within less than a parsec of their central engine (e.g., Malkan and Filippenko 1983). Thus even with *HST's* resolution, this Seyfert 1 continuum should be unresolved, and should appear as a bright point source superposed on a resolved host galaxy.

We have used our ability to discern the bright central point sources in most of our Sy 1 sample as a method of categorizing the Sy 1's. When a nuclear point source is evident, we have categorized it as either a Saturated Sy 1 (SS1) or Unsaturated Sy 1 (US1). The galaxies in both these categories show a distinct point source at their center and have a sharp rise at the 3-5 pixel radius in their surface brightness profiles. Finally, we have grouped into the Resolved Sy 1 (RS1) category those galaxies which were identified as Sy 1 but showed no discernible point source, that is there was no detectable break in their surface brightness profiles at r$\sim$3-5 pixels. If a point source is present in these galaxies, it must typically contribute less than about 45% of the light within the inner one arcsecond.

This classification system admittedly depends on the dynamic range of WFPC2 and the distances to the galaxies, but it has a roughly quantitative flux basis. Out of the 91 Sy 1's 36 (40%) fall into the SS1 category, 21 (23%) fall into the US1 category and 34 (37%) fall into the RS1 category. These ratios do not take into account the distances to the galaxies. To account for the distances, some galaxies from the SS1 category and US1 category were eliminated leaving a total number of 78 Sy 1's. From this sample, 30 (38%) fall into the SS1 category, 27 (18%) fall into the US1 category, and 34 (44%) fall into the RS1 category. These comparisons are summarized in table 7.

We have compared this classification system with other spectroscopic classifications (i.e., 1.8 to 1.9, Goodrich 1995). Of the SS1's only 1 galaxy is classified as a 1.8 and of the US1's only 2 galaxies have an intermediate spectroscopic classification, but 14 galaxies in the RS1 category have a 1.8 or 1.9 designation. Although the numbers are small, this does tend to show that RS1's are closer to being Sy 2's than the US1's or SS1's, in having relatively weaker broad permitted line wings. Also those galaxies that do not carry an inter-

mediate spectroscopic classification may not have been studied carefully enough to decide if such classification is appropriate.

The central magnitudes of the RS1's are very similar to those of Sy 2's. The median 0.″18 diameter magnitude for the Sy 2 galaxies in our sample is 19.30 with a standard deviation of 2.14. For the RS1's, the median magnitude is 18.76 with a standard deviation of 1.23. The median 0.″92 diameter magnitude of the Sy2 's is 16.86 ± 2.02, while that for the RS1's is 17.04 ± 0.93. In contrast, the US1's have a brighter 0.″18 diameter magnitude at 18.53 ±0.63 and a dimmer 0.″92 diameter magnitude of 17.13 ±0.42. The dimmer outer magnitude may be accounted for by the fact that the bulge may be dimmer in these galaxies, thus making the bright point source relatively more prominent.

The similarity between the Sy 2's and the RS1's also extends to their Balmer decrements. Although very few of our observed RS1's had Balmer decrement measurements (there are only 14), the RS1 Balmer decrements (med. = 6.13±1.51) and the Sy 2 Balmer decrements (med. = 5.34±2.53) are higher than the Balmer decrements of the entire Sy 1 sample (med. = 4.48±2.87). The differences (at the 98% confidence level based on the Two-Sample Z Statistic) indicate that their nuclear continua are in many cases weakened by dust reddening. The same does not hold true for the US1's whose Balmer decrements (med. = 3.43±1.56) are more like those of the rest of the Sy1's. Thus in both their spectra and their high-resolution images the RS1's have an observational appearance similar to Sy 2's while the US1's have an appearance and spectra similar to Sy 1's, only less powerful, and with *HST's* high resolution we have been able to attach these spectral characteristics to morphological characteristics.

6. Unusual Seyfert 2 Galaxies

Our atlas confirms that the nonstellar continuum is not viewed directly in Seyfert 2 nuclei. This is the same conclusion reached by Nelson et al. (1996) where they observed in their WF/PC 1 images that Sy 1 galaxies tended to have strong point sources in their nuclei while Sy 2 galaxies did not.

However, two of our classified Sy 2's do seem to show central point sources. IC4870 is actually an "extragalactic HII region" with unusually high ionization lines. The saturated point source near its center is probably a foreground star. IR1832-594 has an even brighter (saturated) central point source. This confirms its reclassification as a Sy 1.8 by Maiolino and Rieke (1995).

Only 7 other Sy 2 images have saturated centers. Mrk 622 was reclassified as an intermediate Seyfert galaxy by Goodrich (1995). Another, NGC 4507, is a heavily obscured hard X-ray (and possibly gamma-ray) source whose X-ray properties mark it as a reddened Sy 1 (Jura et al. 1997). These bright Seyfert 2 nuclei may be intermediate cases: combinations of a direct and a scattered Seyfert 1 continuum where the scattering region is slightly resolved. (The center of the saturated image is often broader than a point source). We have further evidence for its existence in another saturated Sy 2, Mrk 533, which has broad emission lines in polarized flux.

The remaining saturated Sy 2's (F312, F334, IR1121-281, Mrk 1370) have not been scrutinized with such high SNR spectroscopy, which might reveal weak broad lines. Even if they do not show polarized broad lines, there is

still another possibility that our images happened to be obtained when these Sy 2's temporarily "turned on" a visible Seyfert 1 nucleus (broad-line region plus point-like nonstellar continuum). The very low frequency of saturated Sy 2 nuclei in our survey implies that such a transformation from a Sy 2 to Sy 1 is very rare.

7. Quasar-like Seyfert 1 Galaxies

A small fraction of the (more luminous) Seyfert 1 galaxies have nuclei which are far more luminous than their host galaxies. We have singled out five of the most extreme examples, which are indicated as "Quasar-like" in Table 4. In Figure 6, their azimuthally-averaged surface brightness profiles—scaled to have matching brightness in their unsaturated wings—are overplotted (open symbols), along with several field stars (solid symbols). At radii of less than 3 or 4 pixels, the images are saturated to varying degrees. At larger radii, all of these profiles—for both stars and Quasar-like Seyfert 1's—are extremely similar. The distinctions between Seyfert 1 images and stellar images are so subtle that they are not much larger than the differences which appear between different stars.

The existence of quasi-stellar Seyfert 1 galaxies is in part a selection effect that comes from observing more luminous nuclei at higher redshifts. The average z of these galaxies is 0.0296, and their average nuclear luminosities are M_{606}= -23.6 + 5logh_{50}. Operationally, these Seyfert 1's can equally well be classified as "quasars". Three of them appear in the Palomar-Green Bright Quasar Survey (Green, Schmidt, & Liebert 1986). In fact, at a slightly higher redshift they would appear absolutely stellar in the WFPC2 images. At redshifts above a few tenths, even more of our Seyfert 1 galaxies would appear completely unresolved in the PC2 images. These are the low-luminosity counterparts of several PG quasars imaged by Bahcall et al. (1995) with *HST* which lack detectable host galaxies (sometimes misleadingly referred to as "naked quasars".) These Quasar/Seyfert 1 nuclei serve as indicators that there cannot be a very good correlation between the luminosity of the Seyfert 1 nucleus and the luminosity of the host galaxy.

8. Radio Fluxes

Integrated radio fluxes were available from the literature for 48 of our Seyfert 1 galaxies, and 35 of our Seyfert 2's. We used these to look for a correlation between radio luminosity and morphological classification of the Seyfert galaxy, but found none. The Seyfert 1 and 2 nuclei which we believe reside in E (or E/S0) galaxies are *not* stronger radio emitters than those in spirals. This contrasts with claims that radio-loud quasars are more likely to be found in ellipticals, while radio-quiet quasars reside in spirals (e.g., Malkan 1984). If the host galaxy morphology correlates with radio power at high luminosities, the relation must break down at the low luminosities of Seyfert galaxies included in the present study.

9. Morphological Irregularities

It is not possible to capture the rich range of morphologies seen in these images with a simple set of classifications. Nonetheless, to draw statistical conclusions, we have grouped most of the principal observational characteristics we have identified into the following seven categories, most of which are not mu-

tually exclusive[5].

Only ~20% of the galaxies appear, in our subjective estimation, to be completely "normal". By this we mean axisymmetric, with a bulge component that has regular elliptical isophotes, and, for spirals, a thin circular (after deprojection for inclination angle) disk that appears to be roughly planar. Since WFPC2 is also observing non-active galaxies with unprecedentedly high spatial resolution, it is entirely possible that many of them will now no longer meet our definition of "normal", either. Some subjective disagreement is unavoidable, but our approach has been to err on the side of noting too many possible irregularities in these images, rather than too few.

Our search for unusual central structures is necessarily biased against finding them near the middles of Seyfert 1 nuclei. We tried various methods of subtracting off the bright point source; however, none were successful. Glare from the imperfectly subtracted wings of the PSF remained, whether we used theoretical PSF's from Tiny Tim or a library of PSF's extracted from our WFPC2 images. Thus our ability to notice low-contrast features near the galaxy center may be greater in the normal Seyfert 2's and weaker in Seyfert 1 galaxies. We have tested this possibility with a simulation described below.

[5]Although no morphological investigation of galaxy images can be completely objective, we have attempted to note features which are clearly evident to everyone who has viewed them. The more difficult task is in interpreting the significance of these features. Our aim has been to provide the information, with our interpretation, but many features may have different interpretations which are also allowed by the data.

9.1. Evidence of Interactions

One of our principal observational results is that few of these images show clear indications of disturbances or other strongly asymmetric irregularities. Two show tidal features, three have shells of differing brightness, one has strongly warped isophotes, and 10 are in collisions/mergers. Of those galaxies in a collision/merger, there are very few galaxies in our sample which show two distinct nuclei in the final stages of a merger. Gorjian (1995) has already presented 3 cases from these data of galaxies with apparent double or triple nuclei. In only one case, Mrk 516, is this clearly the late stage of a merger. Thus less than 0.5% of Seyfert galaxies show this most unambiguous evidence of being in the late stages of a merger. If mergers are common in our sample, then one of the nuclei must not spend very much time as a recognizably distinct subsystem when it is within the central kiloparsec of the consuming galaxy.

9.2. Inner Bars

About a third of all spiral galaxies in the Third Reference Catalog have isophotes with strong deviations from rotational symmetry in the form of inner isophotes with a $cos2\Theta$ dependence, which is traditionally classified as a strong "Bar" (SB) or "Lens". In the central 10 arcseconds of the PC images, we have identified strong bars in 25 Seyfert 1's (27%), 26 Seyfert 2's (23%), and 6 (12%) HII's.

Many of these galaxies give the appearance of "Integral Signs" or capital "Thetas" in the centers of the galaxies. They also show up as large twists in the isophotes as a function of radius, some of which could be equally well described as "Lenses". By erring on the side of caution, and only searching the central kilo-

parsec regions of the galaxies covered by the PC chip, we have probably missed many bars, especially those on larger spatial scales. This is evidenced by bar classifications in the RC3 which do not match our classifications. If both classifications are combined, then there are 36 (40%) Sy 1's with bars, 58 (51%) Sy 2's with bars, and 17 (33%) HII galaxies with bars.

Barnes and Hernquist (1996) modeled barred potentials and showed that they are effective in driving interstellar matter into the nucleus, and fueling increased non-stellar activity there, assuming a massive black hole is already present. We do not yet have a control sample of non-active spirals available for comparison, but it is not apparent that strong inner bars are unusually common in our sample of Seyfert galaxies, which is in agreement with ground based studies (Heckman 1980, Simkin, Su, & Schwartz 1987, Mulchaey and Regan 1997).

9.3. Filaments and Wisps in Early-Type Galaxies

Ten of the Seyfert 1's (11%) and 24 of the Seyfert 2's (21%) show emission wisps or filaments which are not part of a clear spiral arm pattern (as indicated in Tables 4 and 5 by F/W). In contrast to dust lanes, these features are brighter than the surrounding starlight. Since the $H\alpha$ /[NII] emission lines fall near the peak sensitivity of our broad 606W bandpass, some or even all of this extra light could be due to emission from ionized gas, which can be confirmed by STIS spectroscopy.

We have compared the optical morphologies of our Seyfert galaxies with high-resolution radio maps of the same inner regions (Ulvestad and Wilson 1989, Rush et al. 1996) In most cases there is little correlation. In some cases the filaments show some spatial correlation with the extended radio emission, or at least some alignment, suggesting that both are directly powered by the active nucleus.

In spite of the large quantities of gas and ionizing photons in the H II galaxies, they do not harbor clear examples of these filaments and wisps, although some could have been lost in the "noise" of the irregular background light. We tentatively conclude that these filaments and wisps are in many cases emission-line dominated gas associated with, and photoionized by the active nucleus.

The higher frequency of filament/wisps in the Seyfert 2's compared with the Seyfert 1's is significant at the 96.5% level. This result may well be related to the fact that narrow-band ground-based imaging is more likely to resolve the forbidden line emission in Seyfert 2's than in Seyfert 1's (Poggee 1988).

10. Irregularities from Star Formation and Dust

Most of the galaxies show significant deviations from smooth isophotes caused either by localized excesses of emission (e.g., star clusters and HII regions) or localized deficits (caused by dust absorption).

At one extreme, 5 Seyfert 1 galaxies (6%), 11 Seyfert 2 galaxies (10%), and 19 HII galaxies (37%) are extremely "clumpy." These galaxies have large-amplitude deviations from a smooth isophotal pattern. They contain multiple local maxima which are at least 15% brighter than their surroundings. (As they are usually slightly resolved we know they are not foreground stars in the Milky Way). In most cases these are caused by "knots" which are most likely active star-forming regions–

star "clusters" and their associated H II regions. A special case of emission knots appears in the 8 galaxies we classify as "flocculent spirals". In contrast to "grand design" spirals with a few very long arms, these disks have dozens to hundreds of barely resolved patches wrapped in tight spirals. These are seen in 3% of the Seyfert 1's, 2% of the Seyfert 2's, and 6% of the HII galaxies and are usually too fine-scale to be detected in ground-based images.

Another special case is the 11 (12%) Sy 1, 9 (8%) Sy 2 and 5 (10%) HII galaxies with circumnuclear rings. These rings seem to be the sites of recent star formation , and with the resolution of WFPC2 we resolve some of these rings into many tiny "knots." We note that this resolving of rings into "knots" has already been seen in the ground-based observations of NGC 7469, by Mauder et al. 1994), whose speckle masking image reconstruction shows an excellent similarity to our PC2 image. The marked lumpiness we observe in star-forming regions is consistent with the view that this process may lead to the formation of large star clusters (e.g., Barth et al. 1996)

The H II galaxies are also more likely to appear "Irregular" or "Disturbed." Again the explanation is that these galaxies have the highest fractions of interstellar matter and associated recent star formation. In this, they substantially exceed the average Seyfert galaxy, at least on morphological grounds. In other words, the host galaxies of Seyfert nuclei do *not* show the extremely high star formation rates seen in the most active starburst galaxies at the same low redshifts.

The single most common morphological feature evident in our images is absorption due to interstellar dust in the active galaxy. In many cases the absorption has too little contrast or spatial extent to have been detectable in ground-based images. In the absence of a standardized classification system for dust absorption, we have attempted to identify galaxies which have dust lanes that appear irregular. In lenticular galaxies, which we classify as E or S0 in Tables 4 and 5, we regard any dust absorption as noteworthy, whereas in later-type spirals only extremely distorted dust lanes are classified as "irregular" (DI).

On its face, the low fraction of Seyfert nuclei residing in dust-free and gas-free galaxies appears to distinguish them from a randomly selected sample of normal galaxies. This indication will remain tentative until a comparable sample of nearby normal galaxies is examined with similar *HST* resolution for signs of dust and star clusters.

Two further cases of dust absorption of special interest have been noted even though we do not consider them intrinsically "irregular" for spiral galaxies. 39 galaxies appear to have dust lanes running across their nuclei, giving them a bisected appearance (denoted DC in Tables 3,4,5) Of the Sy 2's, 23 (20%) were designated as DC, contrasted with 12 (13%) of the Sy 1's. Our DC and DI classifications are mutually exclusive. In many of these DC galaxies the small amount of nuclear light that does reach Earth is evidently scattered back into our line of sight, accounting for the nuclear polarizations. It also accounts for their identification as heavily absorbed X-Ray sources: this category may include nearly all known "Narrow-Line X-Ray Galaxies." The nuclear dust lanes in these galaxies have evidently obscured our direct view of the nuclear broad-line region and optical nonstellar continuum, although the hard X-ray emission does leak through.

The second group of galaxies with interesting dust absorption are inclined spirals with extensive dust lanes on one side of their major axis and hardly any on the other side (denoted in Table 3,4,5 as D-[*direction*], where *direction* = N, E, S, W, NE, NW, SE, SW.) This morphology is a simple orientation effect of the bulge light being intercepted by the disk. On the side of the galaxy with the disk tilted towards us, most of the bulge light is behind, and suffers more extinction. The relatively smooth side is the one in which most of the bulge is in front of the disk, which tilts away from Earth. We have noted these cases mostly to help break the usual indeterminacy in knowing which way the disk is tilted, which can be of interest for comparison with the geometry of the extended nuclear non-stellar emission (e.g., in the radio).

11. Nuclear Dust Lanes: Intrinsic Differences Between Seyfert 1 and 2 Host Galaxies

Forty-five (39%) of the Seyfert 2 galaxies show either dust lanes or absorption patches which are irregular (i.e., not associated with a spiral arm pattern) or dust that passes through the center of the galaxy (DI and DC categories). This is significantly higher than the proportion in Seyfert 1 galaxies, 21 (23%) of which fall into this category. Can this difference be attributed to the differing distances of the two samples, which might allow us to detect more fine scale features in the closer galaxies (Sy 2's med z = 0.017), and less in the further galaxies (Sy 1's med. z = 0.024)? To test this hypothesis, we eliminated the Sy 1 and Sy 2 galaxies that had a $z \geq 0.03$ from our sample thereby bringing the median z of the two samples closer together (Table 8). For both Sy 1 and Sy 2 galaxies, the percentage of DC and DI galaxies went up, but the difference in dustiness between the two categories changed very little. Before the z based selection the difference was 16%, after the z based selection it was 14%. Thus we are not likely missing large numbers of DC and DI Sy 1's because of their greater distances.

Another selection effect which may cause the Sy 1's to seem less dusty than the Sy 2's would be because of glare from saturated point sources. We have tested the possibility that dust closer to the nucleus is lost when a saturated point source is present with a simulation. One of us added observed saturated point sources to an anonymous subsample of representative Seyfert 2 images, thus converting them into artificial SS1's. These test images were then reclassified by another one of us, who *independently* obtained the same dust absorption classification in 84% of the galaxies as in their original images.

In only one case– ESO 373-G29 –was dust absorption missed when the saturated point source was added, because it is only visible very close to the center of that galaxy. The only other misclassification went in the opposite sense: IR 2246-195 was noted as having a dust lane which "possibly" extended close to the center (i.e., , with less confidence than any of the other dust detections in the test images). This test indicates that the deficiency of dust detections in the SS1's relative to the Seyfert 2's is not due to the glare of the point source. Such an explanation would require that we missed *half* of the dust features in the SS1's, whereas we in fact missed only one-sixth of them.

Furthermore this effect cannot explain the low rate of dust detections in the Unsaturated Seyfert 1's, which is still significantly below that of the Seyfert 2's. The DC/DI percent-

age in the Sy 1's with point sources (SS1 and US1 category) is 19% (11 out of 57) versus the rate for Sy 1's with no point sources (RS1 category) which is 29% (10 out of 34). This is still below the 39% for the Sy 2's.

This difference is also seen in the Hubble types we assigned for the inner region of each galaxy. Figure 7 shows that the Seyfert 1 galaxies are more skewed to Sa types, and away from Sc's. (The ratio of Sa/Sc galaxies with Seyfert 1 nuclei is 3.9; it is 1.0 for Seyfert 2 galaxies). This skewness toward early-types in Seyfert 1's also shows up in the median morphological class, which is Sa for the Seyfert 1 galaxies and Sb for the Seyfert 2's.

The combination of these robust differences in morphological classes and dust-lane classifications indicate that the centers of Seyfert 2's are *intrinsically more dusty* than the centers of Seyfert 1's. Our spatial resolution is many orders-of-magnitude coarser than the structures that define a Seyfert 1–the broad-emission-line region and the even more compact nonstellar continuum. Thus we could easily fail to see a small opaque dust cloud which is nonetheless large enough to block out the Seyfert 1 nucleus in many galaxies we classify as Seyfert 2's. It seems likely, however, that the dust we see on larger scales would be statistically associated with these small (possibly unseen) dust clouds. Therefore, in a dustier galaxy, more lines-of-sight to the central active nucleus are likely to intersect small but opaque galactic dust clouds. We postulate that these galactic dust clouds are a major reason we cannot see the Seyfert 1 nucleus directly in Seyfert 2 galaxies.

Our imaging evidence for galactic dust clouds along our lines-of-sight to Seyfert 2's is statistical, since we would not be able to see them in every case. The absorption must have a great deal of unresolved fine structure. Since *HST* cannot resolve the small spatial scales on which the Seyfert 1 nucleus can be blocked, we could hardly expect a one-to-one correspondence between a dusty appearance and a Seyfert 2 classification. Thus we have probably missed small galactic dust lanes which lie in front of some Seyfert 2 nuclei which did not appear "dusty" in our PC images. Conversely, it is also plausible that those "dusty" Seyferts classified as type 1 happen to have a relatively dust-free gap along our line-of-sight, which allows at least some of the nuclear light to reach us directly. *HST*'s order-of-magnitude improvement in spatial resolution may well have shown us the tip of the iceberg. With another comparable improvement in resolution, we predict that the correlation between nuclear dust absorption and Seyfert 2 classification will become even stronger than it is on our data.

The suggestion that Seyfert 2 nuclei are more heavily obscured is not new (e.g., Lawrence and Elvis 1982, Malkan and Oke 1983). They are redder than Seyfert 1's at all wavelengths from the far-infrared to the X-rays, and a relatively larger fraction of their total energy output has been reprocessed by warm dust grains (Edelson and Malkan 1986). Because the surviving transmitted continuum is weaker, the scattered continuum light becomes relatively more prominent. The greater dust covering fraction enhances the scattering, and increases the proportion of nuclear luminosity which is re-radiated in the thermal infrared (Spinoglio and Malkan 1989).

We noted above that our full sample may suffer some selection biases. The principal one is that Seyfert 2's are less likely to be included unless they are relatively prominent

(i.e., with unusually high nuclear luminosities or star formation rates). This raises the danger that we are comparing the Seyfert 1 galaxies with Seyfert 2's which are intrinsically more luminous. We have no reason to suppose that more luminous Seyfert 2's should have higher dust covering fractions than less luminous Seyfert 2's. Nonetheless, in testing predictions of the unified scheme, it is desirable to compare Seyfert 1s and 2s which are matched in some isotropic emission property. We have compared those Seyferts with measured low-frequency radio fluxes and [OIII] 5007 emission line fluxes. These quantities, which are believed to be relatively orientation-independent, have *indistinguishable distributions in our Sy 1's and Sy 2's.* Thus we have avoided the most common pitfall in constructing Sy 1/Sy 2 comparison samples to test unified schemes.

Another test is to consider the subsample of Seyfert galaxies which were not selected in the traditional optical/UV searches. Fortunately 29 of our Sy 1's and 31 of our Sy 2's are members of the 12 Micron Galaxy Sample which avoids the usual biases of these other methods (Spinoglio and Malkan 1989; Rush et al. 1993). The morphologies of this subset show the same preference for Sy 1 nuclei to reside in earlier-type galaxies than Sy2 nuclei (Figure 8). The median morphological class is Sab for the Sy 1's and Sbc for the Sy 2's. Since this subsample shows the same distinction as our entire (heterogenous) sample, we believe that the effect is not an artifact of selection.

12. Seyfert Unification: An Alternative to the Orientation Hypothesis

The Seyfert unification hypothesis states that each Seyfert 2 nucleus actually harbors a normal Seyfert 1 nucleus in its center (Peterson 1997). It has long been suspected that the classical observational signatures of the Seyfert 1 nucleus (point-like nonstellar continuum plus broad permitted emission lines) are not visible in Seyfert 2's because of obscuration along our line-of-sight to the central engine (e.g., Lawrence and Elvis 1982; Malkan and Oke 1983). All of the Seyfert 1 nuclei which suffer sufficient extinction (corresponding to more than several magnitudes of visual absorption) will then appear to us as Seyfert 2's. This idea is well established for some Seyfert 2 nuclei which show broad emission lines in polarized light. This powerful observational signature has by no means been shown to be universal among Seyfert 2's. Whether *all* Seyfert 2's harbor obscured Seyfert 1 nuclei is still controversial. (See Lawrence1991 for a review). The present imaging study does not settle this question. In the following discussion we will assume the unification hypothesis is true, and use our data to make further inferences.

The differences in the apparent nuclear dustiness of the Seyfert 1 and 2 host galaxies in these PC images should not depend much, if at all, on the orientation of the nucleus (or the orientation of the galaxy, if that were similar). Our data suggest that this difference does not result from viewing angle, but because *a greater fraction of the sky as seen from a Seyfert 2 nucleus is blocked by obscuration.* This is at least a complication to the simple "unified scheme" in which Seyfert 2's are intrinsically identical to Seyfert 1's except for the angle at which they are viewed. Instead, we argue that those Seyferts which are classified as type 2 are more likely to have larger "dust covering fractions" than the average type 1's. This *intrinsic difference* could ex-

plain some of their different observed broad-band properties (e.g., Edelson et al. 1987, Carleton et al. 1987), as well as most of the usual difficulties with the simple unified scheme (e.g., review by Antonucci 1993).

Still assuming the Seyfert unification hypothesis, an outstanding question remains: What is the nature and location of the absorbers that obscure our view of the Seyfert 1 nucleus, which we suppose is always present in the center of a Seyfert 2 galaxy? One possibility has become well known since it was sketched in Antonucci (1982). That paper described a particular scenario in which our view of the central continuum and broad-line region is occulted by a dusty thick gas ring which surrounds the central engine, and is closely aligned with its rotation axis. A Seyfert which we view at sufficiently high inclination, through its torus, will appear to us as a type 2. A Seyfert nucleus which we view close enough to a face-on orientation would show us a direct view of its BLR, and would thus be classified as type 1. This Accreting Torus Model (ATM) is sketched on the left-side panel of Figure 9.

This specificity also makes the AT model vulnerable to observational tests. Based on the observed fact that Seyfert 2's are somewhat more numerous locally than Seyfert 1's requires that the opening angle of the torus cannot be larger than about π steradians (Edelson et al. 1987; Rush et al. 1993). The inner diameter need only be large enough to engulf the BLR, hardly more than a parsec for the typical low-luminosity Seyferts in our survey. The outer diameter is not expected to be much more than one or two orders of magnitude larger, so that the entire torus structure remains aligned with (and connected to) the central engine, rather than the host galaxy. More than 100 parsecs from the central engine, its gravity is likely to be less important than that of the galactic stars. Assuming the obscuring torus is a small extension of the central engine, and is relatively independent of the host galaxy, we formulated two expectations about our WFPC2 images: a) the obscuring torus will be too small to detect at our typical resolution of a few hundred parsecs; and b) it will not be connected with the galactic dust lanes which we can observe hundreds of parsecs away from the galactic center; and c) therefore any difference between Seyfert 1 and 2 nuclei would only be invisible on the larger size scales probed by our direct images.

These admittedly simplistic expectations are not borne out by our observations. The higher observed incidence of irregular dust absorption in the centers of Seyfert 2 galaxies suggests that we are in some cases directly observing the source of the nuclear extinction: interstellar dust clouds which intercept our line-of-sight to the nucleus. These dust lanes are seen on scales of hundreds of parsecs, and may therefore have *little or no physical connection with the central engine.* This alternative to the AT model, the Galactic Dust model (GDM), is illustrated schematically on the right-hand panel of Figure 9.

The viability of the GDM depends on whether galactic dust outside the nucleus could produce enough extinction to transform a Seyfert 1 nucleus into a Seyfert 2? The answer depends on how much extinction is required, and how much might plausibly be available on scales of a hundred parsecs. The visible and UV traces of a Seyfert 1 nucleus (broad lines and compact continuum) would be substantially obliterated at an extinction above A_V of 10 magnitudes. Even unusually deep

infrared searches are hard pressed to detect buried Seyfert 1 nuclei when A_V is 25 to 50 magnitudes (Ward et al. 1991). These extinctions would completely block soft X-ray emission from the nucleus. Thus for a normal dust/gas ratio the line of sight to the center of a typical Seyfert 2 galaxy would need to intercept 0.2–1.0 $\times 10^{23}$ atoms cm^{-2}. Such column densities are roughly consistent with the average values inferred in Seyfert 2's from limited hard X-ray spectroscopy (Mulchaey et al. 1992).

This amount of extinction would be produced if our line-of-sight to the galactic nucleus intercepted about 10 diffuse molecular clouds, or a single dense molecular cloud core. This might happen in a Milky-Way-type disk at a radius of ~100 parsecs, where the vertical extent of the molecular gas (including extraplanar warps), is comparable to the distance from the nucleus (Sanders, Solomon, & Scoville1984). In fact, the average surface density of molecular gas in the inner 500 parsecs of the Milky Way corresponds to $N_H = 4 \times 10^{22}$ atoms cm^{-2}. This value is probably typical (it is, for example, 10^{23} in the inner few hundred parsecs of Maffei 2–Hurt 1994). Furthermore, our images indicate that the interstellar dust is often *disturbed* in Sy 2's, so that it is not confined to a 100-pc-thick slab in the disk plane.

The ATM is most likely to be applicable to those Seyfert 2's which have Fe Kα emission lines of enormous equivalent width. Assuming this Fe line is produced by X-ray fluorescence, it implies the existence of a bright hard X-ray continuum which is obscured by $N_H \geq 10^{24}$ cm^{-2}, which might be too large for the GDM to explain. There are only a handful of such Seyfert galaxies known currently, NGC 1068 being the most famous (Smith, Done, & Pounds1993), but few sufficiently sensitive observations have been made.

If the GDM is more applicable to most Seyfert nuclei than the ATM, then several major implications would follow:

1) The obscuring region in Seyfert 2's need not surround it on all sides. Complete 360-degree azimuthal symmetry cannot be assumed, and there need not be any well defined "opening angle".

2) Galaxy interactions may be an important mechanism for (temporarily) increasing the dust covering fraction of an active galactic nucleus. According to the GDM, this active nucleus is then more likely to appear as a Seyfert 2. This would be consistent with a higher rate of galaxy interactions in Seyfert 2's than in Seyfert 1 galaxies.

3) The obscuring region may be typically more than 100 parsecs from the central engine. The mutual physical influence of these two regions on each other may be very small.

4) The obscuring region could be observed in emission, but only at long wavelengths. For a typical nuclear luminosity of 10^{43} erg/sec, dust grains at a radius of 100 parsecs should reach an equilibrium temperature around 50 K. Thus if Sy 2's do have dustier centers than Sy 1's, they could be relatively stronger emitters of far-infrared continuum and perhaps CO line emission. Testing this prediction would, however, require observations at wavelengths longer than $100\mu m$. Unfortunately, the spatial resolution required to isolate and map the central 100 parsecs is of order an arcsecond, probably achievable via interferometry.

5) The orientation of this dust lane may have little or no relation to the *intrinsic* orientation of the central engine. Of course it does

affect what we are able to see from Earth. In particular, it blocks our direct view of the central continuum source and the broad line region. It also extinguishes scattered photons from these regions unless they are escaping out of the plane of the dust lane. This explains why some Seyfert 2 nuclei have linear continuum polarizations which are modest (typically a few up to 15%), but always less than would be expected for the very simple, well-defined scattering geometry of a torus plus conical-funnel scattering region (where the expected polarizations can range from 20% to much higher values).

6) The linear or even bi-polar structures which are sometimes seen in the [OIII] line and radio continuum emission in Seyfert nuclei do not require the presence of a geometrically thick dust torus for their existence. These structures, which are sometimes spatially related, appear to be produced by a bipolar outflow of energy along the two opposite poles of the central engine. The central engine tends to eject energy (which could be in the form of relativistic particles or mechanical energy) along what is thought to be the spin axis. As shown in Figure 9, in the ATM, only gas above the poles of the torus sees the ionizing radiation from the central source. In the GDM the central ionizing continuum and the [OIII] line emission need not be bipolar, except for the component of the NLR which is associated with the radio jet. In the few cases where dense molecular gas has been detected orbiting close to an active nucleus, such as NGC 4258, it lies in an extremely thin disk, not a torus.

7) Even though the central engines in Seyfert 1 and 2 nuclei may be intrinsically the same, the inner regions of their host galaxies are *not*. If Seyfert 2 galaxies have nuclei which are covered by a larger fraction of dust clouds, they would be more often observed as Seyfert 2's rather than less obscured Seyfert 1's. This larger areal dust covering fraction is likely to have additional observational manifestations, including more heavily reddened emission line ratios and different thermal dust emission spectra in the infrared (e.g., Edelson et al. 1987).

8) If much of the obscuring medium is not fixed to the central engine, it may well be moving across our line-of-sight. Typical orbital speeds for galactic dust clouds are up to 0.1% the speed of light. Thus fine structure in the dust lane can traverse the nucleus in as little as 1000 light-crossing times. This would correspond to changes in the reddening/extinction of the nuclear continuum on timescales as short as weeks, and changes in the reddening/extinction of the broad emission lines over less than a decade. Statistically, we could expect the partially covered nuclei (our RS1's) to show the strongest reddening variations, and much more so in the continuum than in the lines. If the projected cloud edges are relatively straight as they move across the nucleus, this kind of extinction variability could provide a kind of tomography of the central engine, somewhat different from the information gleaned from reverberation.

9) Assuming the central engine of the Seyfert nucleus has a symmetry (rotation?) axis, its viewing angle is probably *not* simply related to its apparent classification. Thus, for example, we probably view some Seyfert 1 nuclei at high inclinations, just as we probably view some Seyfert 2 nuclei close to "face-on."

13. Summary

Our large sample of high-resolution images of the centers of nearby Seyfert 1, 2 and HII galaxies has allowed us to search for statistical differences in their morphologies.

The Seyfert galaxies do not, on average, resemble the HII galaxies. The latter have more irregularity and lumpiness associated with their high rates of current star formation. Conversely, none of the HII galaxies have the filaments or wisps which are sometimes seen in Seyfert 1 and 2 galaxies, and are evidently gas filaments photoionized by the active nucleus.

Sixty-three percent (63%) of the galaxies classified as Seyfert 1 have an unresolved nucleus, 52% of which are saturated. Some (6%) have such dominant nuclei that they would appear as "naked quasars" if viewed at somewhat higher redshifts. The presence of an unresolved nucleus, particularly a saturated one, is anti-correlated with an intermediate spectroscopic classification (such as Seyfert 1.8 or 1.9) and is also anti-correlated with the Balmer decrement. This implies that those Seyfert 1's with weak nuclei in the PC2 images are extinguished and reddened by dust.

The vast majority of the Seyfert 2 galaxies show no central point source. In fact, the only two of these that do (IRAS 1832-594 and IC 4870) are mis-classified galaxies. If all Seyfert 2's actually harbor point-like continuum sources like those in Seyfert 1's, they are at least an order of magnitude fainter on average. In those galaxies without any detectable central point source (37% of the Seyfert 1's; 98% of the Seyfert 2's, and 100% of the H II's), the central surface brightnesses are statistically similar to those observed in the bulges of normal galaxies.

Seyfert 1's and 2's both show circumnuclear rings in about 10% of the galaxies. We identified strong inner bars as often in Seyfert 1 galaxies (27%) as in Seyfert 2 galaxies (22%). In some cases we see a strong assymetry of the dust absorption across the major axis, which allows us to infer which half of the disk is nearer to us: the side which more strongly absorbs the smooth light of the bulge behind it.

The Seyfert 2 galaxies are more likely than Seyfert 1's to show irregular or disturbed dust absorption in their centers as well as galactic dust lanes which pass very near their nuclei. They also, on average, tend to have latter morphological types than the Seyfert 1's. This difference remains in Seyfert 1 and 2 subsamples matched for redshift, [OIII] and radio luminosities. It also holds true when we restrict our consideration to sub-samples of the data which are less biased by selection effects. Thus it appears that the host galaxies of Seyfert 1 and 2 nuclei are *not* intrinsically identical. A galaxy with more nuclear dust and in particular more irregularly distributed dust is more likely to harbor a Seyfert 2 nucleus. This indicates that the higher dust-covering fractions in Seyfert 2's are the reason for their spectroscopic classification: their compact Seyfert 1 nucleus may have been obscured by galactic dust. This statistical result contradicts the simplest and most popular version of the unified scheme for Seyfert galaxies. We suggest that the obscuration which converts an intrinsic Seyfert 1 nucleus into an apparent Seyfert 2 often occurs in the host galaxy hundreds of parsecs from the nucleus. If so, this obscuration need have no relation to a hypothetical fat dust torus surrounding the equator of the central engine. Also then the orientation of the central en-

gine with respect to our line-of-sight does *not* determine whether an active nucleus will appear to us as a Seyfert 1 or as a Seyfert 2.

We thank Wayne Webb and Randall Rojas for help in the early stages of this research, and M. Regan for insightful refereeing. This research has made use of the NASA/IPAC Extragalactic Database (NED), which is operated by the Jet Propulsion Laboratory, Caltech, under contract with NASA.

REFERENCES

Adams, T.F. 1977, ApJS, 33, 19

Antonucci, R. 1982, Nature299, 605

Antonucci, R. 1993, ARA&A, 31, 473

Bahcall, J.N., Kirhakos, S., Saxe, D.H., and Schneider, D.P. 1997, ApJ, 479, 642

Barnes, J.E., & Hernquist, L. 1995, ApJ, 471, 115

Barth, A.J., Filippenko, A.V., Gorjian, V., Malkan, M.A., Sargent, W.L.W., Hubble Space Telescope Images of Nuclear Rings in Barred Galaxies, 1996, A.S.P. Conf. Ser. 91, 94

Brindle, C.,Hough, J.H., Bailey, J.A., Axon, D.J., Ward, M.J., Sparks, W.B., McLean, I.S. 1990, MNRAS, 244, 577

Burrows, C.J., Hubble Space Telescope Wide Field Planetary Camera 2 Instrument Handbook, Version 2.0 (Baltimore:STSci)

Bushouse, H.A. 1986, AJ, 91, 255

Carleton, N.P., Elvis, M., Fabbiano, G., Willner, S.P., Lawrence, A., Ward, M. 1987, ApJ, 318, 595

Corwin, H.G., Buta, R.J., and De Vaucouleurs, G. 1994, AJ, 108, 2128

Dahari, O. 1985, AJ, 90, 1772

Dahari, O. 1985, ApJS, 57, 643

Edelson, R.A., & Malkan, M.A. 1986, ApJ, 308, 59

Edelson, R.A., Malkan, M.A., and Rieke, G.H. 1987, ApJ, 321, 233

Fuentes-Williams, T. & Stocke, J., 1988 AJ, 96, 1235

Goodrich, R.W. 1990, ApJ, 355, 88

Goodrich, R.W. 1995, ApJ, 440, 141

Gorjian, V. 1995, ApJ, 450, 511

Green, R.F., Schmidt, M., & Liebert, J. 1986, ApJS, 61, 305

Heckman, T.M. 1980, A&A, 87, 142

Hernquist, L., & Mihos, C.J. 1996, AJ, 471, 115

Holtzman, J.A., et al. 1995,PASP,107,1065

Hurt, R.L. 1994, PASP, 106, 549

Jura, M. 1997, in preparation

Kennicut, R.C. Jr., & Keel, W.C. 1984, ApJ, 2791, 5

Koski, A.T. 1978, ApJ223, 56

Kotilainen, J.K, Ward, J.M., Williger, G.M., 1993, MNRAS, 263, 655

Lawrence, A., & Elvis, M. 1982, ApJ, 256, 410

Lawrence, A. 1991, MNRAS, 252, 586

Maiolino, R., & Rieke, G.H. 1995, ApJ, 454, 95

Malkan, M.A. 1983, ApJ, 268, 582

Malkan, M.A. 1984, ApJ, 287, 555

Malkan, M.A., & Filippenko, A.V. 1983, ApJ, 275, 477

Malkan, M.A., & Oke, J.B. 1983, ApJ, 265, 92

Mulchaey, J.S., Mushotzky, R.F., Weaver, K.A. 1992, ApJ, 390, 69

Mulchaey, J.S. et al. 1994, ApJ, 436, 586

Mulchaey, J.S., & Regan, M.W. 1997, ApJ, 482, 135l

Mauder, W., Weigelt, G., Appenzeller, I., Wagner, S.J. 1994, A&A, 285,44

Nelson, C.H., Mackenty, J.W., Simkin, S.M., Griffiths, R.E. 1996, ApJ, 466, 713

Osterbrock, D.E. 1977, ApJ, 215, 733

Osterbrock, D.E., & Pogge, R.W. 1985, ApJ, 297, 166

Osterbrock, D.E., & Pogge, R.W. 1987, ApJ, 323, 108

Peterson, B. 1997, An Introduction to Active Galactic Nuclei, Cambridge University Press, Cambridge, UK, Ch. 7

Petrosian, A. R., 1983, Astrofizika 18, 548

Phillips, A.C., Illingworth, G.D., MacKenty, J.W., Franx, M. 1996, AJ, 111, 1566

Pogge, R.W. 1988, PASP, 100, 1296

Polleta, M.,Bassani, L.,Malaguti, G., Palumbo, G.G.C., Caroli, E. 1996, ApJS, 106, 414

Rix, H., Rieke, M., & Carleton, N.P. 1990, ApJ, 363, 480

Rush, B., Malkan, M.A., & Edelson, R.A. 1996, ApJ, 473, 130

Sanders, D.B., Solomon, P.M., & Scoville, N.Z., 1984, ApJ, 276, 182

Schwartz, M. 1981, ApJ, 247, 77

Shlosman, I., Frank, J., & Begelman, M. 1989, Nature, 338, 45

Shlosman, I., Frank, J., & Begelman, M. 1990, Nature, 345, 679

Simkin, S.M., Su, H.J., & Schwarz, M.P. 1980, ApJ, 237, 404

Smith, D.A., Done, C., & Pounds, K.A. 1993, MNRAS, 263, 54

Spinoglio, L., & Malkan, M.A. 1989, ApJ, 342, 8

Steiner, J.E. 1981, ApJ, 250, 469

Tran, H.D., Osterbrock, D.E., Martel, A. 1992, AJ, 104, 2072

Ulvestad, J.S., & Wilson, A.S. 1989, ApJ, 343, 659

Véron-Cetty, M.P., & Véron, P. 1986, A&AS, 66, 335

Véron-Cetty, M.P., & Véron, P., 1987, ESO Sci. Rep., No. 5

Ward, M.J., Blanco, P.R., Wilson, A.S., Nishida, M. 1991, ApJ, 382, 115

This 2-column preprint was prepared with the AAS LaTeX macros v4.0.

TABLE 1

SEYFERT 1 GALAXIES

Galaxy	Alternate Designation	z	12μm	Inner Mag.[a]	Outer Mag.[b]	Seyfert Class	Saturated Unsaturated, Resolved
ESO 215-g14		0.019		17.56	15.92	1	US1
ESO 323-g77		0.015		16.69	···	1	SS1
ESO 354-g4		0.033		18.42	16.66	1	US1
ESO 362-g18	MCG -5-13-17	0.013	X	···	···	1	RS1
ESO 438-g9	IRAS 11083-2813	0.024		17.44	···	1.5	SS1
FRL 51	ESO 140-g43	0.014		17.17	···	1	SS1
FRL 1146		0.032		16.54	14.40	1.5	RS1
H -1-0307-73	H0307-730	0.028		18.29	···		SS1
H 1143-182		0.033		17.16	···	1	SS1
H 2106-099		0.027		16.87	···	1.2	SS1
IC 1816	ESO 355-g25	0.017		18.10	···	1	RS1
IC 4218	UGC 8348	0.019		18.68	17.41	1	US1
IC 4329a	ESO 445-g50	0.016	X	16.91	···	1	SS1
IRAS 1319-164	MCG -3-34-64	0.017	X	16.43	···	1.8	RS1
IRAS 13329-340	MCG -6-30-15	0.008	X	17.26	···	1	SS1
MCG 6-26-12	KUG 1136+342	0.032		18.43	17.52	1.5	US1
MCG 8-11-11	UGC 3374	0.020		17.07	···	1.5	SS1
MRK 6	IC 0450	0.019	X	16.77	···	1.5	SS1
MRK 10	UGC 4013	0.030		18.46	16.85	1	US1
MRK 40	ARP 151	0.020		18.68	17.03	1	US1
MRK 42		0.024		19.01	17.54	1	RS1
MRK 50		0.023		18.35	17.12	1	US1
MRK 79	UGC 3973	0.022	X	16.92	···	1.2	SS1
MRK 279	UGC 8823	0.031		16.66	···	1	SS1
MRK 290		0.029		17.65	···	1	SS1
MRK 334	UGC 6	0.022		17.99	···	1.8	RS1
MRK 335	PG 0003+199	0.025	X	16.51	···	1	SS1
MRK 352		0.015		18.53	17.04	1	US1
MRK 359	UGC 1032	0.017		17.97	···	1.5	SS1
MRK 372	IC 1854	0.031		18.70	16.88	1.5	RS1
MRK 382		0.034		18.44	···	1	SS1
MRK 423	MCG 6-25-72	0.032		18.96	16.49	1.9	RS1
MRK 471	UGC 9214	0.034		19.42	17.78	1.8	RS1
MRK 493	UGC 10120	0.031		18.67	17.13	1	US1
MRK 516	IRAS 21538+0707	0.028		17.70	16.48	1.8	RS1
MRK 530	NGC 7603	0.029	X	16.97	···	1.5	SS1
MRK 543	NGC 7811	0.026		18.42	···	1	SS1
MRK 590	NGC 863	0.027		16.76	···	1.2	SS1
MRK 595		0.028		18.56	16.48	1	RS1
MRK 609	IRAS 03229-0618	0.032		17.48	···	1.8	RS1
MRK 699	IIIZW77	0.034		18.42	17.11	1.2	US1
MRK 704		0.029	X	17.45	···	1.5	SS1
MRK 744	NGC 3786	0.010		17.05	···	1.8	SS1
MRK 766	NGC 4253	0.012	X	17.13	···	1.5	SS1
MRK 817	UGC 9412	0.033	X	17.43	···	1.5	SS1
MRK 833		0.039		22.46	19.33		RS1
MRK 871	IC 1198	0.034		18.61	···	1.5	SS1
MRK 885		0.026		19.95	17.80	1.5	RS1
MRK 896		0.027		18.30	···	1	US1
MRK 915	MCG -2-57-23	0.025		19.11	17.10	1	RS1
MRK 1040	NGC 931	0.016	X	18.46	···	1.5	SS1
MRK 1044		0.016		17.15	···	1	SS1
MRK 1126	NGC 7450	0.010		18.75	16.80	1.5	RS1
MRK 1218	NGC 2622	0.028		18.66	16.82	1.8	RS1
MRK 1330	NGC 4593	0.009	X	17.11	···	1	SS1
MRK 1376	NGC 5506	0.007	X	19.41	16.99	1.9	RS1
MRK 1400	CGCG 414-001	0.029		20.07	17.54	1	RS1
MRK 1469	MCG 9-20-136	0.031		18.98	17.18	1.5	RS1
MS 1110+2210	MS 1110.3+2210	0.030		20.74	18.37	1	RS1
NGC 235		0.022		18.72	16.16	1	RS1
NGC 526a		0.018	X	17.98	···	1.5	RS1
NGC 1019		0.024		18.75	17.11	1	US1
NGC 1566		0.004	X	16.84	···	1	RS1
NGC 2639		0.011	X	19.41	16.33	1	RS1
NGC 3227	UGC 5620	0.003	X	16.33	···	1.5	SS1
NGC 3516	UGC 6153	0.009	X	15.83	···	1.5	SS1
NGC 3783	ESO 378-g14	0.009		17.43	···	1	SS1
NGC 4051		0.002	X	16.28	···	1	SS1
NGC 4235	UGC 7310	0.007		18.60	16.78	1	RS1
NGC 4748	IRAS 12495-1308	0.014	X	17.57	···	1	SS1
NGC 5252		0.022		19.47	17.08	1.9	RS1
NGC 5548	MRK 1509	0.017	X	16.55	···	1.5	SS1
NGC 5674		0.025		19.12	16.77	1.9	RS1
NGC 5940	UGC 9876	0.033		18.75	17.30	1	US1
NGC 6104		0.028		19.88	18.01	1.5	RS1
NGC 6212		0.030		20.03	17.48	1	RS1
NGC 6860		0.015	X	17.37	···	1	SS1
NGC 7213		0.006	X	16.85	···	1	US1
NGC 7314	ESO 533-g53	0.006	X	19.75	18.23	1.9	RS1
NGC 7469	MRK 1514	0.017	X	16.38	···	1	SS1
PG 1310-108	IISZ10	0.034		18.00	···		SS1
PKS 0518-458		0.034		18.82	17.41		US1

TABLE 1—*Continued*

Galaxy	Alternate Designation	z	12μm	Inner Mag.[a]	Outer Mag.[b]	Seyfert Class	Saturated Unsaturated, Resolved
TOL 1059+105		0.034		19.26	17.64	1	US1
TOL 2327-027	UM 163	0.033		19.59	17.75	1	US1
UGC 1395	UM 146	0.017		19.69	17.46	1.9	US1
UGC 3223		0.018		18.76	17.14	1	RS1
UGC 7064	WAS 45	0.024	X	18.40	15.98	1.9	RS1
UGC 10683b		0.031		18.49	17.18	1	US1
UGC 12138	IRAS 22377+0747	0.025		17.67	···	1.8	US1
UM 614		0.033		18.60	16.69	1	US1
X 0459+034	MS 0459.5+0327	0.016		16.43	···	1	RS1

[a]2 pixels radius (or 0.″09)

[b]11 pixels radius (or 0.″5), ··· indicates no central magnitude available due to saturation of central pixels

TABLE 2

SEYFERT 2 GALAXIES

Galaxy	Alternate Designation	z	12μm	Inner Mag.[a]	Outer Mag.[b]
ESO 137-g34		0.009		19.28	15.90
ESO 138-g01		0.009		16.69	14.37
ESO 139-g12		0.017		16.87	14.83
ESO 353-g9		0.017		19.25	16.45
ESO 362-g8		0.016		16.41	13.50
ESO 373-g29	IC 2510	0.009		18.89	16.93
ESO 509-g66		0.034		18.54	16.42
ESO 509-g66-c		0.045		20.64	18.52
FRL 294		0.017		19.21	16.83
FRL 312	IC 3639	0.011		[17.06]	...
FRL 315		0.016		18.90	16.47
FRL 316		0.016		19.95	17.36
FRL 334	IC 4777	0.018		[17.58]	...
FRL 341	IC 4995	0.016		19.03	16.68
IC 184		0.018		20.96	18.03
IC 4870		0.003		[19.54]	...
IRAS 0147-076	IRAS 01475-0740	0.017	X	19.24	17.56
IRAS 0258-1136	MCG -2-8-39	0.030	X	17.84	17.20
IRAS 0450+039	CGCG 420-015	0.030		18.84	16.99
IRAS 0450-032	PGC 16226	0.016		20.88	18.28
IRAS 0457-756	ESO 33-g2	0.019	X	19.23	16.80
IRAS 1121-281	IRAS 11215-2806	0.014		—	—
IRAS 1305-241	IRAS 13059-2407	0.014		19.81	16.84
IRAS 1443+272	IRAS 14434+2714	0.029		19.11	17.43
IRAS 1548-037	IRAS 15480-0344	0.030	X	19.29	17.12
IRAS 1832-594	FRL 49	0.019		[17.58]	...
IRAS 1833-654	ESO 103-g35	0.013		19.34	16.86
IRAS 2246-195	MCG -3-58-7	0.033	X	18.83	16.55
IRAS 2302-000	UGC 12348	0.030		19.35	16.95
IRAS 2346+019	IRAS 23461+0157	0.031	X	19.11	17.82
MCG -5-27-13	ESO 439-g9	0.023		21.31	18.25
MRK 1		0.016		18.45	16.78
MRK 3	UGC 3426	0.014		18.39	15.59
MRK 176	UGC 6527	0.027		18.87	16.53
MRK 198		0.024		19.71	17.00
MRK 266NE	NGC 5256	0.028	X	20.77	18.00
MRK 270	NGC 5283	0.009		18.74	16.17
MRK 313	NGC 7465	0.006		18.99	16.40
MRK 348	NGC 262	0.014	X	18.82	16.77
MRK 403		0.024		20.14	17.87
MRK 533	NGC 7674	0.029	X	[17.58]	...
MRK 573		0.017		18.97	16.37
MRK 577	UGC 1282	0.017		19.30	16.63
MRK 607	NGC 1320	0.009	X	18.81	16.59
MRK 612		0.020		19.61	16.90
MRK 620	NGC 2273	0.006		19.24	16.64
MRK 622	UGC 4229	0.023		[17.30]	...
MRK 686	NGC 5695	0.014		19.51	16.77
MRK 917		0.025		19.05	16.58
MRK 937		0.030		19.41	17.68
MRK 938	NGC 34	0.019	X	18.78	16.31
MRK 955		0.035		20.49	17.58
MRK 993	UGC 987	0.017		19.28	16.85
MRK 1058		0.018		19.35	17.09
MRK 1066	UGC 2456	0.012		18.67	16.24
MRK 1073		0.023		19.63	16.84
MRK 1157	NGC 591	0.015		19.20	16.86
MRK 1193		0.032		19.74	17.57
MRK 1210	UGC 4203	0.013		18.40	16.46
MRK 1370		0.024		18.91	17.16
NGC 424	TOL 0109-383	0.011	X	[18.05]	...
NGC 513		0.016	X	20.08	17.33
NGC 788		0.013		18.95	16.52
NGC 1125		0.011	X	17.73	17.25
NGC 1144		0.029	X	20.29	17.33
NGC 1241		0.013	X	19.90	17.22
NGC 1358		0.013		19.58	16.62
NGC 1386		0.002	X	18.92	15.86
NGC 1410	IIIZW55N	0.025		20.50	17.48
NGC 1667		0.015	X	19.81	16.93
NGC 2110		0.007		18.86	16.50
NGC 2992		0.007	X	19.22	16.91
NGC 3081		0.007		19.19	16.82
NGC 3362		0.028		20.38	17.96
NGC 3393		0.012		19.49	16.57
NGC 3982		0.003	X	19.29	17.12
NGC 4156		0.022	X	19.33	17.34
NGC 4507	ESO 322-g29	0.012		[17.05]	...
NGC 4922b	NGC 4922 NED01	0.024	X	19.34	16.71
NGC 4939		0.010		19.84	16.84
NGC 4968	ESO 508-g6	0.009	X	18.82	16.76
NGC 5135	ESO 444-g32	0.013	X	19.13	16.81

TABLE 2—*Continued*

Galaxy	Alternate Designation	z	12μm	Inner Mag.[a]	Outer Mag.[b]
NGC 5347		0.008	X	19.10	16.83
NGC 5427		0.009		19.72	17.52
NGC 5929	UGC 9851	0.008	X	20.00	17.03
NGC 5953		0.007	X	19.05	16.00
NGC 5995		0.025	X	19.00	16.82
NGC 6211		0.020		18.25	15.55
NGC 6217		0.005	X	18.32	15.63
NGC 6221	ESO 138-g3	0.004		19.56	16.55
NGC 6300		0.003		20.59	17.63
NGC 6393	IRAS 17296+5940	0.028		21.92	19.05
NGC 7130	IC 5135	0.016	X	18.53	16.02
NGC 7172		0.008	X	21.63	18.14
NGC 7212	UGC 11910	0.026		19.41	16.94
NGC 7319	UGC 12102	0.022		20.95	18.16
NGC 7410		0.006		20.57	17.33
NGC 7582	ESO 291-g16	0.005	X	19.27	16.43
NGC 7590		0.005	X	19.82	16.87
NGC 7592		0.024		20.87	18.44
NGC 7682	UGC 12622	0.017		20.16	17.36
NGC 7743		0.007		18.30	15.54
PKS 2048-572	IC 5063	0.011	X	19.46	17.10
PKS 2158-380		0.033		19.50	16.79
Q 1234+0848	TOL 1234+088	0.028		21.69	19.74
UGC 3255		0.019		21.68	18.77
UGC 4332	A 0816+21	0.018		21.04	17.78
UGC 6100	IRAS 10587+4555	0.029		19.23	17.02
UM 105	IC 123	0.030		20.83	18.18
UM 319		0.016		21.66	18.65
UM 625		0.025		19.55	17.55
WAS 2		0.033		19.01	16.67
ZW 1408+137	IRAS 14082+1347	0.017		19.88	17.71
ZW 1541+286	IRAS 15418+2840	0.032		19.78	17.55

[a] 2 pixels radius (or 0.″09)

[b] 11 pixels radius (or 0.″5), ··· indicates central magnitudes are unavailabe due to saturation of central pixels

[....] denote upper limits on magnitude

TABLE 3
H II GALAXIES

Galaxy	Alternate Designation	12 μ	z	Inner Mag.[a,c]	Outer Mag.[b,c]	Morphology MGT	RC3	Comments[d]
ESO 185-ig13			0.019	19.86	16.73	?		CL,
ESO 325-ig41			0.006	...	...	Irr		CL
ESO 350-ig38			0.020	...	...	Irr		CL, DC
FRL 280			0.010	...	...	SBb	SBb	B,CL
G 1307-1608			0.032	20.80	18.79	Irr		faint nucleus, dwarf
G 1314-1532			0.013	23.96	21.15	?		B
IC 3576			0.003	...	...	none	Sm	CL
IC 4687			0.017	...	...	Sd	Sb	interacting
KUV 13000+29	KUV 13000+2908		0.020	21.72	18.92			
MRK 25			0.010	19.80	17.08	Sb?	E	B
MRK 52			0.007	...	...	Sc	SB0	
MRK 171			0.010	...	...	Irr		CL
MRK 201			0.008	18.76	16.43	Irr	Im	CL
MRK 298			0.034	20.45	17.76	no	SA0	DI
MRK 308			0.024	...	...	S?	Irr	CL
MRK 567			0.033	20.14	17.25	Sc		flocculent
MRK 703			0.013	...	...	SBc	Sab	R,B
MRK 759	NGC 4152		0.006	...	...	SBd	SABc	DI,B
MRK 789			0.032	19.96	17.15	Irr		collision
MRK 930			0.019	...	...	Irr		CL
MRK 1087			0.028	...	...	?	S0	D-E
MRK 1133			0.024	19.23	17.01	Sa		bright central disk
MRK 1149			0.021	...	...	SBc		B,DC
MRK 1261			0.026	20.30	17.38	Sc/d	Irr	DC
MRK 1308			0.004	...	...	?	S0	CL, DI
MRK 1408			0.034	...	...	SBb		B
MRK 1414			0.014	...	...	Sd		
MRK 1459			0.027	...	...	Irr		CL, collision
MRK 1490			0.026	...	...	Sa		R(partial)
NGC 625*			0.001	...	...	Irr	SBm	
NGC 1614			0.015	...	...	Irr	SBc	CL,collision
NGC 2377			0.007	20.64	17.94	Sd	SAc	R
NGC 2989			0.013	...	...	Sd	SABbc	flocculent, B?
NGC 3032			0.005	...	...	Sa/b	SAB0	bright central disk
NGC 3310			0.003	...	...	Sc/d	SABbc	CL, DC
NGC 3353			0.003	...	...	Irr	Sb	CL
NGC 3504			0.005	...	...	Sb	Sab	flocculent
NGC 3738*			0.001	...	...	Irr	Irr	CL
NGC 4694			0.004	...	...	?	SB0	CL
NGC 4700*			0.004	...	...	Irr	SBc	
NGC 4990	MRK 1344		0.010	...	...	Sa	S0	
NGC 5253*			0.001	...	...	Irr	Irr	
NGC 5597			0.008	...	...	Irr	SABcd	CL
NGC 5757			0.008	19.85	17.03	SBc	SBb	B,R, Sersic Pastoriza
NGC 7552			0.005	...	...	Sd	SBab	B, flocculent
NGC 7714			0.009	...	...	Ir	SBb	CL, collision
Q 1209-1105	[oh91] s08		0.016	...	...	?		DI
Q 1241+1624	[hb91] 1241+164		0.026	22.25	19.77	?		dwarf
SZ 80			0.026	20.71	18.80	Irr		bright nucleus
UGC 8929	WAS 87		0.027	...	...	?		R
WAS 96			0.034	21.56	18.49	Irr		CL

[a] 2 pixels radius (or 0.″09)
[b] 11 pixels radius (or 0.″5)
[c] magnitudes only appear when there is no ambiguity as to the central point source
[d]

DI = irregular dust
B = bar
CL = cluster, lumpy HII region, knots
DC = dust disk/dust lane passing close or through center (ie bisected nucleus)
D-[direction] = dust lanes on one side of major axis, where direction is N, S, E, W, NW, NE, SW, or SE
F/W = filaments/wisps
R = ring

*400x400 pixel images

TABLE 4

SEYFERT 1 GALAXIES

Galaxy	θ	ϵ	Morphology MGT	RC3	Comments*
ESO 215-g14			Sa		SB0 (or tidal tail), faint galaxy
ESO 323-g77			Sa/b		CL, asymmetric sprial arms
ESO 354-g4	31	0.14	Sa	Sb	normal
ESO 362-g18			Sa	S0/a	spiral elongated nucleus, normal
ESO 438-g9			SBc/d	Sab	B
FRL 51	23	0.46	Sa	Sb	D-E
FRL 1146	72	0.41	Sb		D-E
H -1-0307-73			S(B)a		B
H 1143-182			Irr		F/W, quasar-like
H 2106-099			L		galaxy not detectable, quasar-like
IC 1816			SBa/b	Sab	R, B
IC 4218			Sa	S?	DI
IC 4329a			Sa	S0	DC, nearly edge-on
IRAS 1319-164			Sb?	SB?	edge of chip
IRAS 13329-3402			S0		D-SW
MCG 6-26-12			SB0	S?	B
MCG 8-11-11			SB0	SB?	F/W, low surface brightness
MRK 6			S0	SB0	DI, E
MRK 10	51	0.21	Sa/b	Sb	normal
MRK 40			S0	S0	R, DI, smooth tidal tail
MRK 42			SBa	SB?	R, B, classic sersic/pastoriza
MRK 50			S0		DI
MRK 79			SBc	SBb	F/W
MRK 279			Sa	S0	normal Sa
MRK 290			E	E	quasar-like
MRK 334			Irr	Pec	CL, disturbed
MRK 335			?		F/W(1″to NE), quasar-like
MRK 352	79	0.11	E	S0	smooth, low surface brightness
MRK 359			SBb/c	Pec	normal
MRK 372			Sa		normal
MRK 382			SBa	S?	B
MRK 423			Sb	S0?	normal, some tidal disruption
MRK 471			SBc	SBb	B, DC, fragment to south
MRK 493	148	0.22	S(B)a	SBb	R
MRK 516			Sc		D-N, double nucleus merger
MRK 530			Sa	Sb	D-NE, CL
MRK 543			Sc	Im	normal
MRK 590			Sa	Sa	normal
MRK 595			Sa		D-SW, faint
MRK 609			Sa/b	Im	flocculent?
MRK 699			E		smooth, faint
MRK 704			SBa	S?	B
MRK 744			Sb	Sa	DI
MRK 766			SBc	Sa	B, F/W, DI?
MRK 817			SBc	S?	B
MRK 833			Irr		CL, disturbed
MRK 871			Sb	S?	D-N, DC
MRK 885			SBb	S?	B
MRK 896			Sc	S?	R(inclined)
MRK 915			Sa	S?	F/W, DC, disturbed
MRK 1040			Sb	Sbc	DC, highly-inclined
MRK 1044			Sa	S?	Sersic/Pastoriza
MRK 1126			Sb	SBa	tight spiral arms nearly make a circle
MRK 1218			SBa	S?	B
MRK 1330			Sb/c	SBb	DC
MRK 1376			edge on	Sa	DC, F/W
MRK 1400	53	0.3	Sa		normal, highly inclined
MRK 1469	101	0.47	Sa		D-S, DC
MS 1110+2210			E		
NGC 235	119	0.36	Sa/b	S0	normal
NGC 526a			E/S0		DI
NGC1019	11	0.18	SBb	SBbc	R, B
NGC 1566			Sb	SBbc	DC
NGC 2639			Sb	Sa	DC, flocculent
NGC 3227			?	SBa	F/W, D-SW, dusty
NGC 3516			S0	S0	DI, B?
NGC 3783			Irr	SBab	B
NGC 4051			Sb	SBbc	D-SW
NGC 4235			?	Sa	DC
NGC 4748			Sa		R
NGC 5252	17	0.44	S0	S0	R(polar)
NGC 5548			Sa	S0/a	normal
NGC 5674			SBc	SBc	normal
NGC 5940			SBc	SBab	B
NGC 6104			SBb	S?	B, disturbed spiral pattern
NGC 6212			Sb	S?	flocculent spiral
NGC 6860			Sb	SBb	normal, D-S
NGC 7213			Sa	Sa	normal
NGC 7314			Sd	SBbc	DC
NGC 7469			Sb/c	SBa	R
PG 1310-108			?		F/W, quasar-like
PKS 0518-458			E		

TABLE 4—*Continued*

Galaxy	θ	ϵ	Morphology MGT	RC3	Comments*
TOL 1059+105			S0		
TOL 2327-027			SB		CL, R
UGC 1395			SBa	Sb	DI
UGC 3223			S(B)b/c	SBa	D-N
UGC 7064			Sa	S?	R
UGC 10683b			SBa	S0	B
UGC 12138			SBa	SBa	normal
UM 614	-11	0.29	S0		normal
X 0459+034			E		F/W, smooth halo

*

DI = irregular dust
B = bar
CL = cluster, lumpy HII region, knots
DC = dust disk/dust lane passing close or through center (ie bisected nucleus)
D-[direction] = dust lanes on one side of major axis, where direction is N, S, E, W, NW, NE, SW, or SE
E/S0 = Elliptical
F/W = filaments/wisps
R = ring

TABLE 5

SEYFERT 2 GALAXIES

Galaxy	θ	ϵ	Morphology MGT	Morphology RC3	Comments*
ESO 137-g34			S0	SB0/a	CL, DI
ESO 138-g01			L	E?	DI
ESO 139-g12	285	0.04	Sa	Sbc	normal
ESO 353-g9			SBb	SBbc	DC, B
ESO 362-g8			Sa	S0	DC
ESO 373-g29			Sb	SBab	DI, F/W, R, fragmentary dust tendril
ESO 509-g66			?		much of image is off chip
ESO 509-g66-c			S(B)a		normal spiral
FRL 294			SBa	SB0	normal
FRL 312			SBb	SBbc	B, inclined dust disk
FRL 315			SBa	SB0	R
FRL 316			S0	S0	
FRL 334			S(B)b	SB0	B, DC
FRL 341			Sa?	S0	D-NE
IC 184			SBb	SBa	B, inner + outer shells
IC 4870			?	Im	F/W
IRAS 0147-076			E?		R(inner + outer)
IRAS 0258-1136	50	0.3	S0/a	SBa	pretty smooth
IRAS 0450+039			Sa		normal
IRAS 0450-032			Sc		DC, two dust lanes not co-planar
IRAS 0457-756	217	0.25	SB0		B, old faded Sersic/Pastoriza
IRAS 1121-281			S0		smooth, very thin, part of image is off chip
IRAS 1305-24i			Sc?		DC
IRAS 1443+272			SBa		B
IRAS 1548-037			S0		smooth
IRAS 1832-594			Sa		F/W, point source
IRAS 1833-654	28	0.38	E	S0?	DI
IRAS 2246-195			Sb		normal
IRAS 2302-000			L		DI, R(broken)
IRAS 2346+019			SBc		F/W, R, compact center
MCG -5-27-13			Sb	SBa	DC, F/W, dusty, bubbles along minor axis
MRK 1	66	0.36	Sc	S	D-S, elongated east-west nucleus
MRK 3			S0	S0	F/W, bright linear center
MRK 176	51	0.45	Sa?	Sa	DI, nearly edge on, inner + outer rings
MRK 198			Sa/b	SB0/a	R?
MRK 266NE			Irr	Pec	DI, collision
MRK 270			E	S0	D-S, F/W
MRK 313			Irr	SB0/a	DI, B, collision?
MRK 348			S0	S0/a	double nuclei
MRK 403			SB0/a		B
MRK 533	95	0.28	S(B)c	Sbc	F/W, R(partial)
MRK 573			S0	SB0	F/W
MRK 577	54	0.25	S0	S0/a	
MRK 607			Sb	Sa	D-SW
MRK 612			SB0/a	SB0/a	DC, flocculent, compact nucleus
MRK 620	67	0.5	SBb	SBa	F/W, center not extended along bar
MRK 622			S0	S?	DI
MRK 686			Sb	S?	D-SW, inclined spiral
MRK 917			Sc	SBa	CL
MRK 937			SBa/b		B, DC
MRK 938			Sc	Pec	CL
MRK 955			S(B)b	S?	CL, Sersic/Pastoriza hot spot
MRK 993	29	0.31	Sb	Sa	D-SE, DC, highly-inclined
MRK 1058	108	0.41	Sb	S?	D-N, normal, inclined
MRK 1066			Sc	SB0	F/W, dusty
MRK 1073			Sc	SBb	F/W, Irregular
MRK 1157			Sb/c	SB0/a	R
MRK 1193			SBb		B, F/W
MRK 1210			Sa	S?	normal
MRK 1370	34	0.3	Sa		B(north-south)
NGC 424			Sb	S0/a	D-S
NGC 513			Sb/c	S?	normal
NGC 788	112	.1-.3	S0	S0/a	DI, F/W
NGC 1125			Sb/c	SB0/a	DC
NGC 1144			Irr	Ring B	DI, collision
NGC 1241			Sb/c	SBb	normal
NGC 1358			SB0	SB0/a	B, DI
NGC 1386			Sb/c	SB0	DC
NGC 1410			S0	E pec	F/W, collision: polar dust ring
NGC 1667			Sc	SBc	DI
NGC 2110			Sa	SB0	D-W
NGC 2992			?	Sa	DC
NGC 3081			SB0/a	SB0/a	DI
NGC 3362			Sb	SBc	F/W, hook-like protrusion from nucleus
NGC 3393			Sa	SBa	F/W, like MRK 573
NGC 3982			Sb/c	SBb	normal
NGC 4156	63	0.27	SBa/b	SBb	DI
NGC 4507			S(B)a/b	SBb	D-SE, B, twisted isophote
NGC 4922b	148	0.12	E		DI, dust splotches
NGC 4939			Sa	Sbc	F/W, D-W
NGC 4968			Sa	SB0/a	DI

TABLE 5—*Continued*

Galaxy	θ	ϵ	Morphology MGT	RC3	Comments*
NGC 5135			Sc	SBab	CL
NGC 5347			Sb	SBab	normal
NGC 5427			Sc	Sc	normal
NGC 5929			S0	Sab	DC
NGC 5953			Sc	Sa	flocculent
NGC 5995			S(B)c		normal
NGC 6211	40	0.32	E	SB0/a	shell
NGC 6217			Sc	SBbc	CL, DC
NGC 6221			Sd	SBc	CL, Irregular
NGC 6300			Sd	SBb	DI
NGC 6393			S(B)c	SBb	DC
NGC 7130			Sd	Sa	CL, DC
NGC 7172			?	Sa	DC
NGC 7212			Irr?	S?	F/W, DI
NGC 7319			Irr?	SBbc	F/W, DI, shells
NGC 7410			E/S0	SBa	DC
NGC 7582			?	SBab	DC, F/W, inclined dust disk
NGC 7590			Sd	Sbc	DC
NGC 7592			Irr	S0	CL, Irregular
NGC 7682			SB0	SBab	CL, F/W, early type
NGC 7743			S0	SBab	F/W, DI, early type
PKS 2048-572	81	0.68	E?	S0	DC, F/W(turbulent)
PKS 2158-380			Sa	SB0	D-N
Q 1234+0848			Irr	SBb	dwarf
UGC 3255			Sb/c	S?	DC
UGC 4332				Sa	DC
UGC 6100			Sb	Sa?	normal
UM 105			Sc?		DI
UM 319			Sc		CL, dusty
UM 625			S0		R(partial)
WAS 2			SB0		B
ZW 1408+137			?		DI, disturbed dust
ZW 1541+286			SBa		B, lens

*

DI = irregular dust
B = bar
CL = cluster, lumpy HII region, knots
DC = dust disk/dust lane passing close or through center (ie bisected nucleus)
D-[direction] = dust lanes on one side of major axis, where direction is N, S, E, W, NW, NE, SW, or SE
E/S0 = Elliptical
F/W = filaments/wisps
R = ring

TABLE 6

FIELD STARS IN PC2 IMAGES

Image Frame	Position	Estimated 606W Mag.†	Comment
MRK 915	NE	15.87	saturated
NGC 6300	NW	14.44	saturated
PKS 1718-649	NW	15.88	saturated
ESO 137-g34	W	14.53	saturated
MRK 1133	SW	18.04	unsaturated
ESO 323-g77	NE	18.73	unsaturated
ESO 325-g41	NE	18.17	unsaturated
IRAS 0457-756	SW	18.42	unsaturated
MRK 290	SE	18.45	unsaturated

†magnitudes are in STMAGs

TABLE 7. SS1, US1, & RS1 Statistics

Classification	Number	Median z	z adjusted number[a]	Median z
SS1	36 (40%)	0.018	30 (38%)	0.023
US1	21 (23%)	0.030	14 (18%)	0.024
RS1	34 (37%)	0.025	34 (44%)	0.025

[a]The adjusted numbers were arrived at after some of the SS1's and US1's were removed from the total list so that their median z values would be closer to the median z value of the RS1's

TABLE 8. Seyfert 1 and Seyfert 2 Statistics

	Median z	Total No.	No. of DC & DU	DC & DU %
Sy 1 (Full Sample)	0.024	91	21	23%
Sy 2 (Full Sample)	0.017	114	45	39%
Sy 1 (z<0.03)	0.019	65	18	28%
Sy 2 (z<0.03)	0.016	99	42	42%

FIGURE CAPTIONS

Figure 1 — These are images of galaxies that in NED were classified as Seyfert 1 - 1.9. The arrowhead points North and the bar is East. The length of the eastern bar is 2" in the PC images. Those galaxies that fell on the Wide field chip are designated with an asterisk. The length of the eastern bar in the WF images is 4". The scale is based on H_o=50 km s^{-1} Mpc^{-1} . Note the strong point source in the centers of these galaxies and the fact that the host galaxies are generally earlier in type.

Figure 2 — These are images of galaxies that in NED were classified as Seyfert 2's. The arrowhead points North and the bar is East. The length of the eastern bar is 2" in the PC images. Those galaxies that fell on the Wide field chip are designated with an asterisk. The length of the eastern bar in the WF images is 4". The scale is based on H_o=50 km s^{-1} Mpc^{-1} . Note that the host galaxies appear to be later in type and that some of their dust is in a non-spiral pattern.

Figure 3 — These are images of the galaxies that in NED were classified as HII region galaxies. The arrowhead points North and the bar is East. The length of the eastern bar is 2" in the PC images. Those galaxies that fell on the Wide field chip are designated with an asterisk. The length of the eastern bar in the WF images is 4". The scale is based on H_o=50 km s^{-1} Mpc^{-1} . NGC's 625, 3738, 4700, 5253 were too large so they have been reproduced more extensively. Note that although most of the galaxies are very complex, they do not show any emission filaments or wisps.

Figure 4 — These are plots of redshift vs. inner and outer magnitude. The upper plot is for the magnitudes with a radius of 0".09 and the lower plot is for the magnitudes with a radius of 0".46. The filled symbols are from our derived magnitudes of the saturated centers.

Figure 5 — These are examples of matching the brightness profile of a point source to the central brightness profile of a galaxy. The cross symbols represent the profile of the galaxy and the star symbols represent the profile of the star. The profile of the star is multiplicatively scaled to match the profile of the galaxy at the 3-5 pixel range.

Figure 6 — These are radial profiles of a sample of stars, filled symbols, and our 5 quasar-like Sy 1's (open symbols). Note the similarity of the two profiles and how the differences between the Sy 1's is no more than the differences between the different stars.

Figure 7 — These are histograms of the Hubble classes for the full sample of Sy 1 and Sy 2 galaxies. The black part of the histograms represent the number of barred galaxies in each class. Note the higher proportion of Sy 1's in Sa's relative to Sc 's.

Figure 8 — These are histograms of the Hubble classes for the $12\mu m$ sample of Sy 1 and Sy 2 galaxies. The black part of the histograms represent the number of barred galaxies in each class. Note that in this different subsample that a higher proportion of Sy 1's in Sa's relative to Sc 's.

Figure 9 — Two schematic representations of competing schemes for unifying Sy 1's and Sy 2's. The Accreting Torus Model (ATM) requires a geometrically thick dusty torus to block out most of the light from the central Sy 1 engine, while the Galactic Dust Model (GDM) depends on dust obscuration present in the inner regions of the host galaxy. In the GDM model the Narrow Line Region (NLR) has two energizing mechanisms. The accretion disk provides a more distributed

energy output, while jets from the central black hole would provide energy for " ionization cones." Due to space limitations, the counter jet/cones have not been included in the schematic. In the ATM, Sy 1's are viewed closer to pole-on, while Sy 2's are viewed closer to edge-on. In the GDM this generalization does not hold.

Sy 1

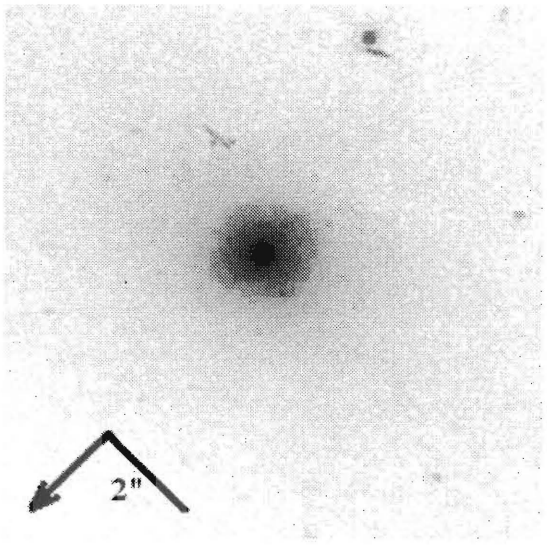

ESO 215-G14 (551 pc/")

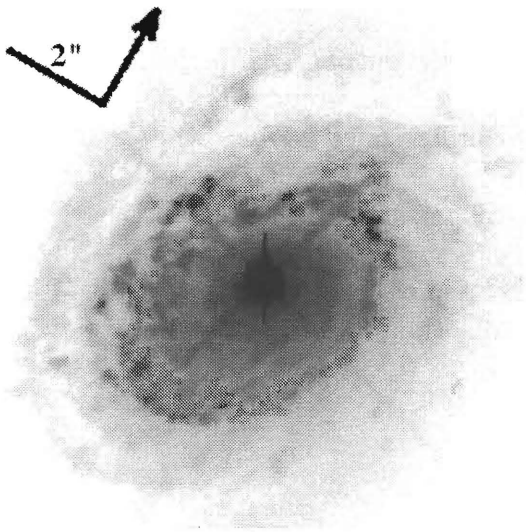

ESO 323-G77 (435 pc/")

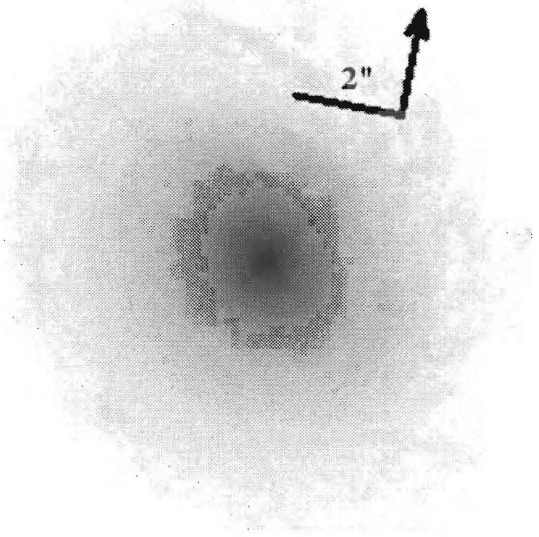

ESO 354-G4 (958 pc/")

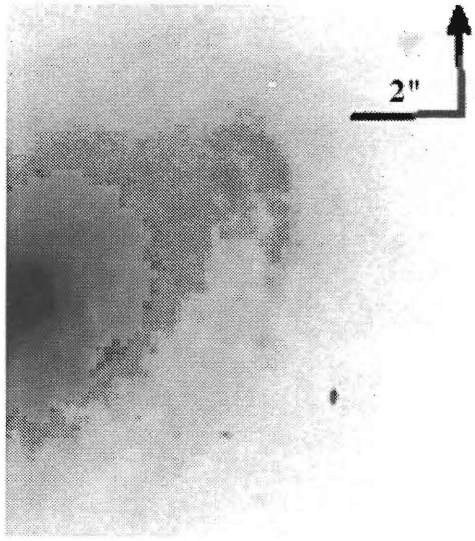

ESO 362-G18 (377 pc/")

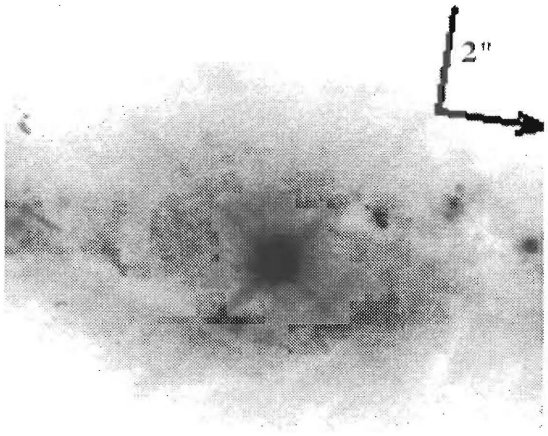

ESO 438-G9 (696 pc/")

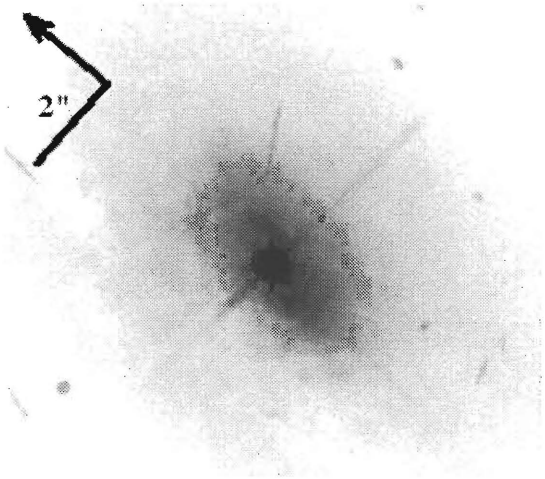

F 51 (406 pc/")

Sy 1

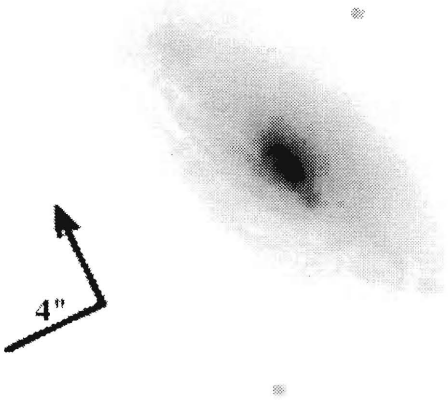

F 1146* (929 pc/")

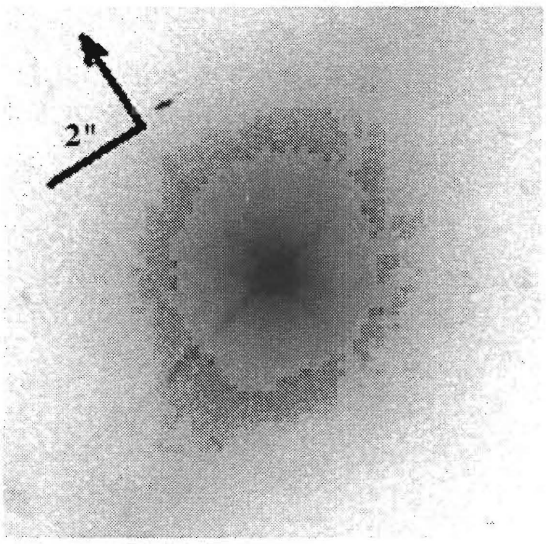

HEAO 1-0307-730 (813 pc/")

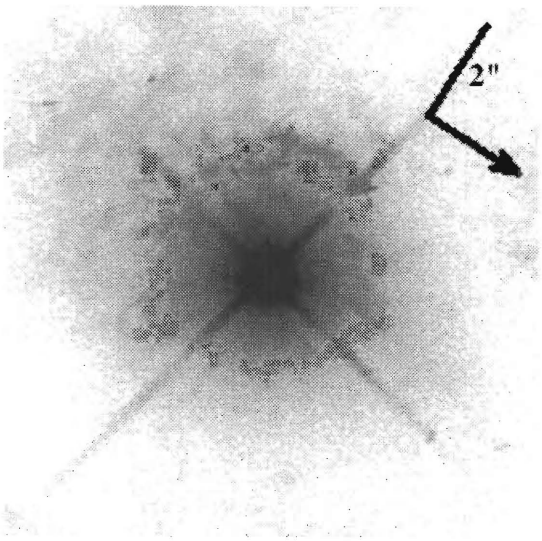

HEAO 1143-181 (958 pc/")

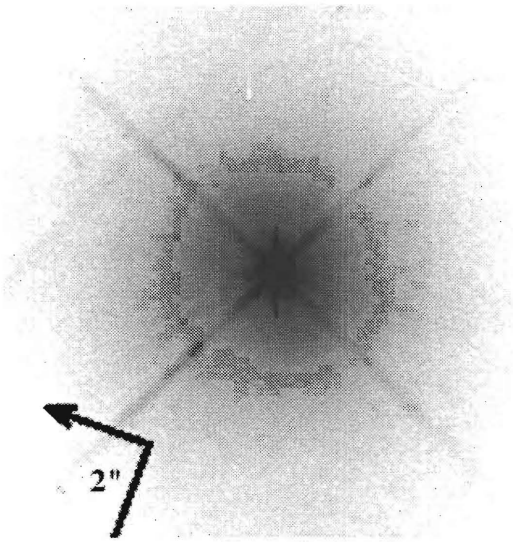

HEAO 2106-098 (784 pc/")

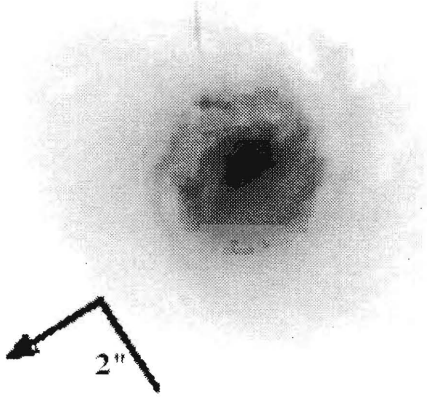

IC 1816 (493 pc/")

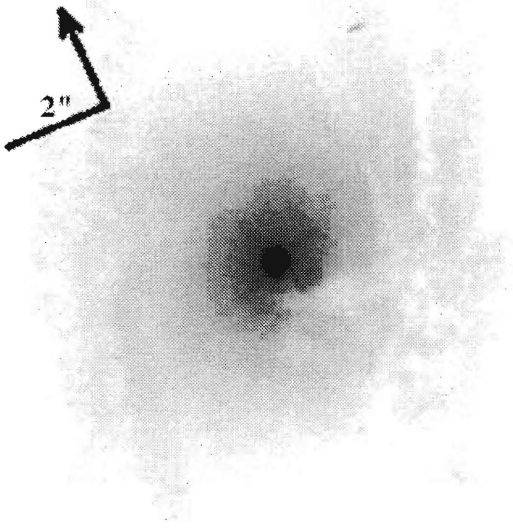

IC 4218 (551 pc/")

Sy 1

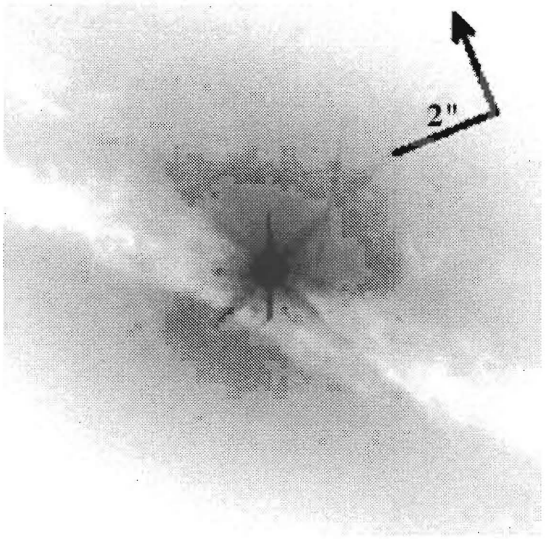

IC 4329a (464 pc/")

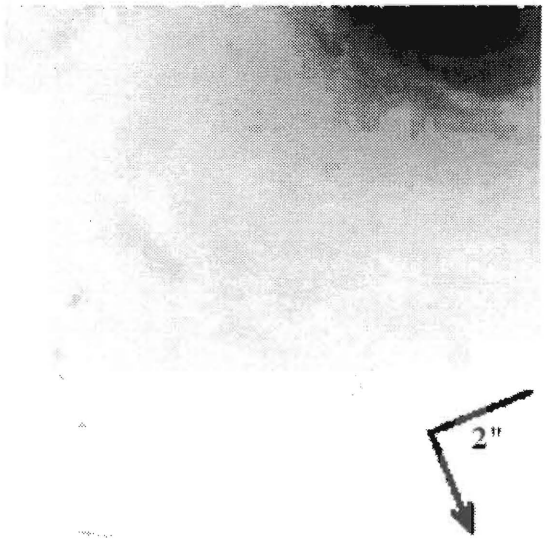

IR 1319-164 (493 pc/")

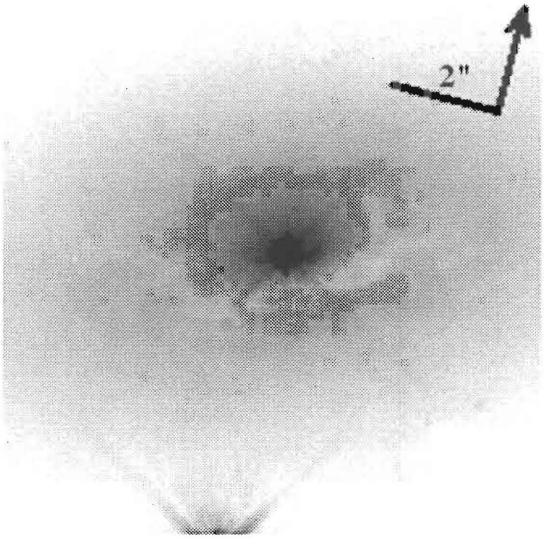

IR 1333-340 (232 pc/")

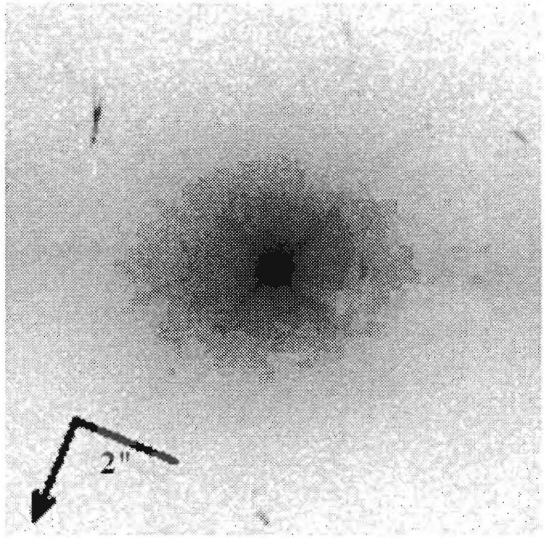

MCG 6-26-12 (929 pc/")

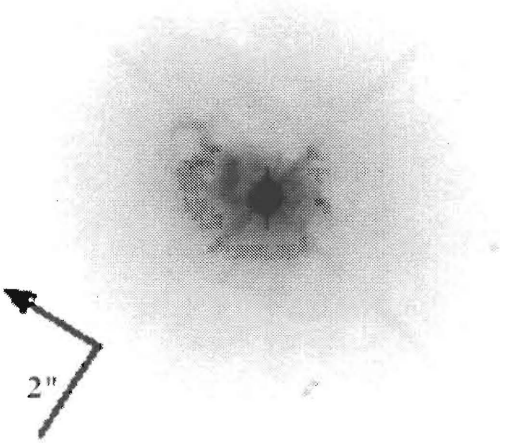

MCG 8-11-11 (580 pc/")

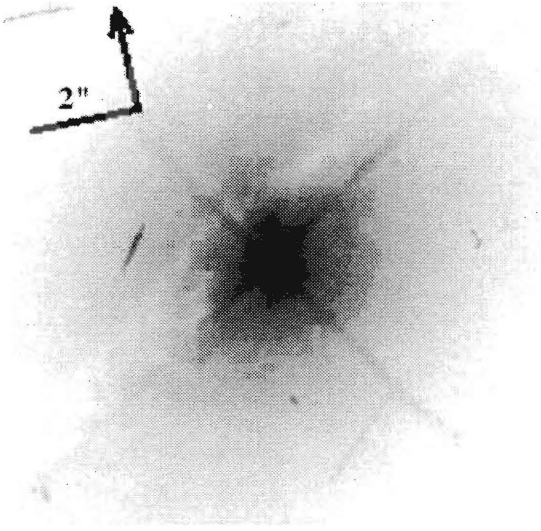

MRK 6 (551 pc/")

Sy 1

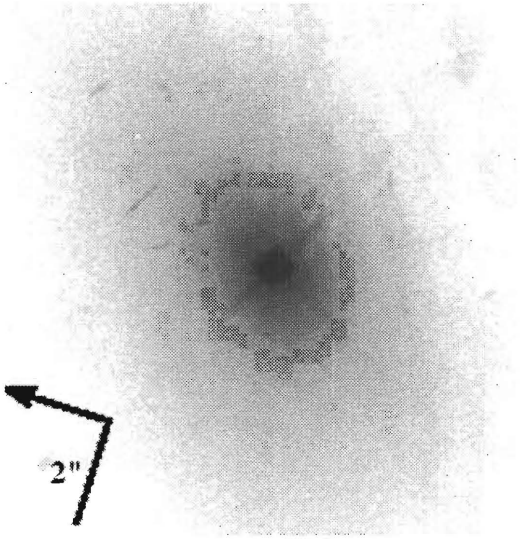

MRK 10 (871 pc/")

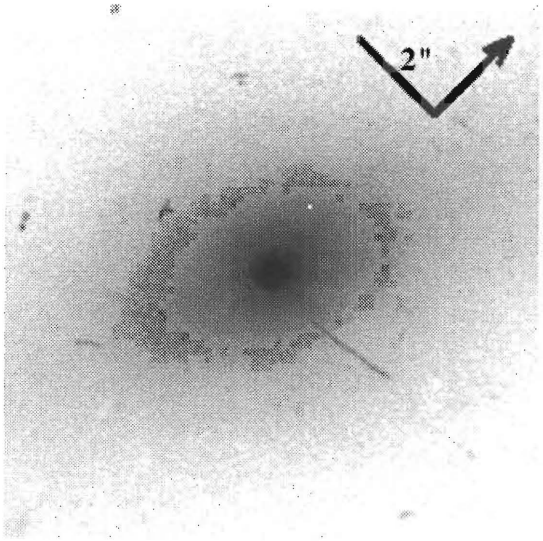

MRK 40 (580 pc/")

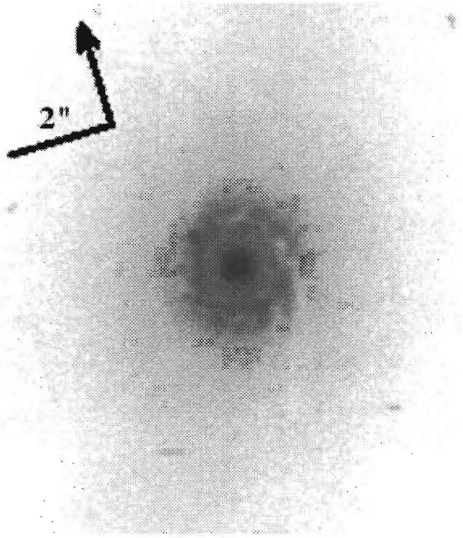

MRK 42 (696 pc/")

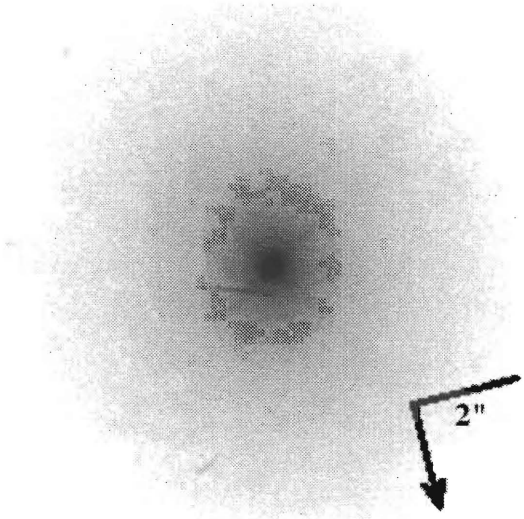

MRK 50 (667 pc/")

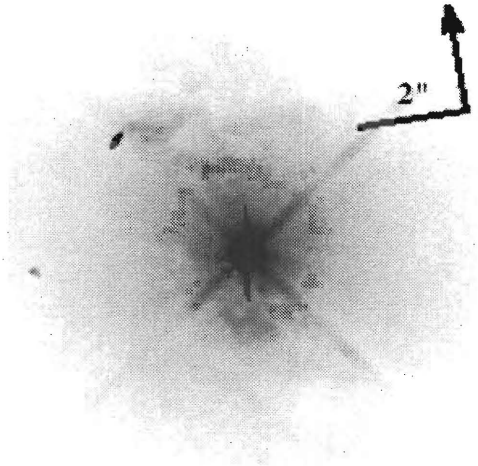

MRK 79 (638 pc/")

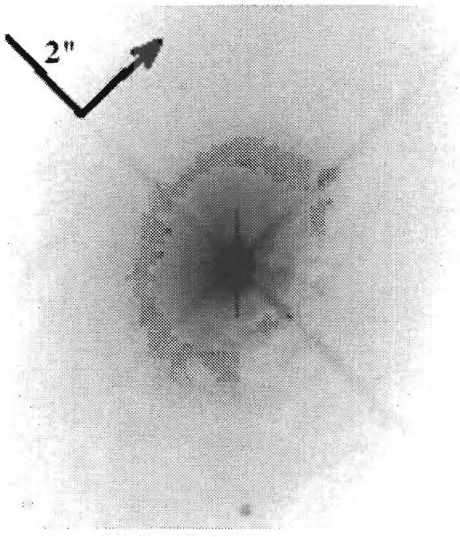

MRK 279 (900 pc/")

Sy 1

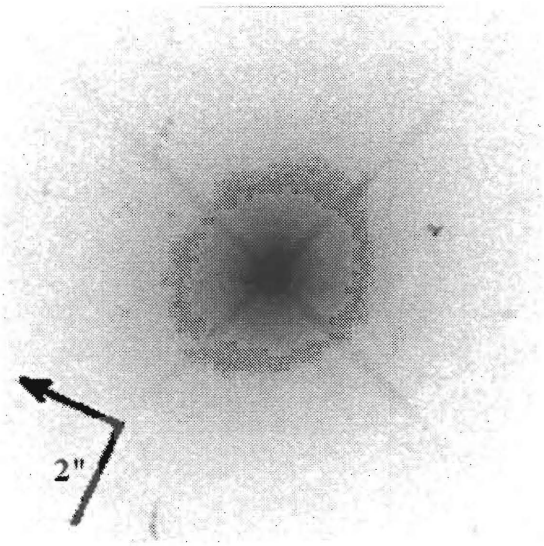

MRK 290 (842 pc/")

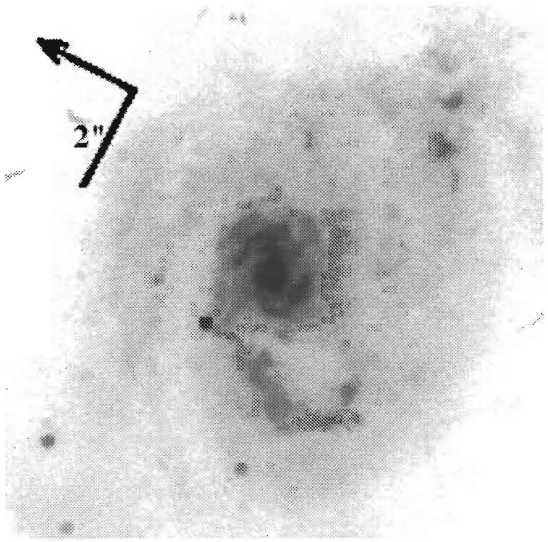

MRK 334 (638 pc/")

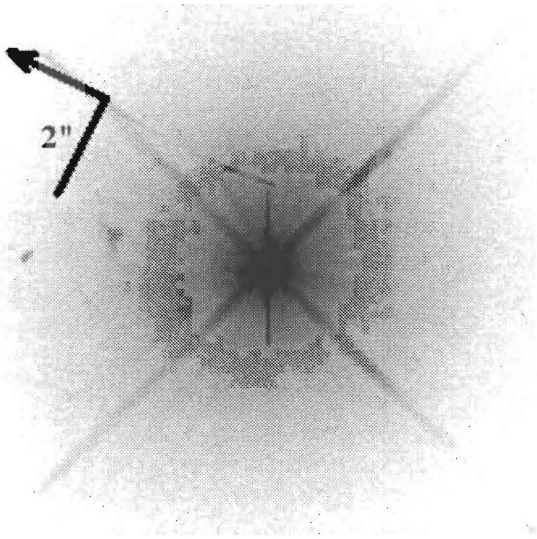

MRK 335 (638 pc/")

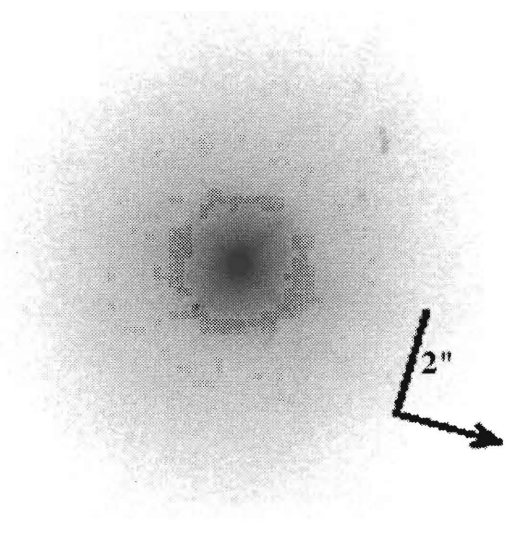

MRK 352 (435 pc/")

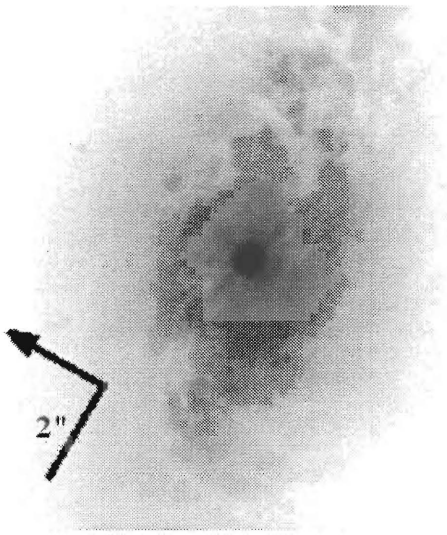

MRK 359 (493 pc/")

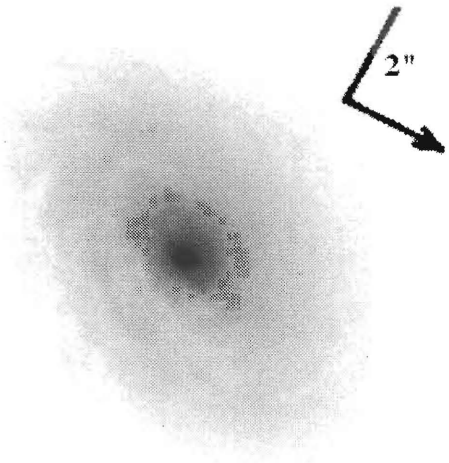

MRK 372 (900 pc/")

Sy 1

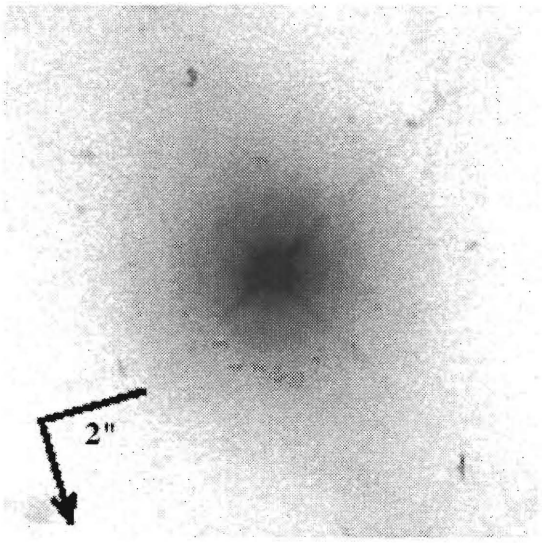

MRK 382 (987 pc/")

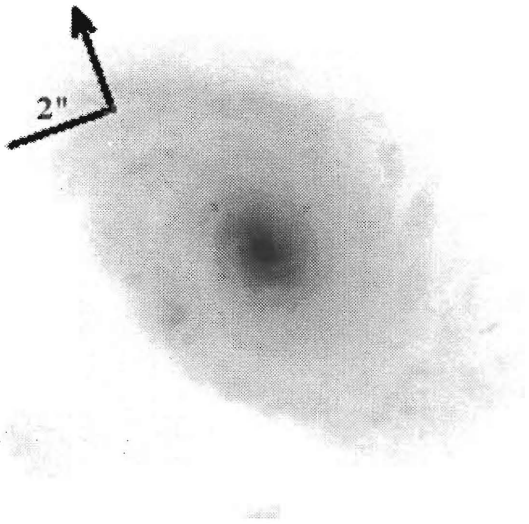

MRK 423 (929 pc/")

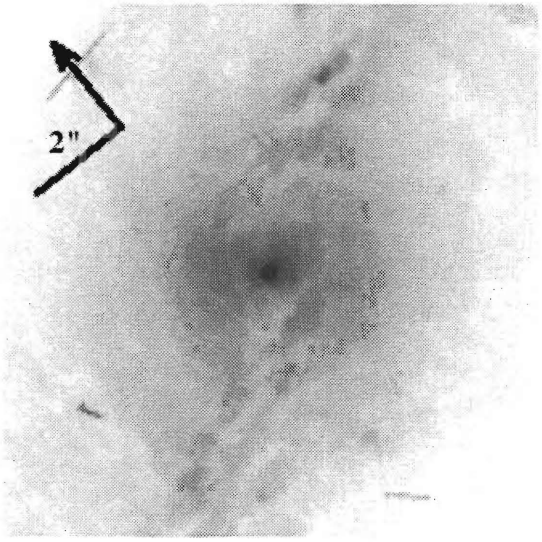

MRK 471 (987 pc/")

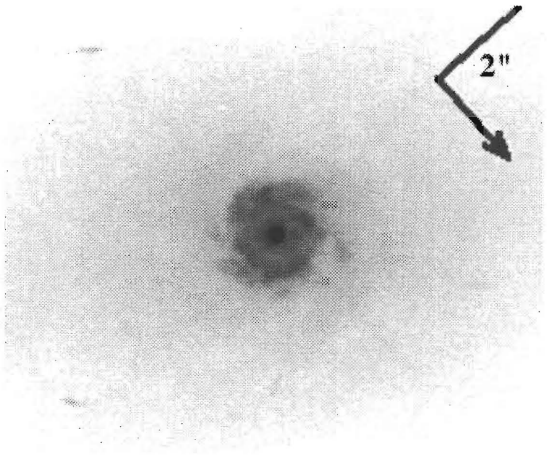

MRK 493 (900 pc/")

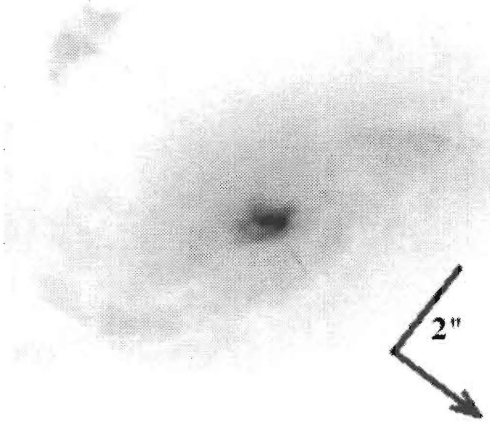

MRK 516 (813 pc/")

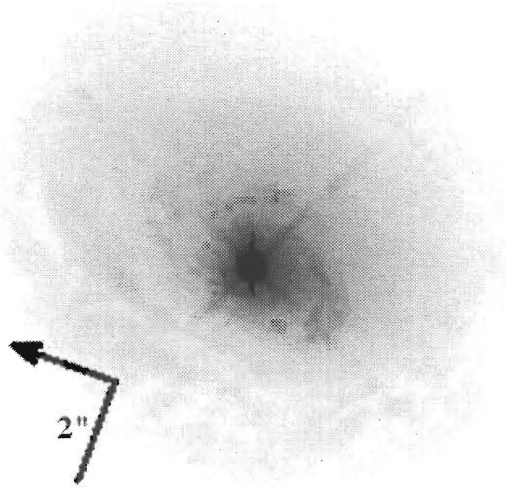

MRK 530 (842 pc/")

Sy 1

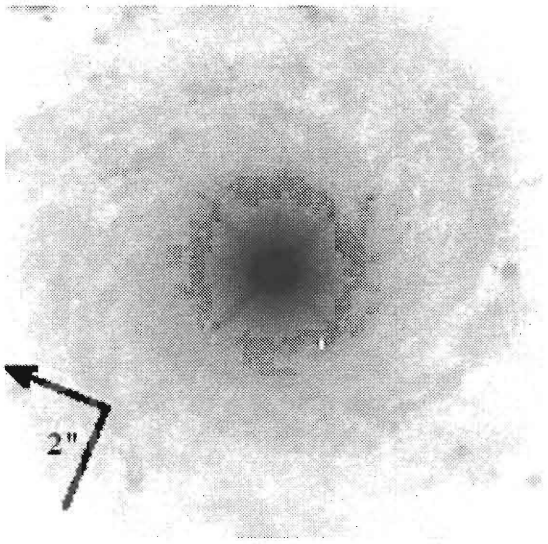

MRK 543 (755 pc/")

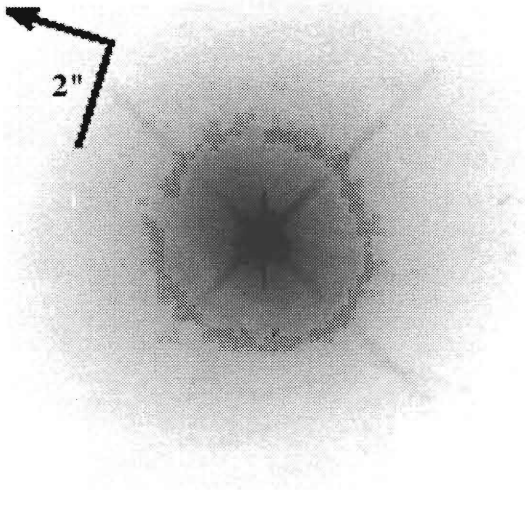

MRK 590 (784 pc/")

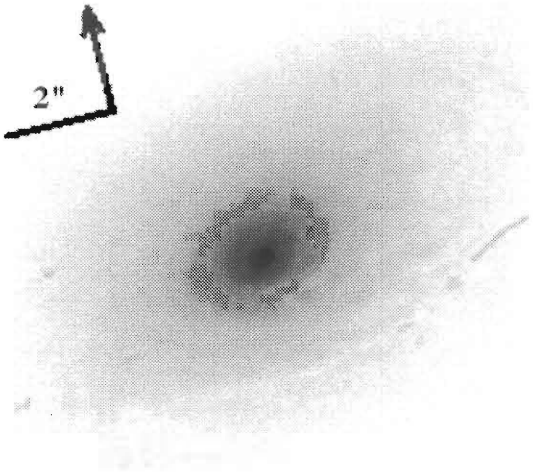

MRK 595 (813 pc/")

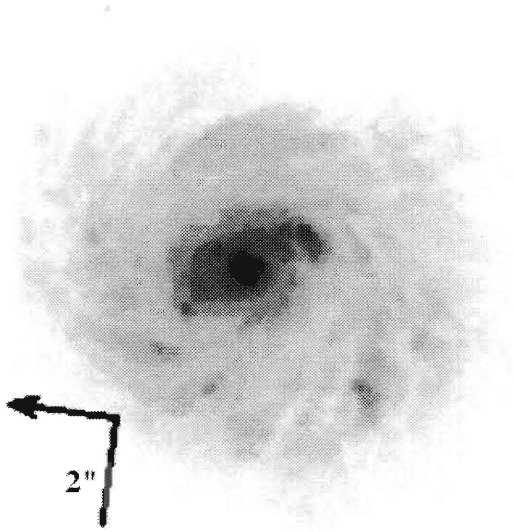

MRK 609 (929 pc/")

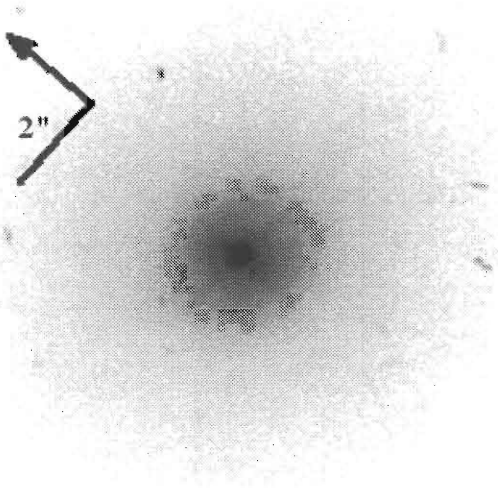

MRK 699 (987 pc/")

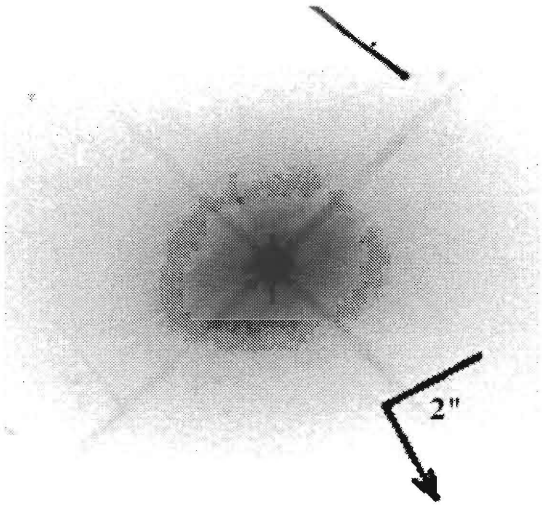

MRK 704 (842 pc/")

Sy 1

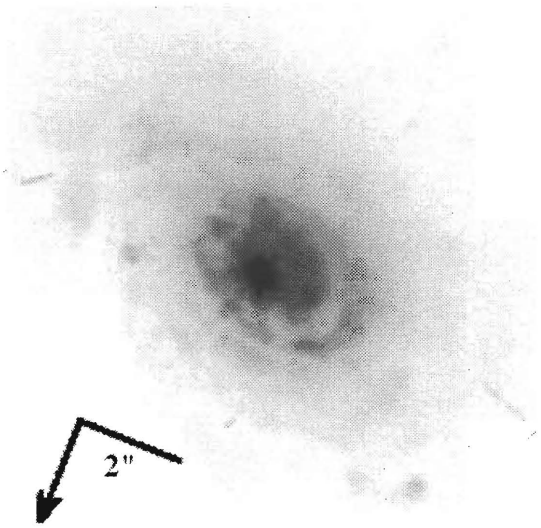

MRK 744 (290 pc/")

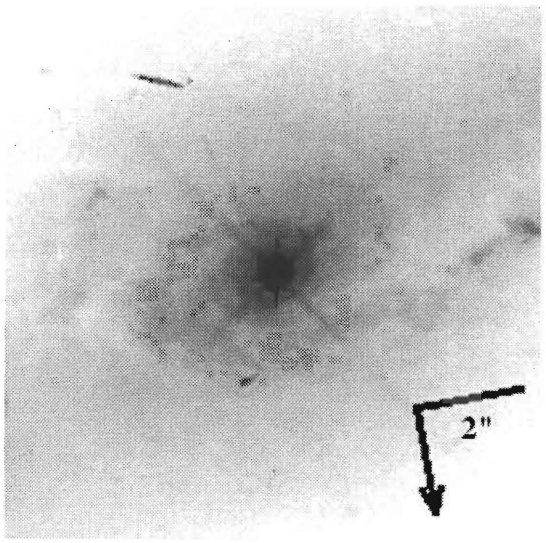

MRK 766 (348 pc/")

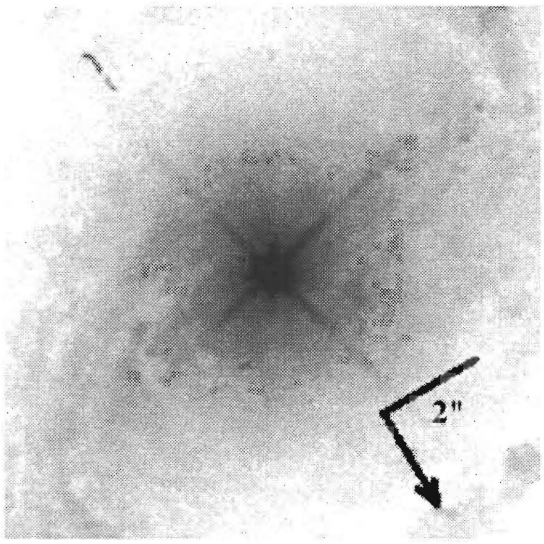

MRK 817 (958 pc/")

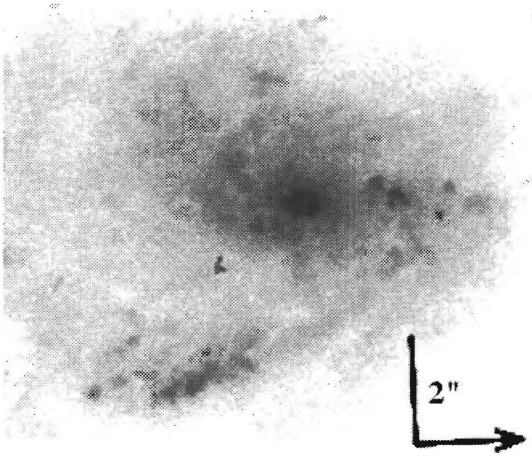

MRK 833 (1132 pc/")

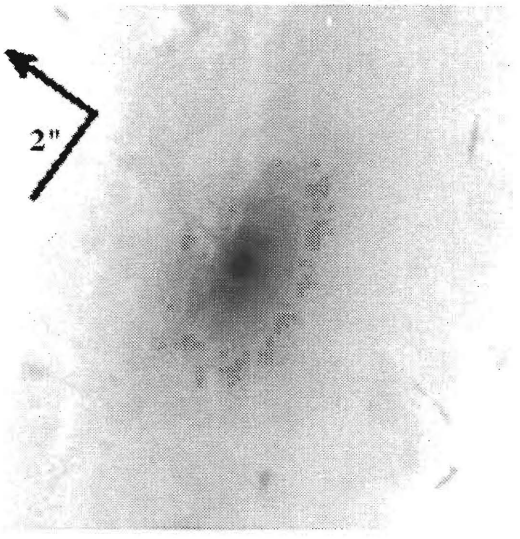

MRK 871 (987 pc/")

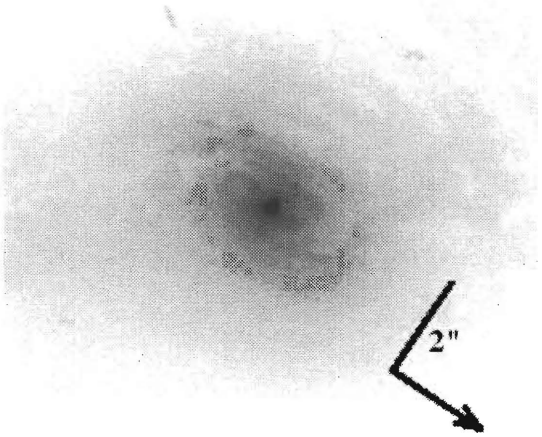

MRK 885 (755 pc/")

Sy 1

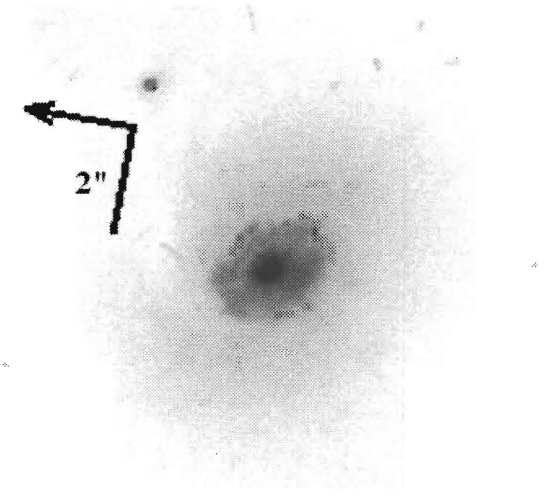

MRK 896 (784 pc/")

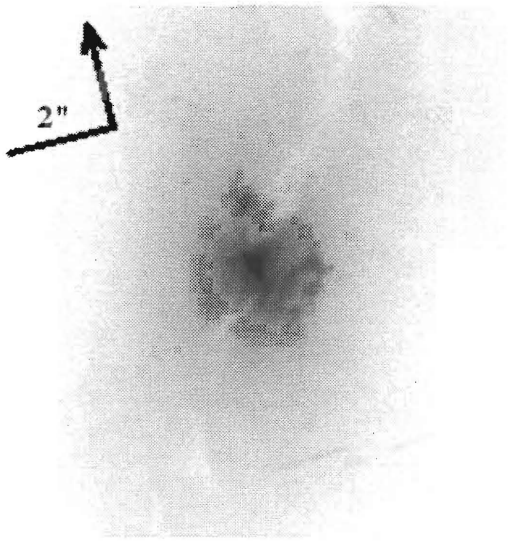

MRK 915 (726 pc/")

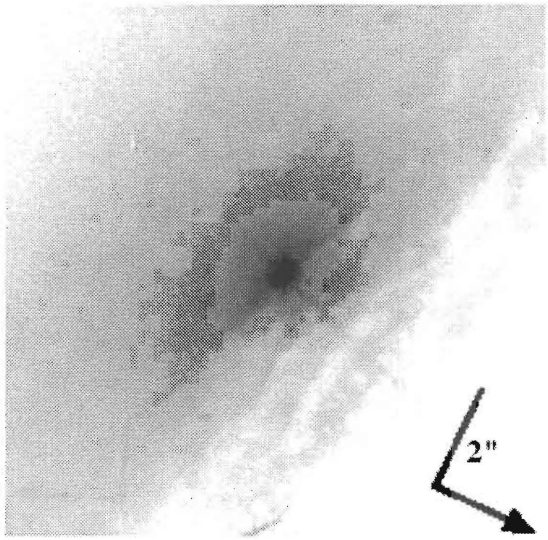

MRK 1040 (464 pc/")

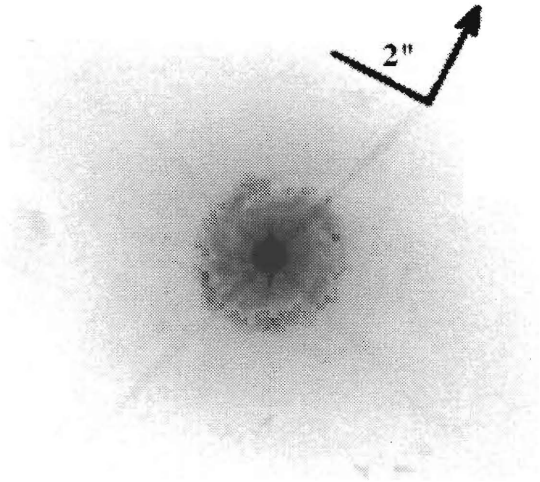

MRK 1044 (464 pc/")

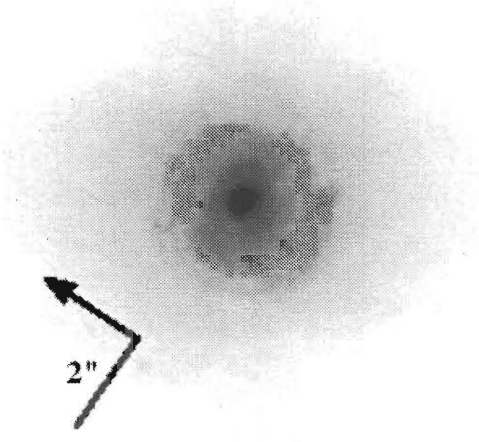

MRK 1126 (290 pc/")

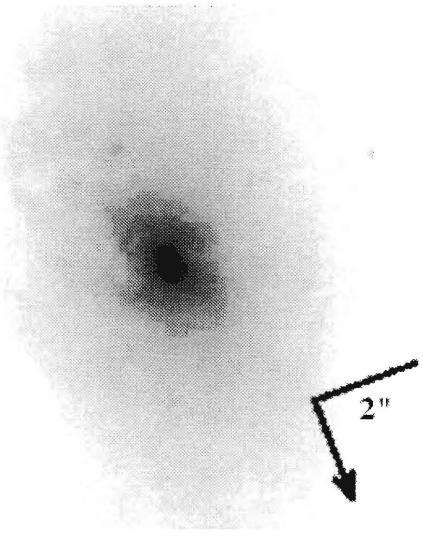

MRK 1218 (813 pc/")

Sy 1

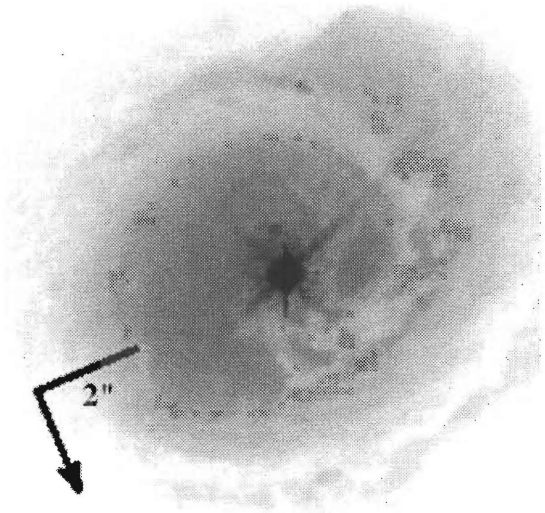

MRK 1330 (261 pc/")

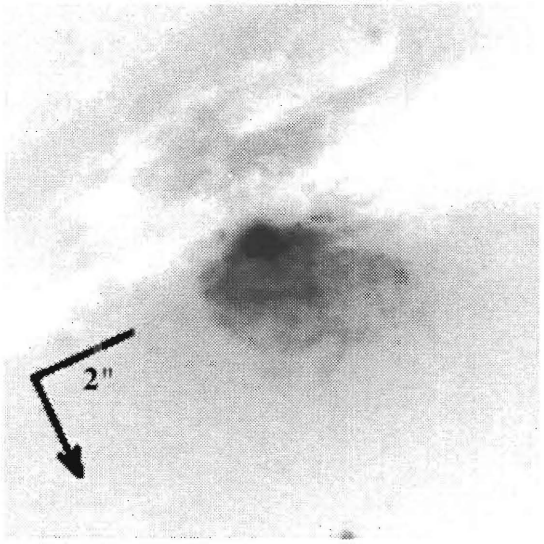

MRK 1376 (203 pc/")

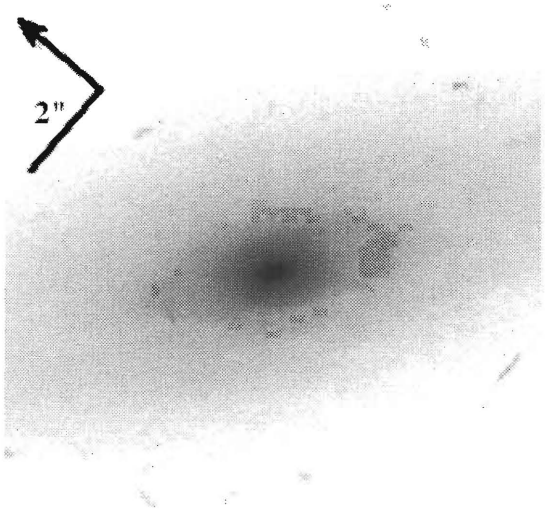

MRK 1400 (842 pc/")

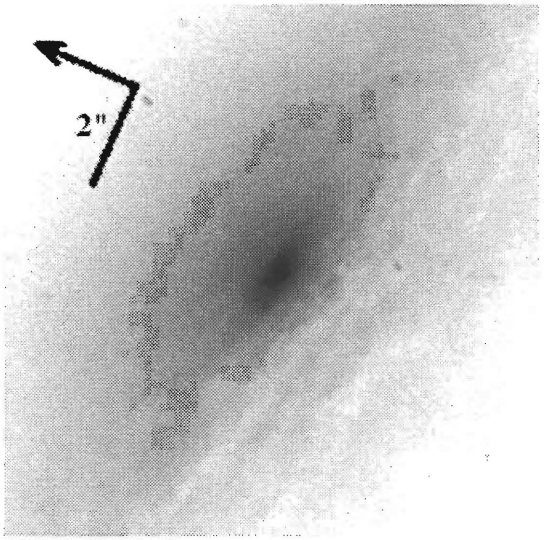

MRK 1469 (900 pc/")

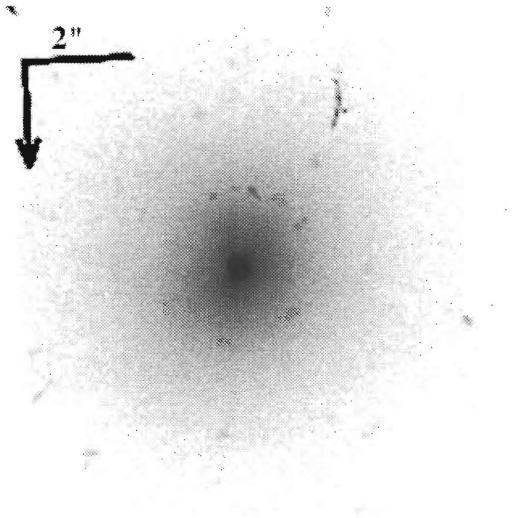

MS 1110+2210 (871 pc/")

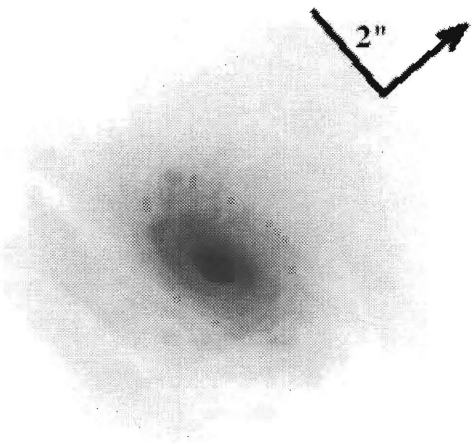

NGC 235 (638 pc/")

Sy 1

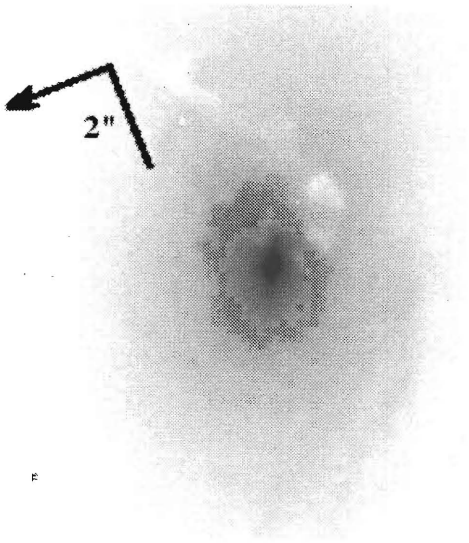

NGC 526a (522 pc/")

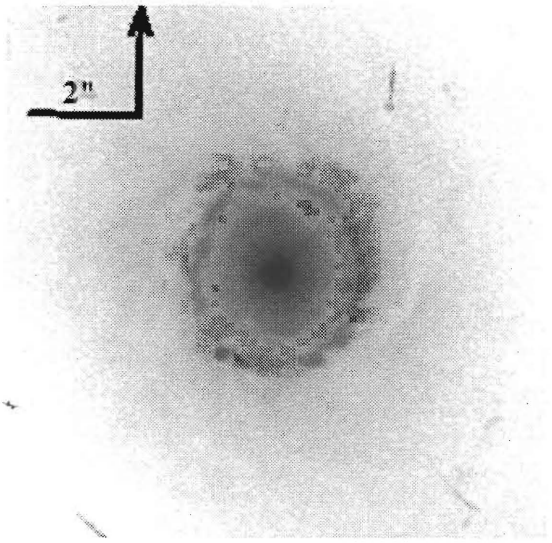

NGC 1019 (696 pc/")

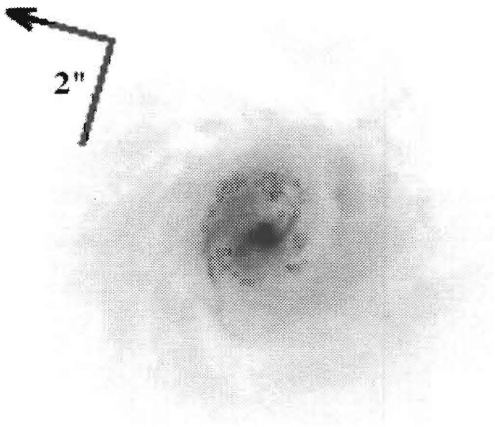

NGC 1566 (116 pc/")

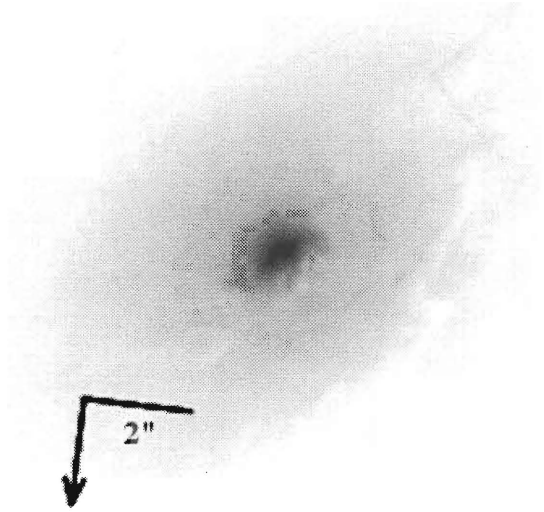

NGC 2639 (319 pc/")

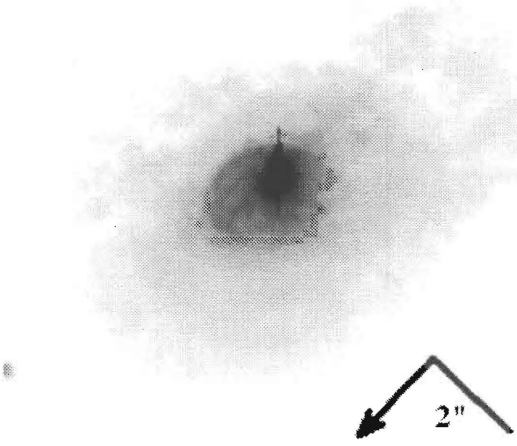

NGC 3227 (87 pc/")

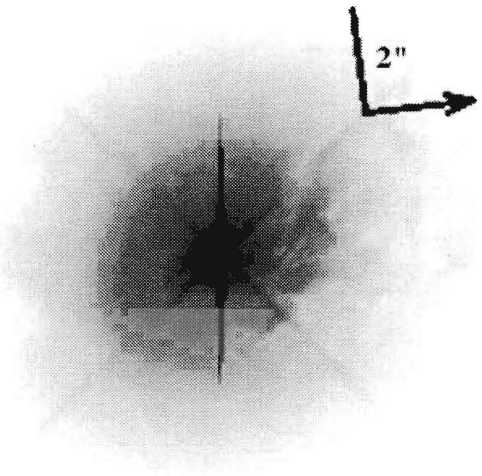

NGC 3516 (261 pc/")

Sy 1

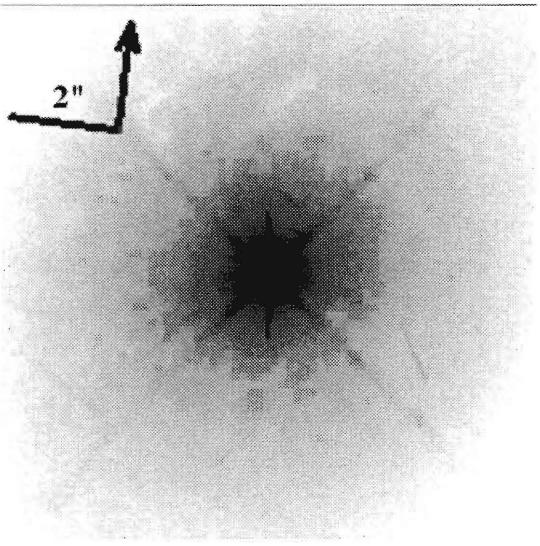

NGC 3783 (261 pc/")

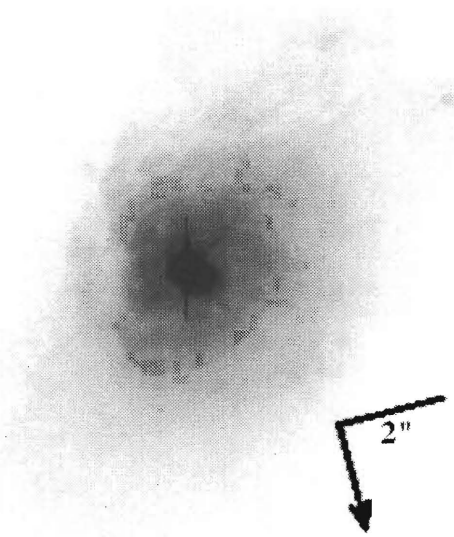

NGC 4051 (203 pc/")

NGC 4235 (203 pc/")

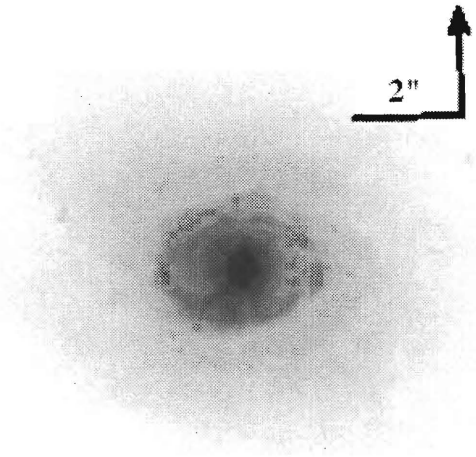

NGC 4748 (406 pc/")

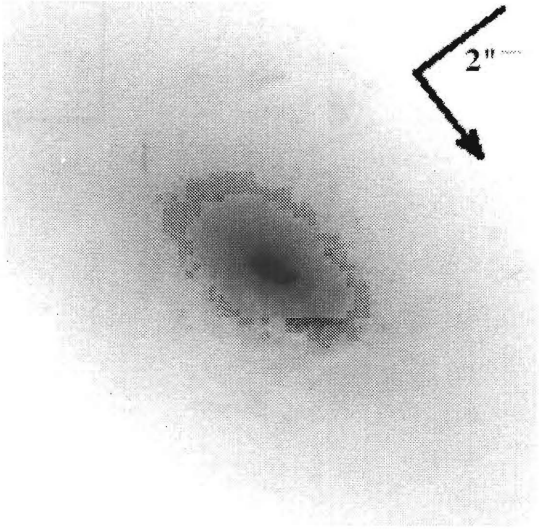

NGC 5252 (638 pc/")

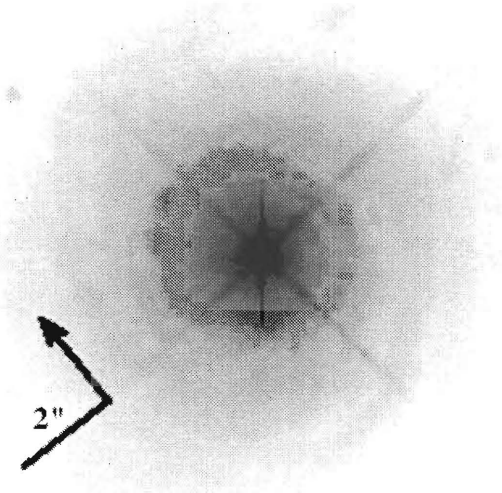

NGC 5548 (493 pc/")

Sy 1

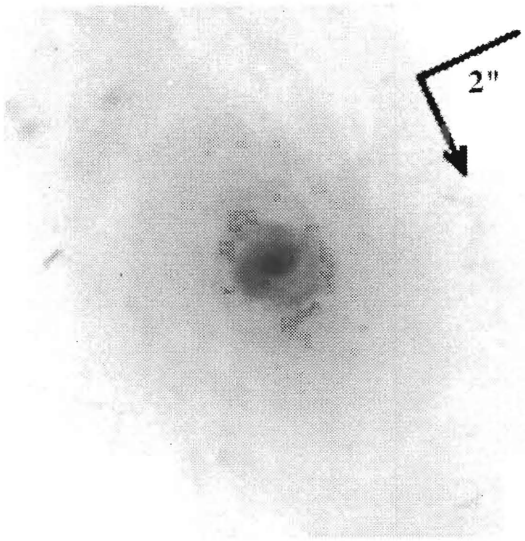

NGC 5674 (726 pc/")

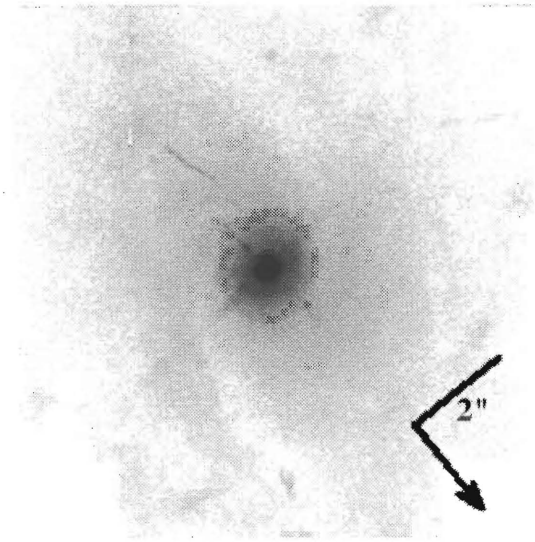

NGC 5940 (958 pc/")

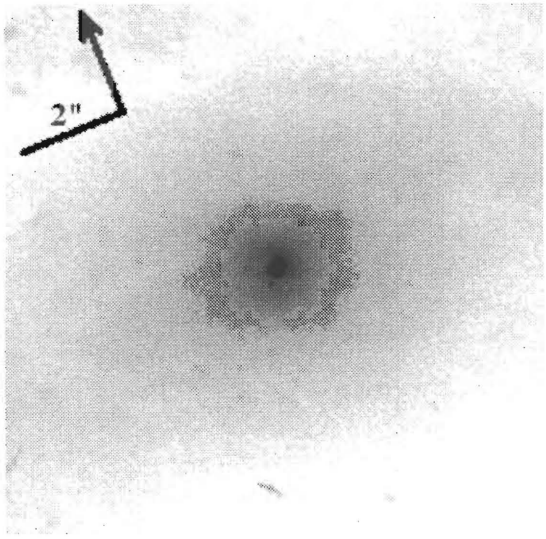

NGC 6104 (813 pc/")

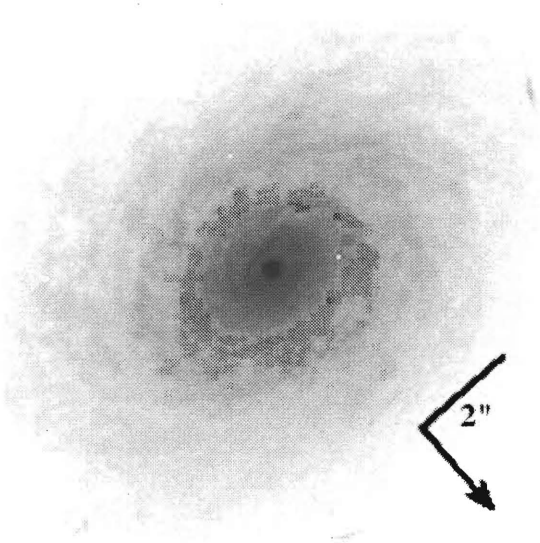

NGC 6212 (871 pc/")

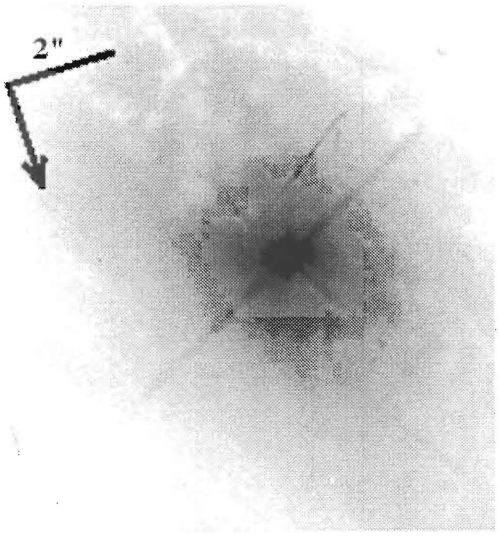

NGC 6860 (435 pc/")

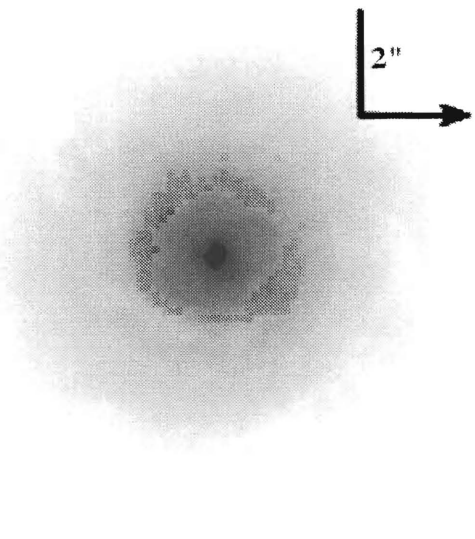

NGC 7213 (174 pc/")

Sy 1

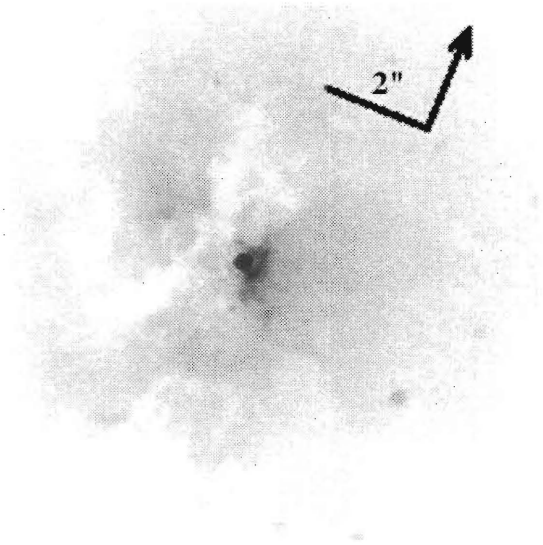

NGC 7314 (174 pc/")

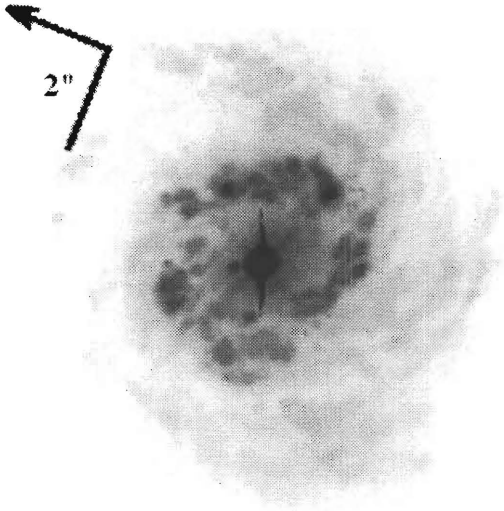

NGC 7469 (493 pc/")

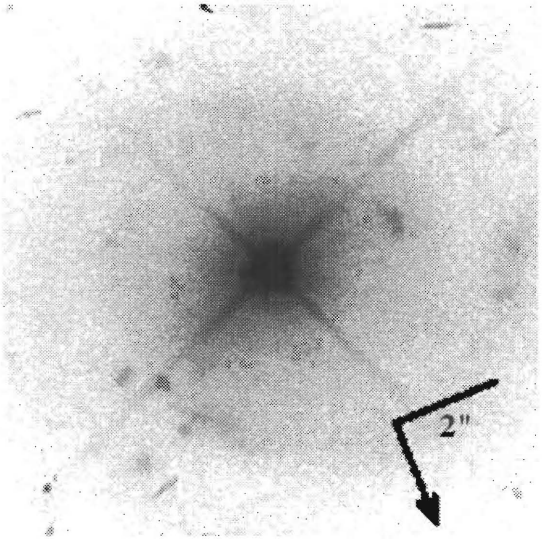

PG 1310-108 (987 pc/")

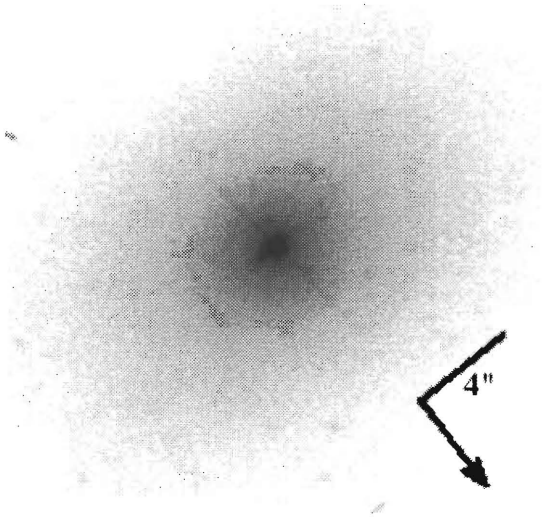

PKS 0518-458* (987 pc/")

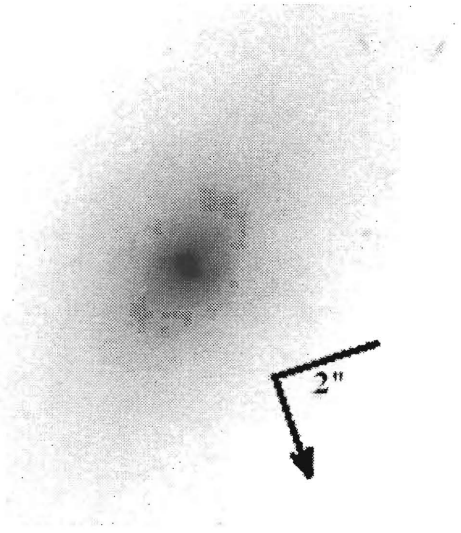

TOL 1059+105 (987 pc/")

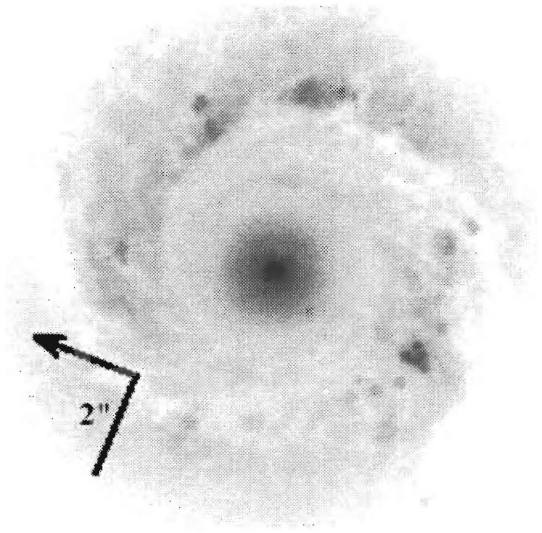

TOL 2327-027 (958 pc/")

Sy 1

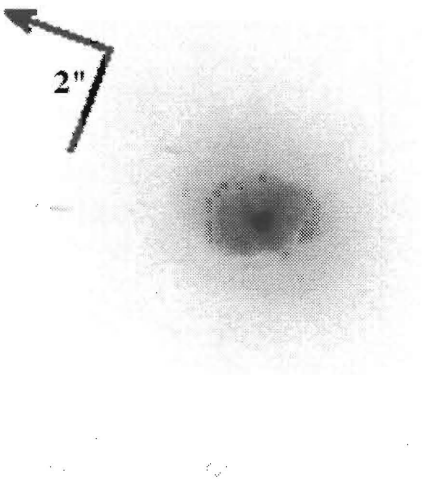

UGC 1395 (493 pc/")

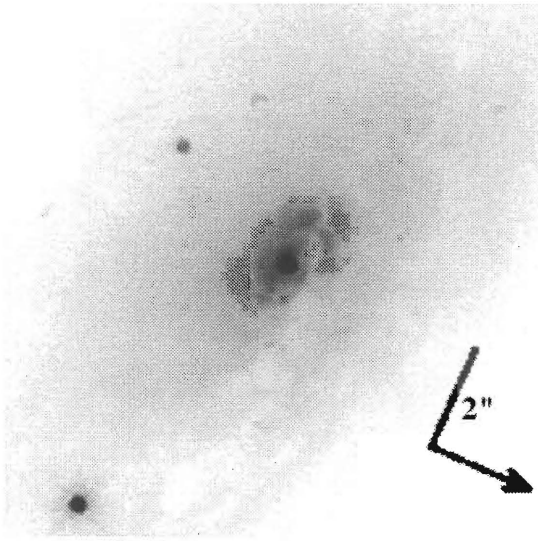

UGC 3223 (522 pc/")

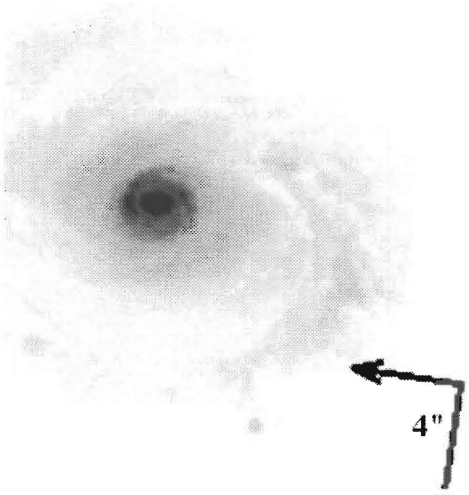

UGC 7064* (696 pc/")

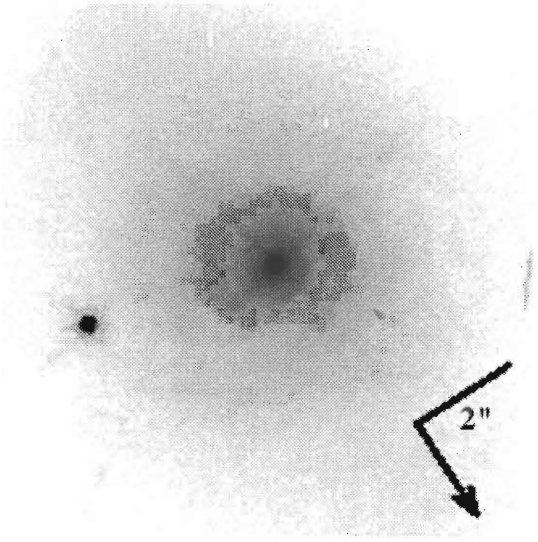

UGC 10683b (900 pc/")

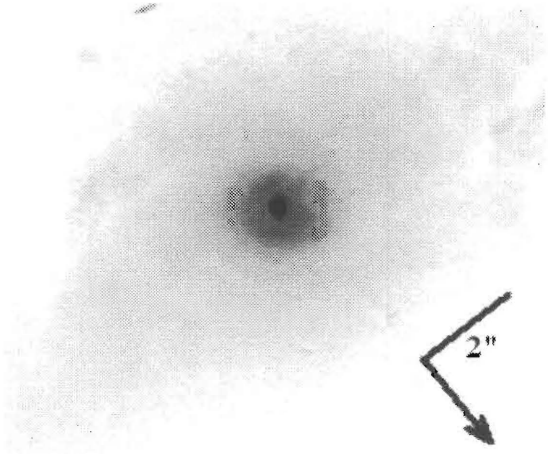

UGC 12138 (726 pc/")

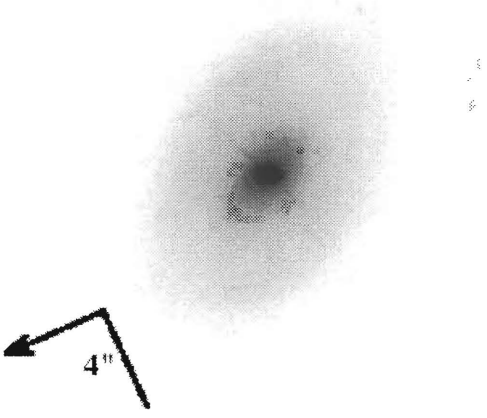

UM 614* (958 pc/")

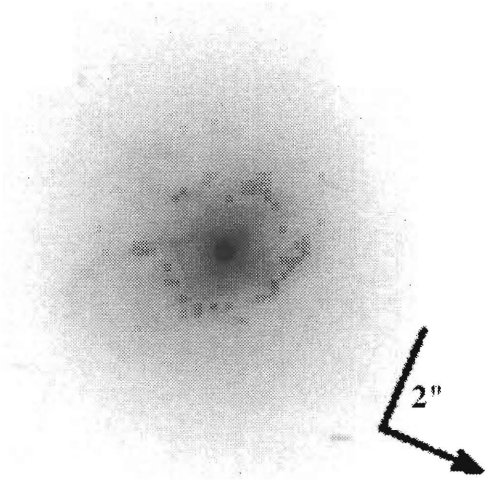

X 0459+034 (464 pc/")

Sy 2

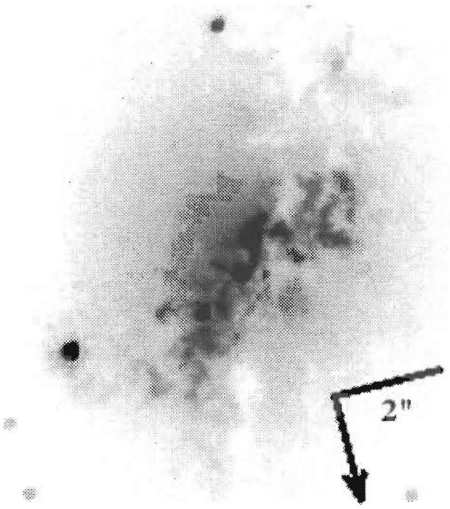

ESO 137-G34 (261 pc/")

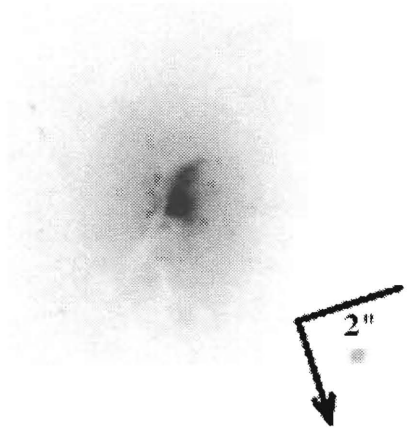

ESO 138-G1 (261 pc/")

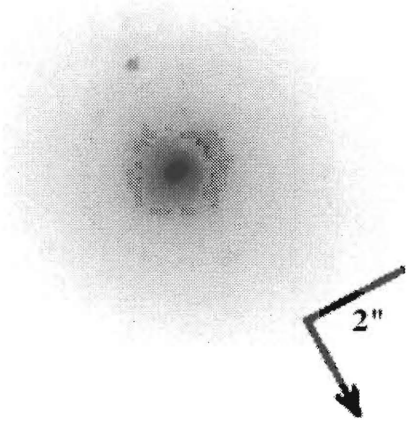

ESO 139-G12 (493 pc/")

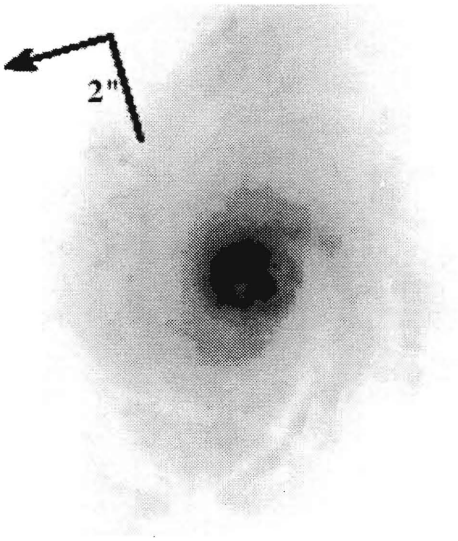

ESO 353-G9 (493 pc/")

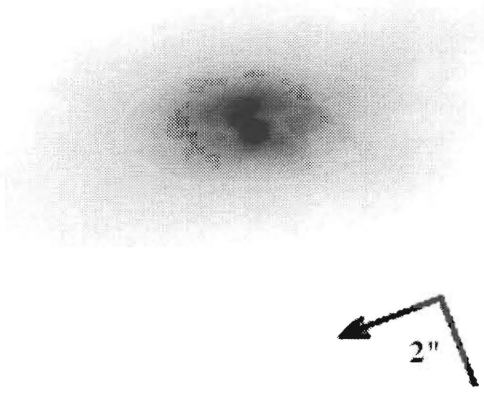

ESO 362-G8 (464 pc/")

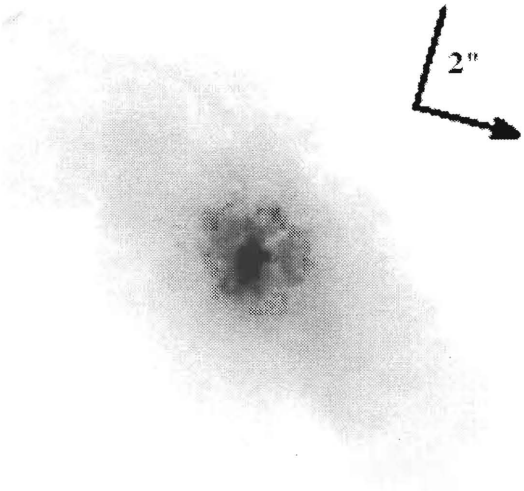

ESO 373-G29 (261 pc/")

Sy 2

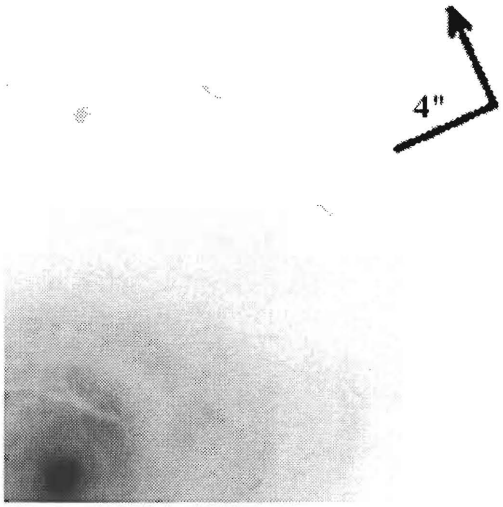

ESO 509-G66* (987 pc/")

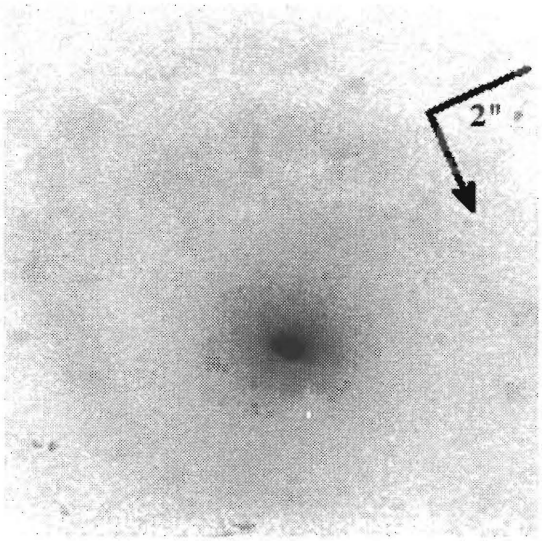

ESO 509-G66-comp (987 pc/")

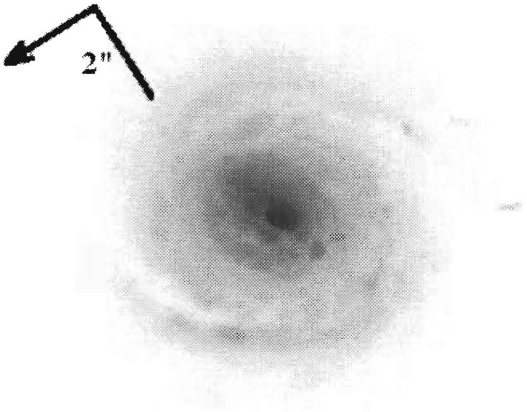

F 294 (493 pc/")

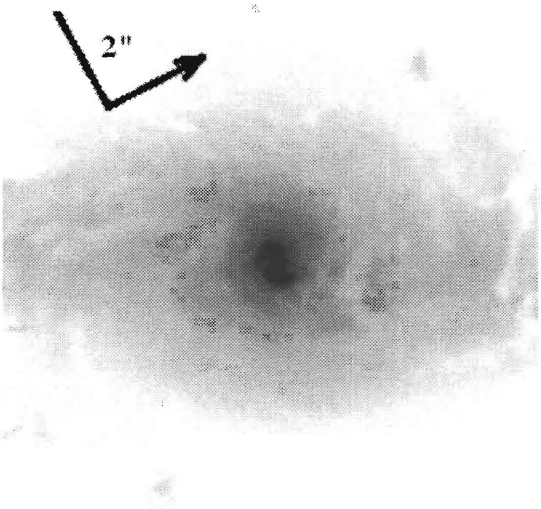

F 312 (319 pc/")

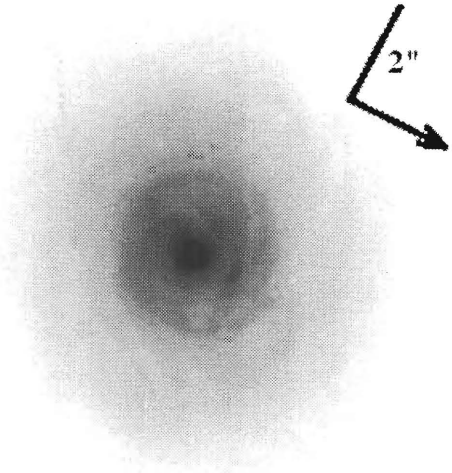

F 315 (464 pc/")

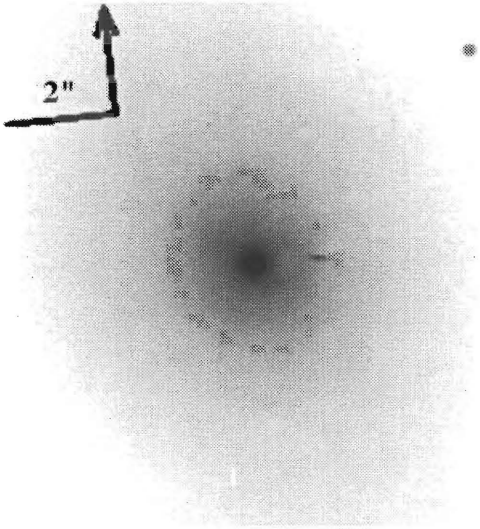

F 316 (464 pc/")

Sy 2

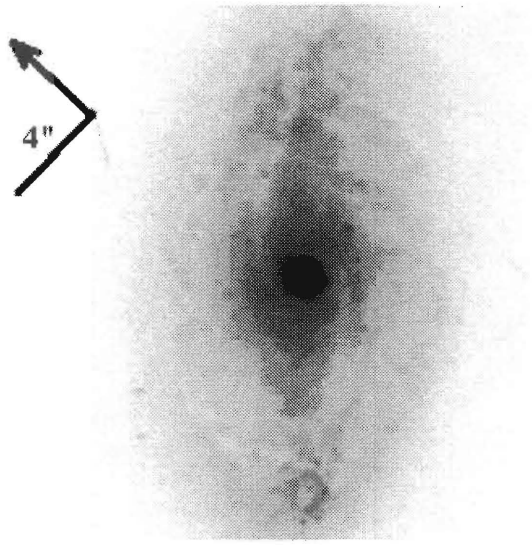

F 334* (522 pc/")

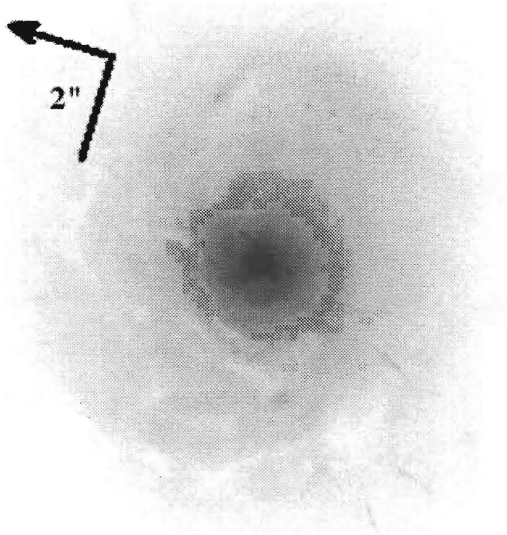

F 341 (464 pc/")

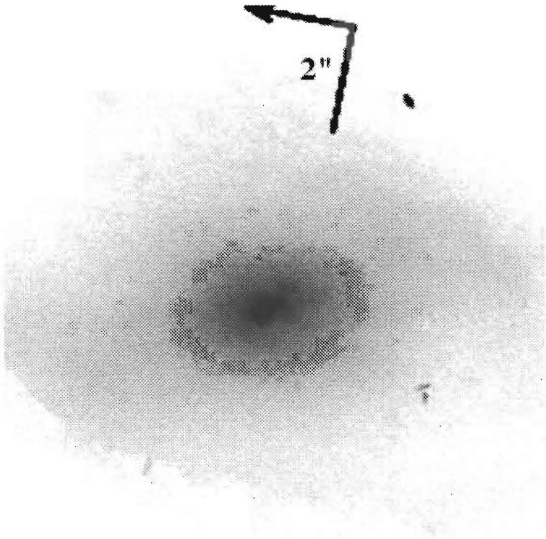

IC 184 (522 pc/")

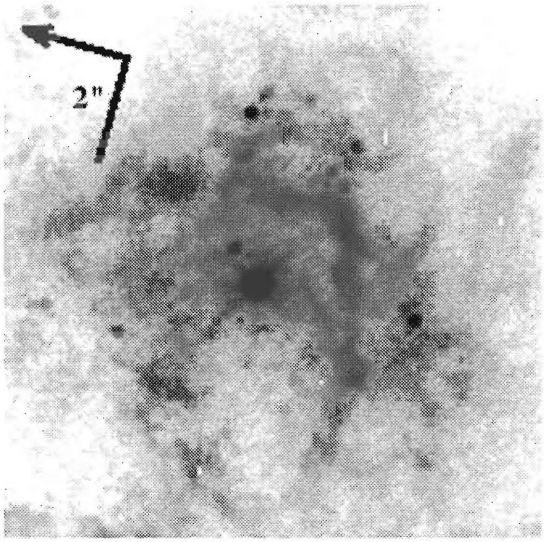

IC 4870 (87 pc/")

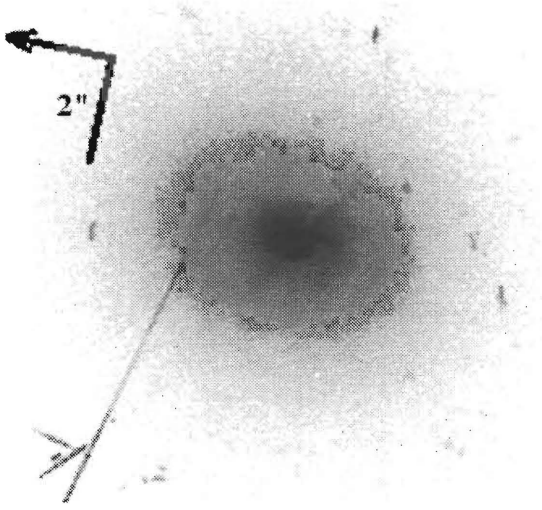

IR 0147-074 (493 pc/")

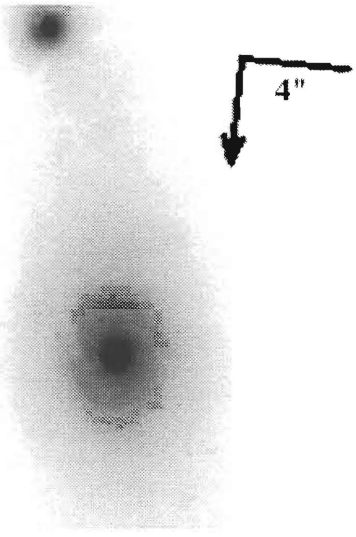

IR 0258-1136* (870 pc/")

Sy 2

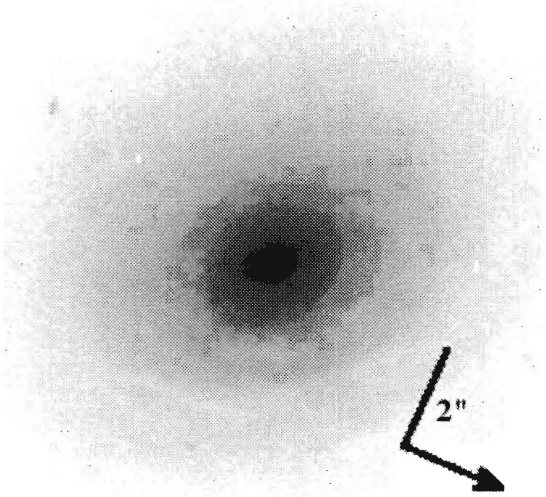

IR 0450+039 (873 pc/")

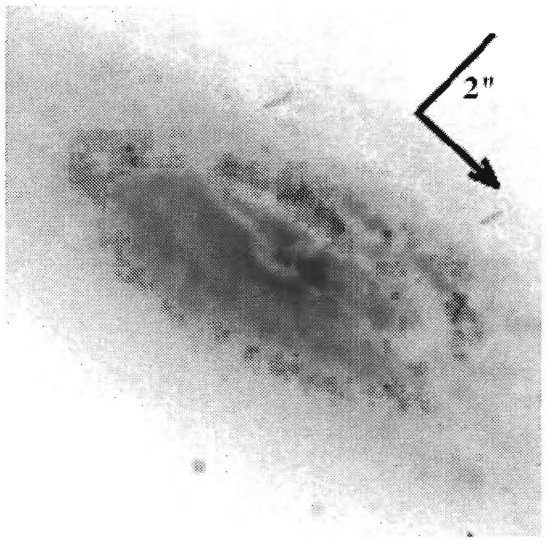

IR 0450-032 (464 pc/")

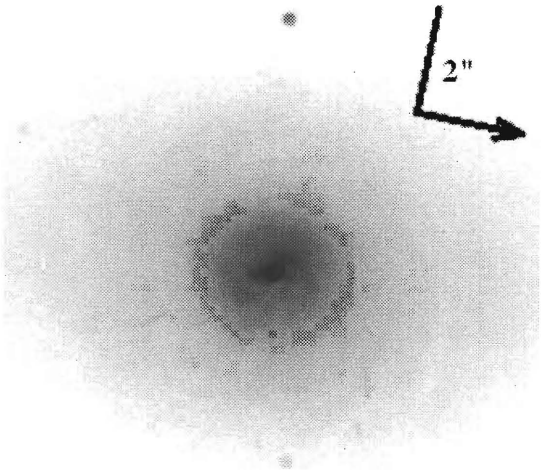

IR 0457-756 (553 pc/")

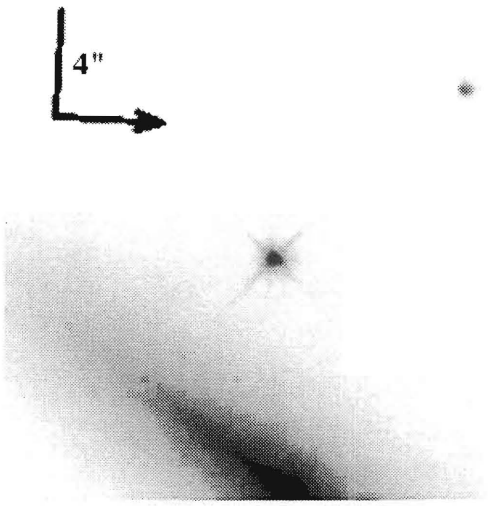

IR 1121-281* (407 pc/")

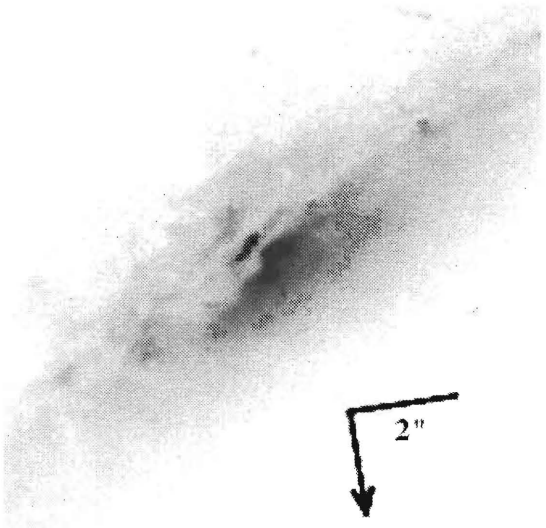

IR 1305-241 (406 pc/")

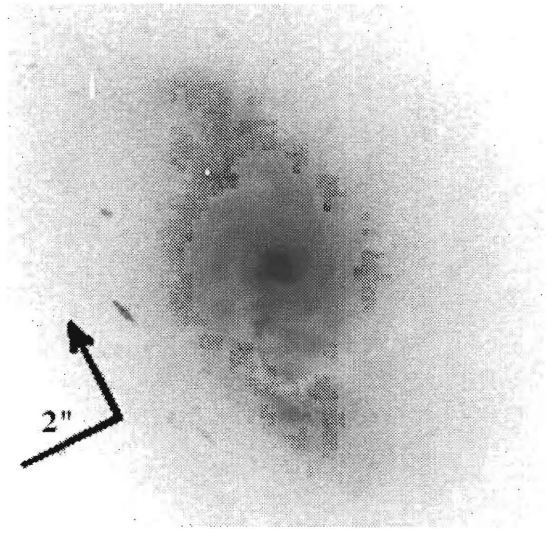

IR 1443+272 (842 pc/")

Sy 2

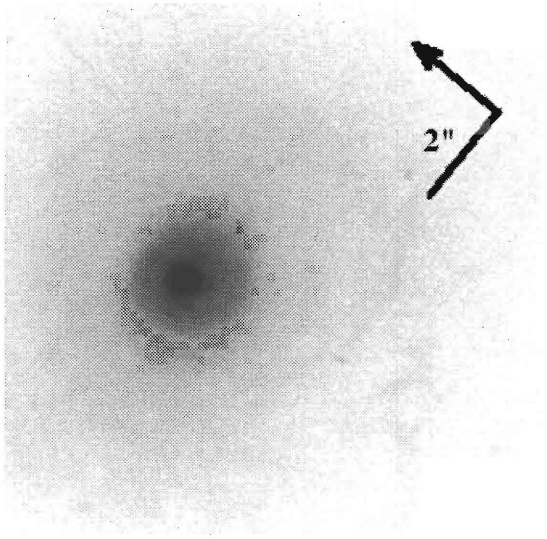

IR 1548-037 (871 pc/")

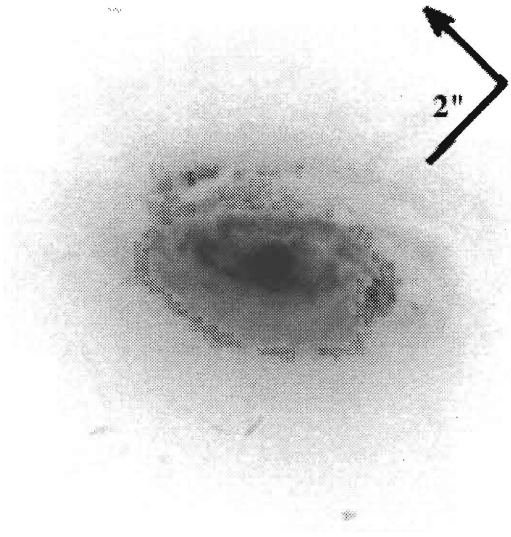

IR 1832-594 (551 pc/")

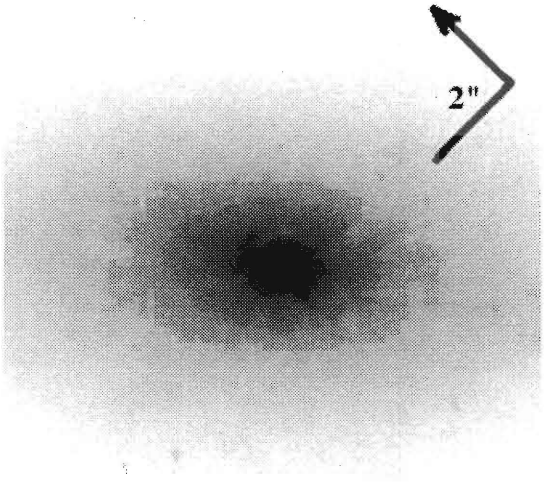

IR 1833-654 (377 pc/")

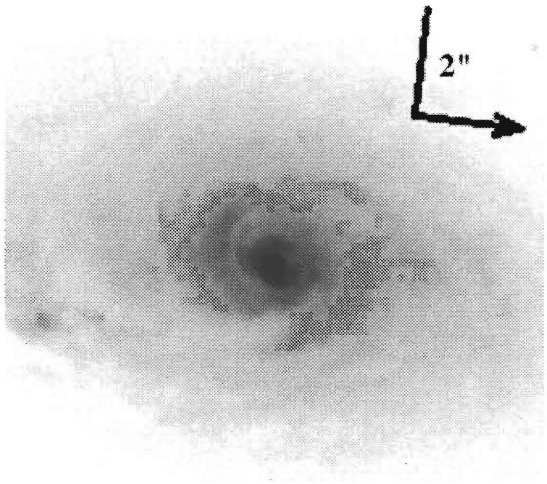

IR 2246-195 (958 pc/")

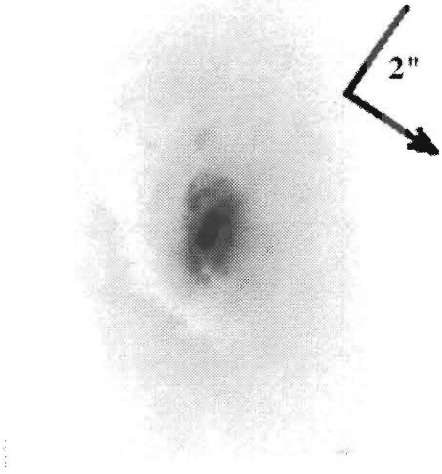

IR 2302-000 (871 pc/")

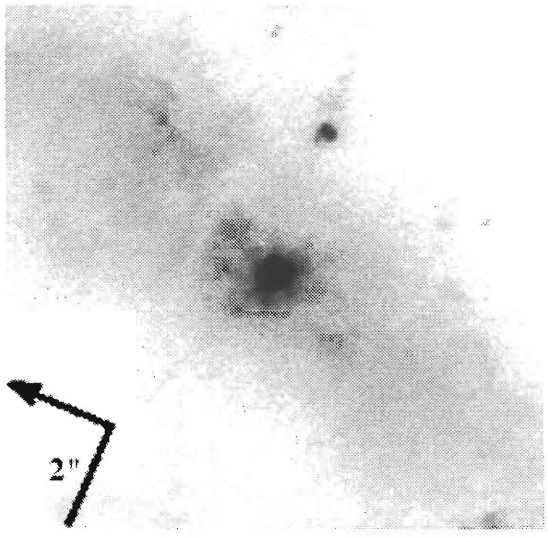

IR 2346+019 (900 pc/")

Sy 2

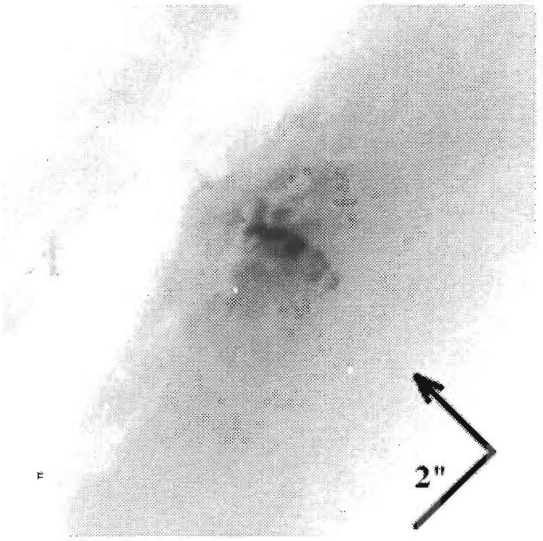

MCG -5-27-13 (669 pc/")

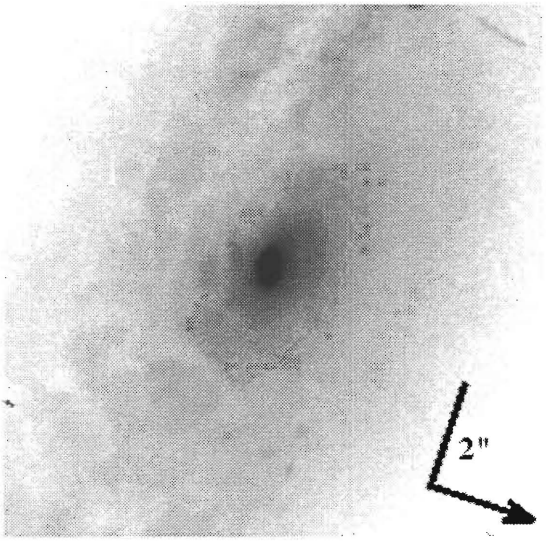

MRK 1 (464 pc/")

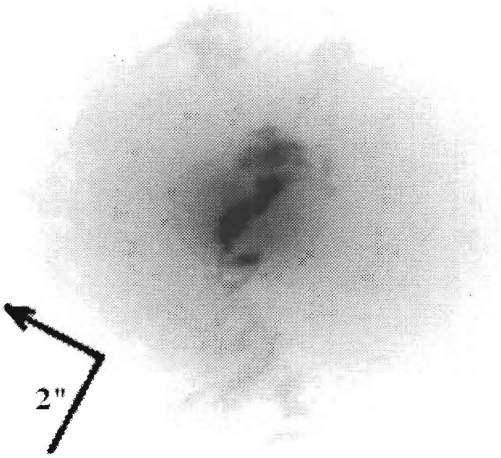

MRK 3 (406 pc/")

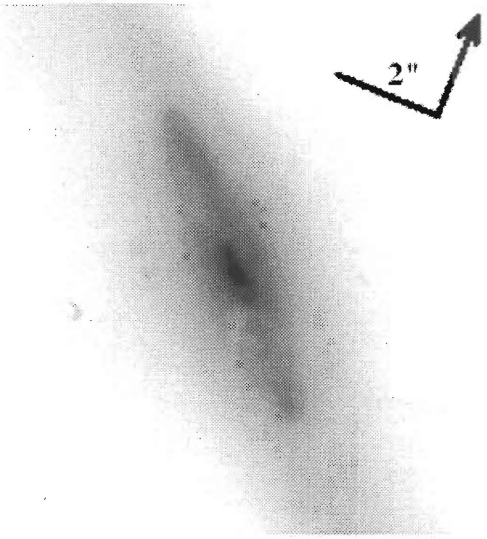

MRK 176 (784 pc/")

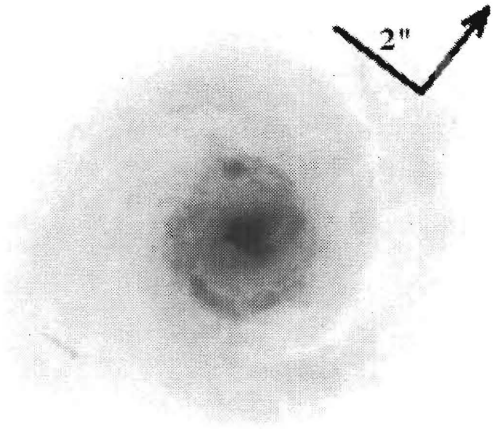

MRK 198 (696 pc/")

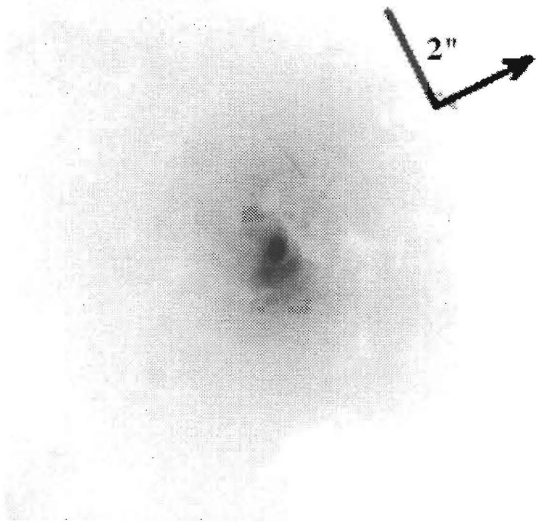

MRK 266NE (813 pc/")

Sy 2

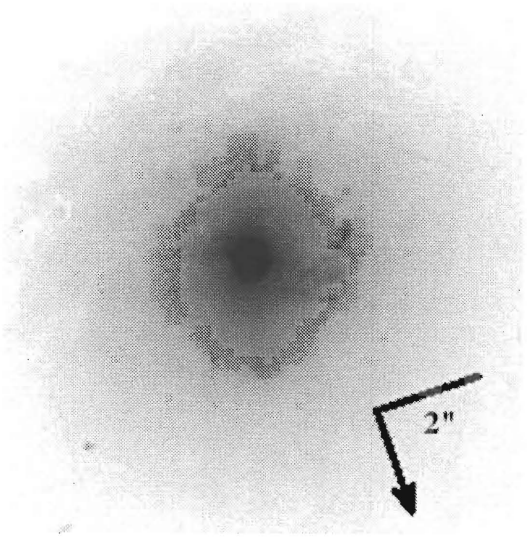

MRK 270 (261 pc/")

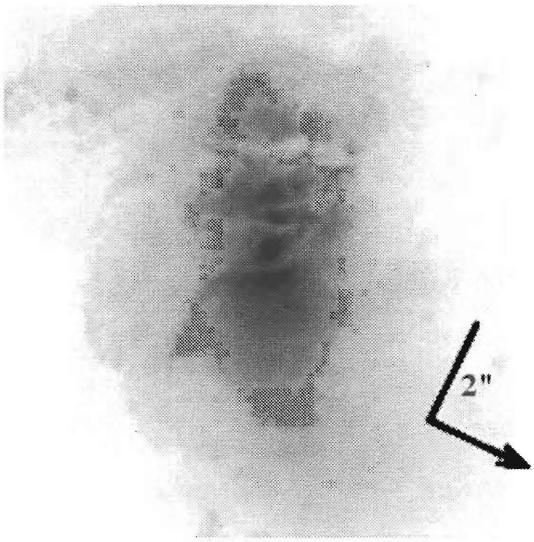

MRK 313 (174 pc/")

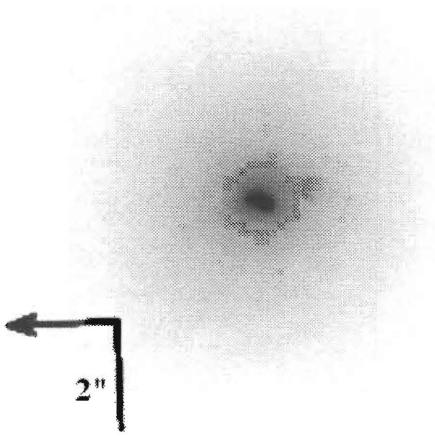

MRK 348 (406 pc/")

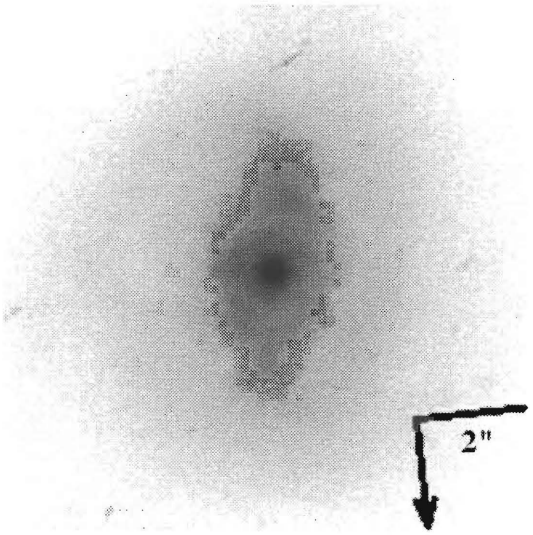

MRK 403 (696 pc/")

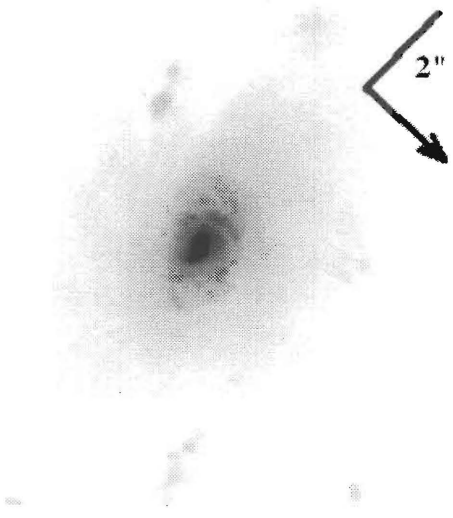

MRK 533 (pc/")

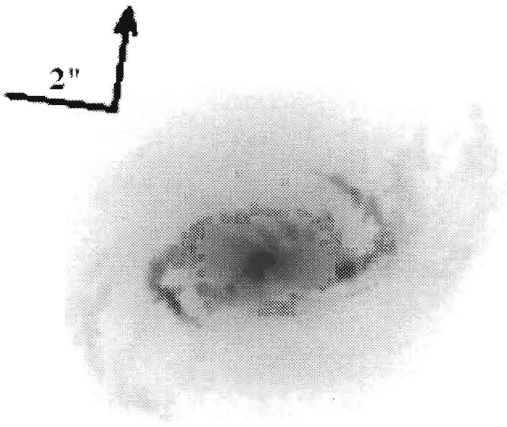

MRK 573 (493 pc/")

Sy 2

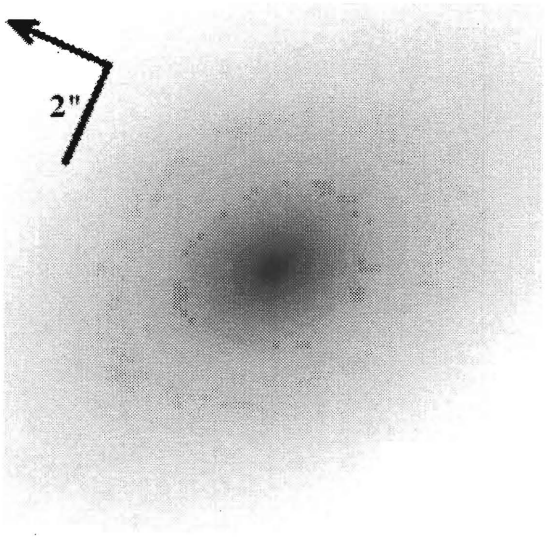

MRK 577 (495 pc/")

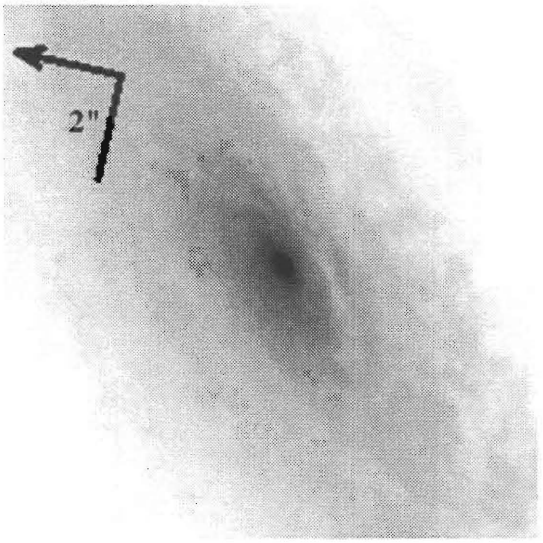

MRK 607 (261 pc/")

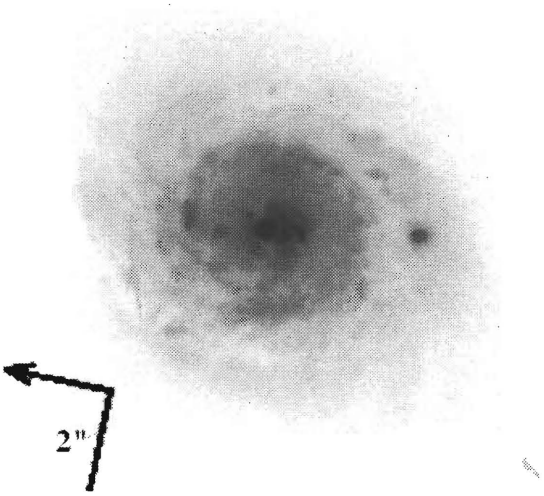

MRK 612 (580 pc/")

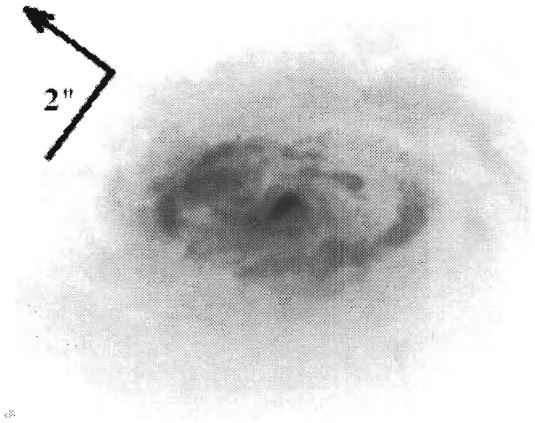

MRK 620 (174 pc/")

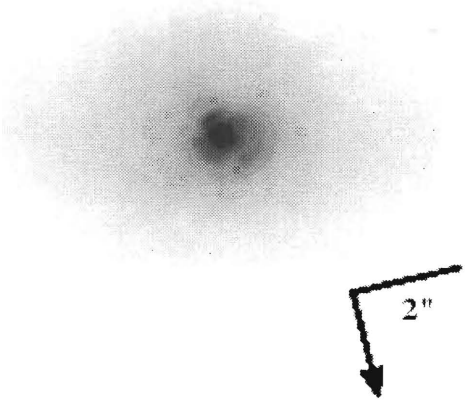

MRK 622 (667 pc/")

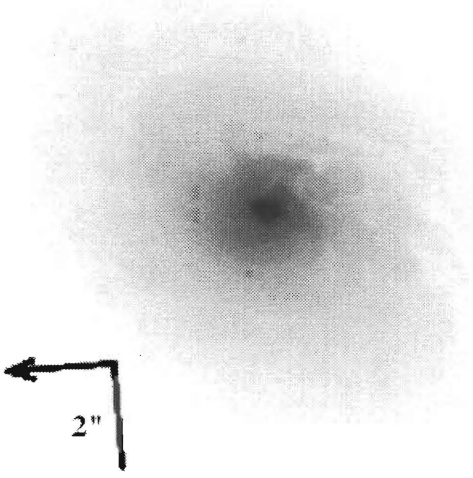

MRK 686 (406 pc/")

Sy 2

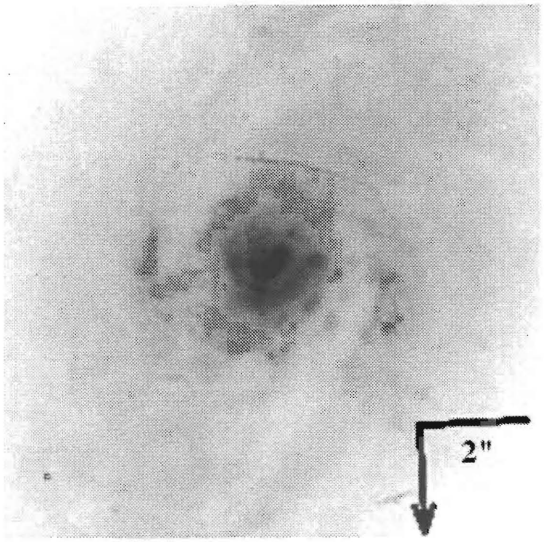

MRK 917 (726 pc/")

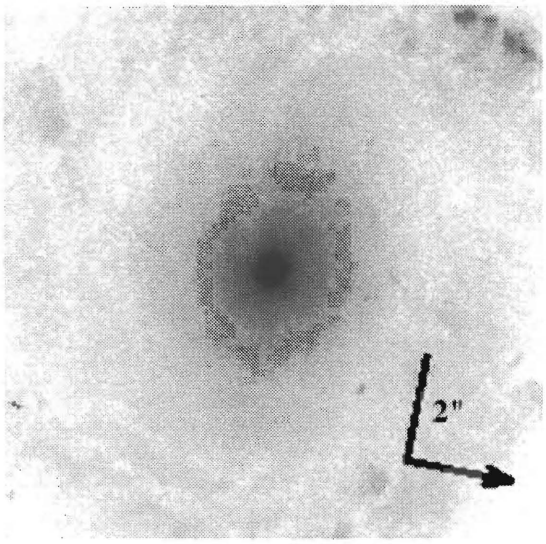

MRK 937 (873 pc/")

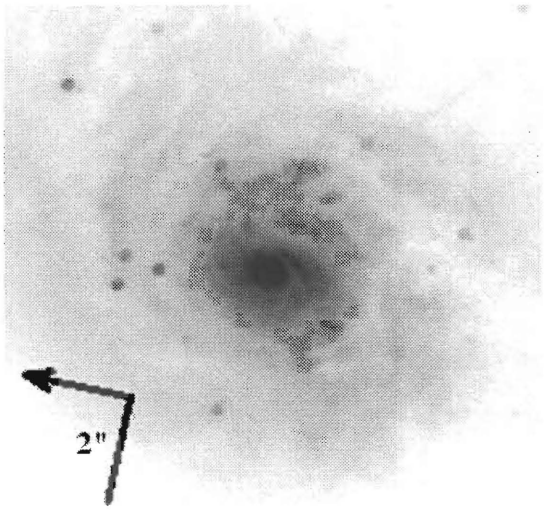

MRK 938 (551 pc/")

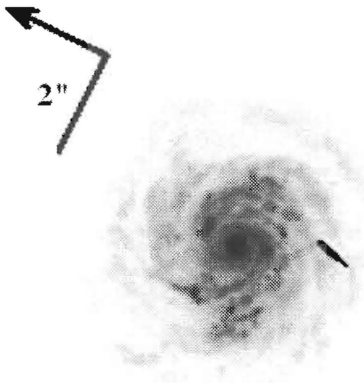

MRK 955 (1020 pc/")

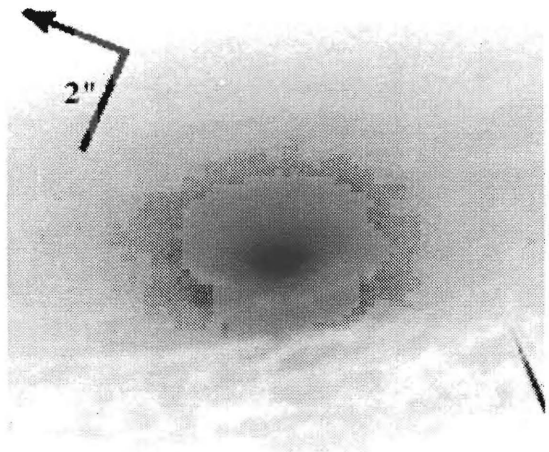

MRK 993 (493 pc/")

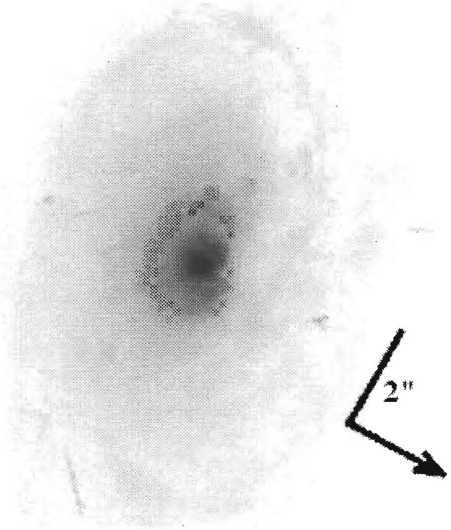

MRK 1058 (522 pc/")

Sy 2

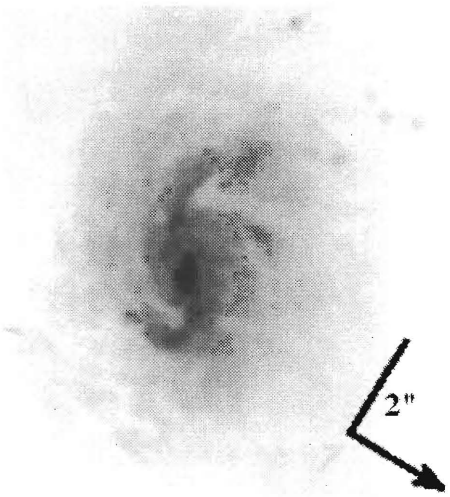

MRK 1066 (348 pc/")

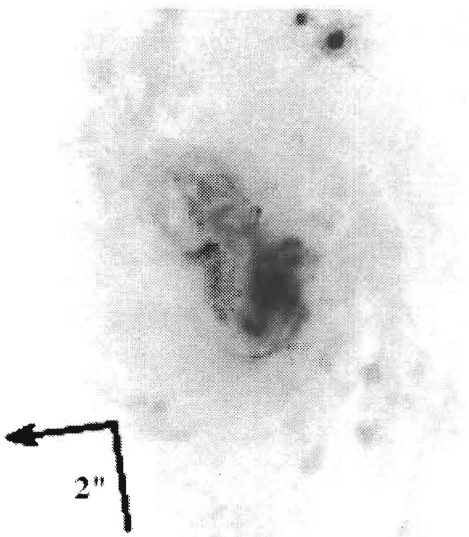

MRK 1073 (667 pc/")

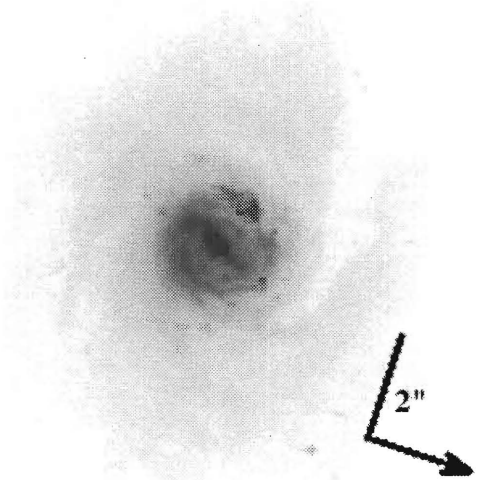

MRK 1157 (435 pc/")

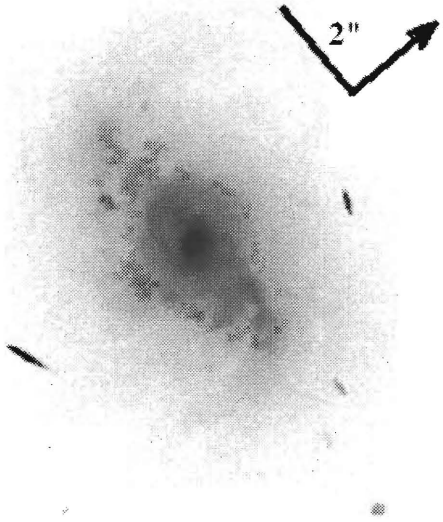

MRK 1193 (929 pc/")

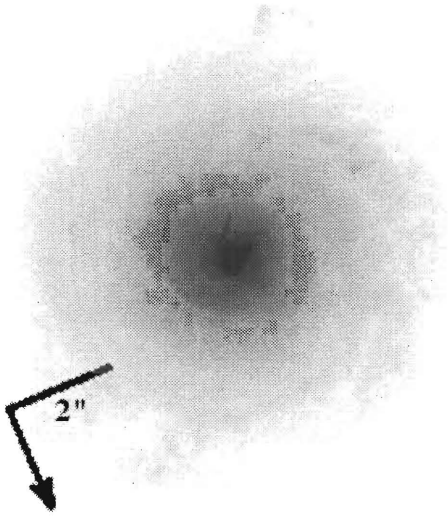

MRK 1210 (929 pc/")

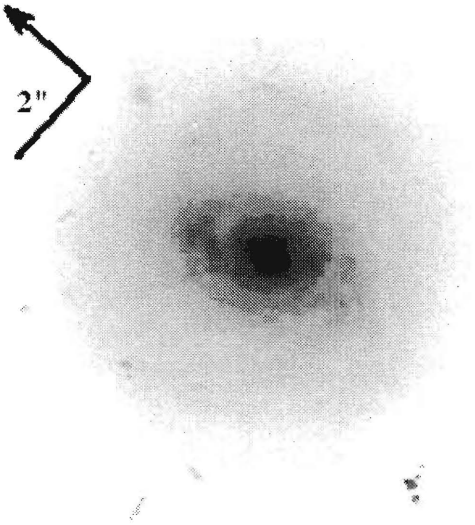

MRK 1370 (696 pc/")

Sy 2

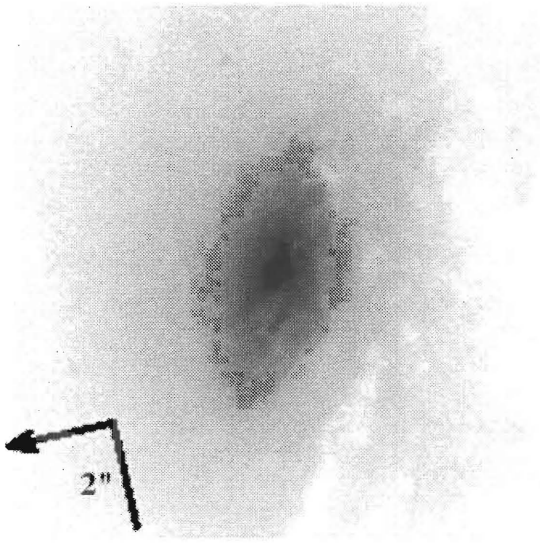

NGC 424 (696 pc/")

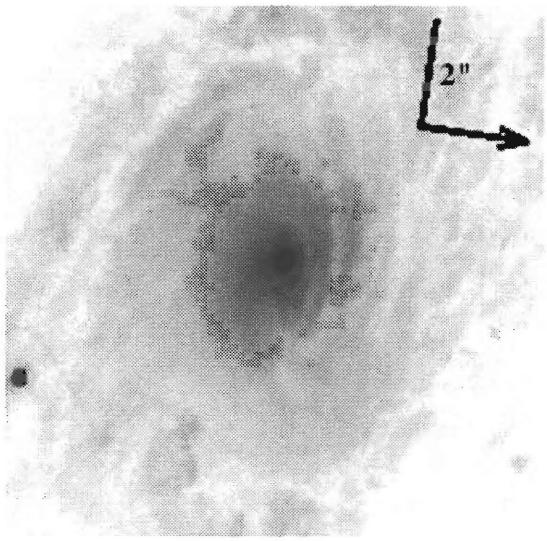

NGC 513 (464 pc/")

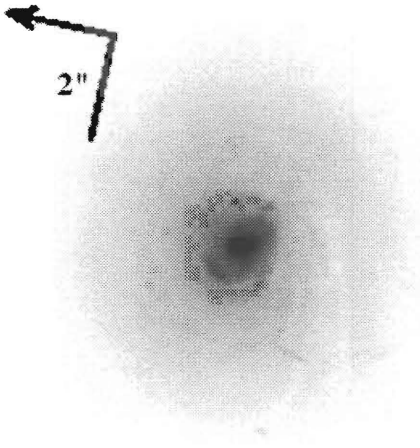

NGC 788 (377 pc/")

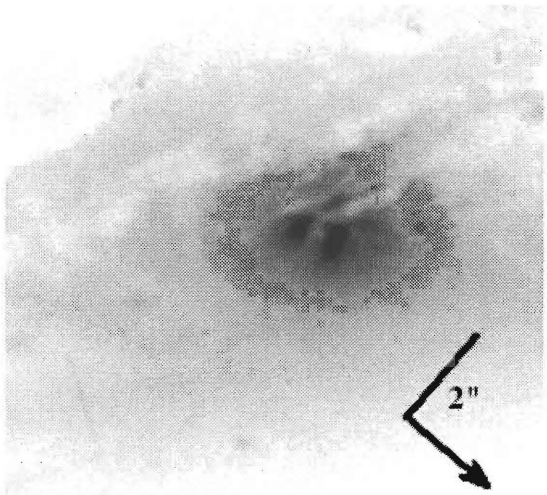

NGC 1125 (319 pc/")

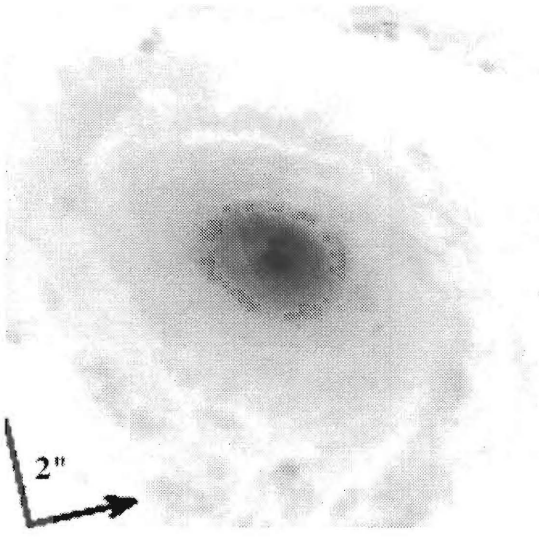

NGC 1144 (842 pc/")

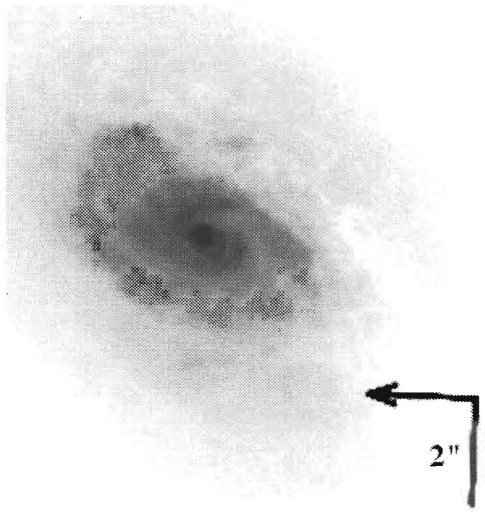

NGC 1241 (377 pc/")

Sy 2

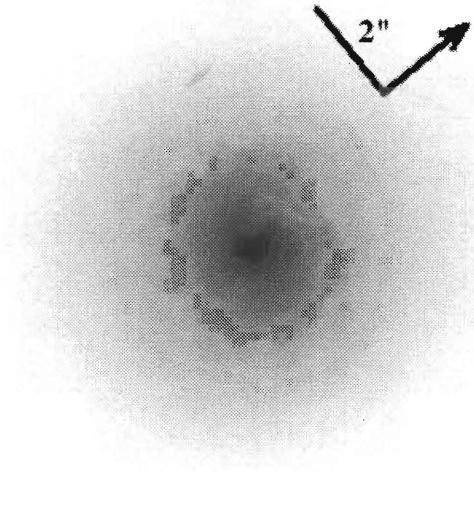

NGC 1358 (377 pc/")

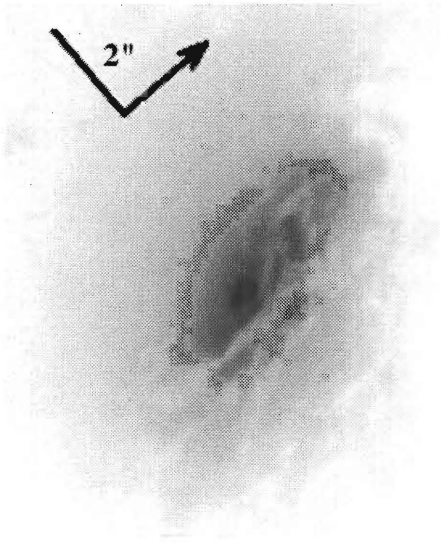

NGC 1386 (58 pc/")

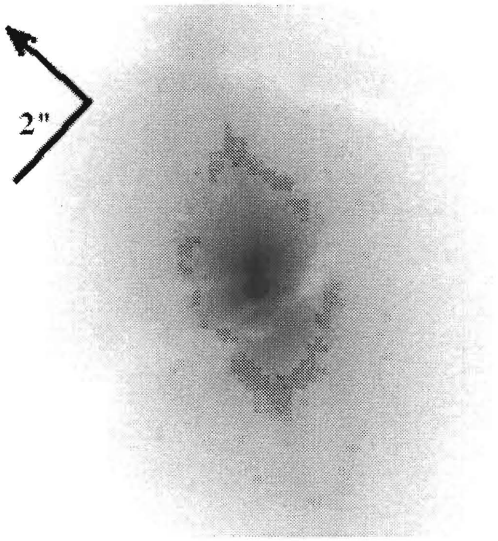

NGC 1410 (727 pc/")

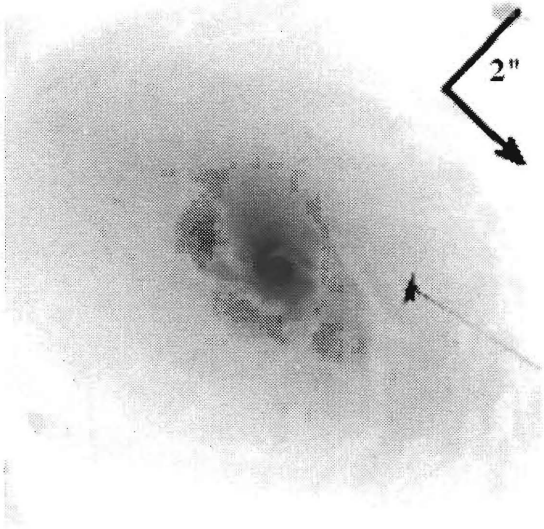

NGC 1667 (435 pc/")

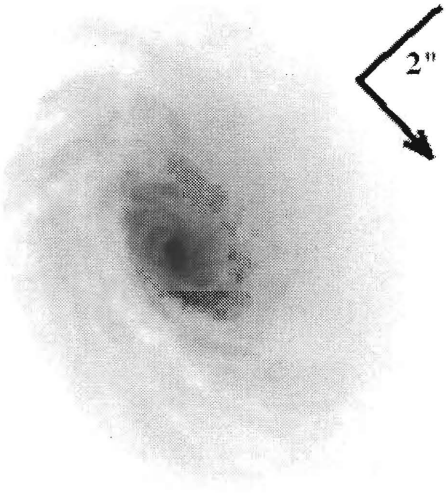

NGC 2110 (203 pc/")

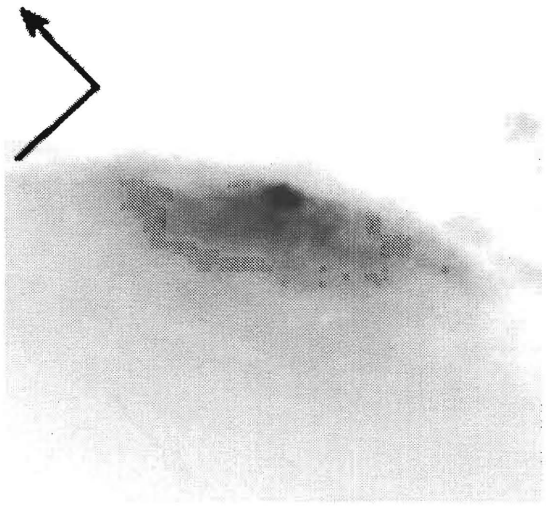

NGC 2992 (203 pc/")

Sy 2

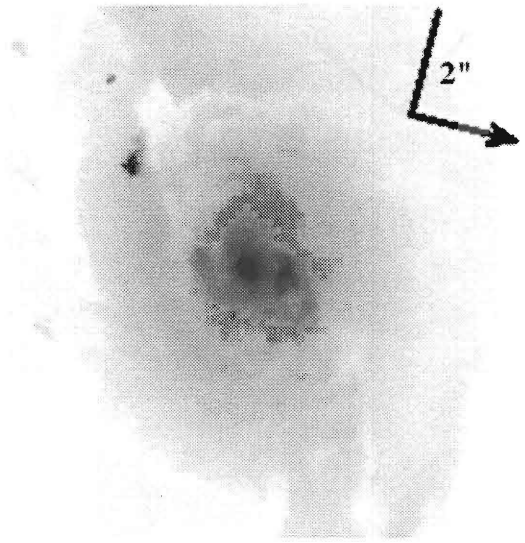

NGC 3081 (203 pc/")

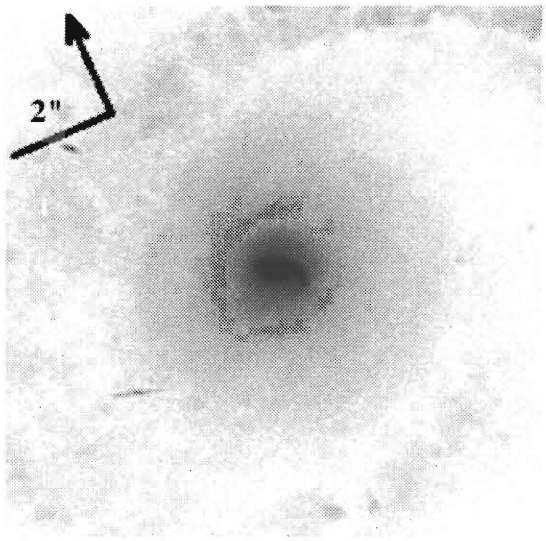

NGC 3362 (813 pc/")

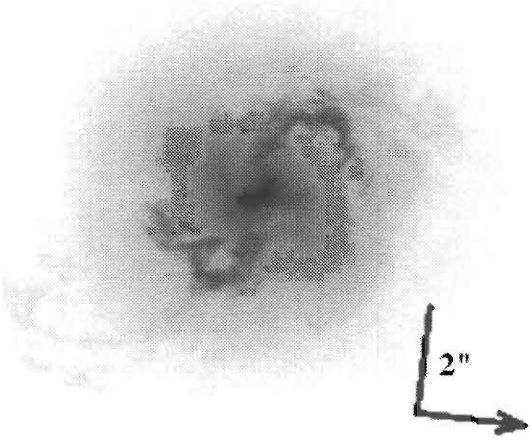

NGC 3393 (348 pc/")

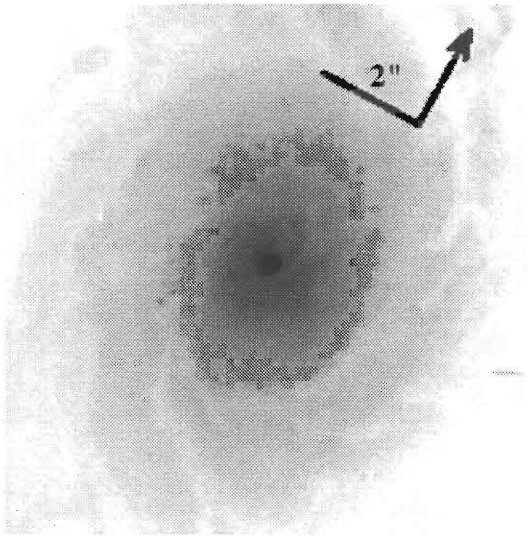

NGC 3982 (87 pc/")

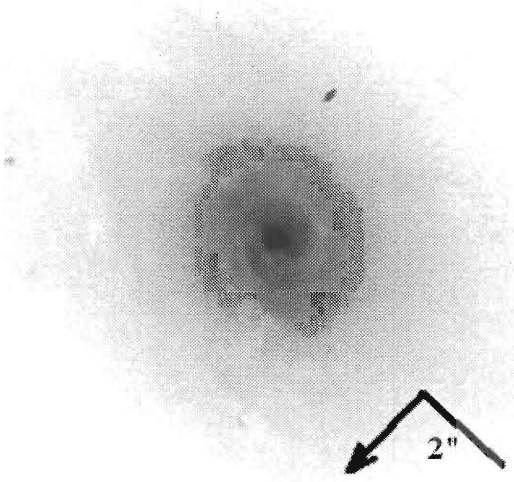

NGC 4156 (638 pc/")

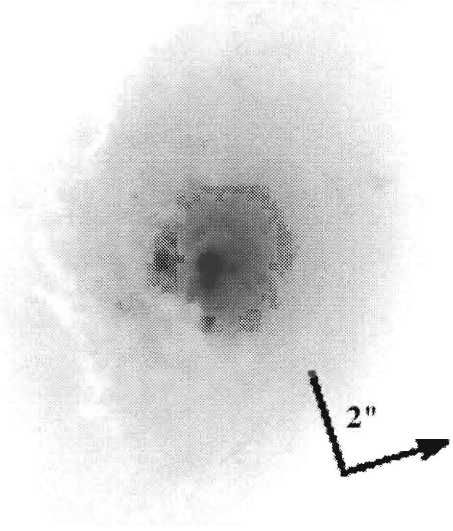

NGC 4507 (348 pc/")

Sy 2

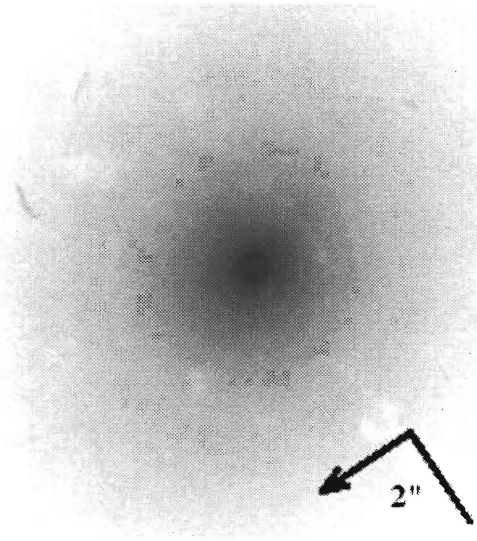

NGC 4922b (696 pc/")

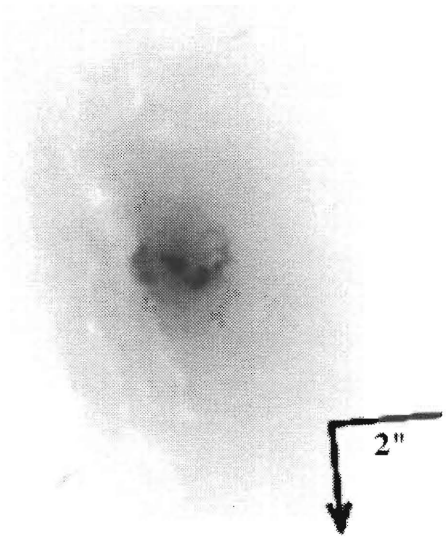

NGC 4939 (290 pc/")

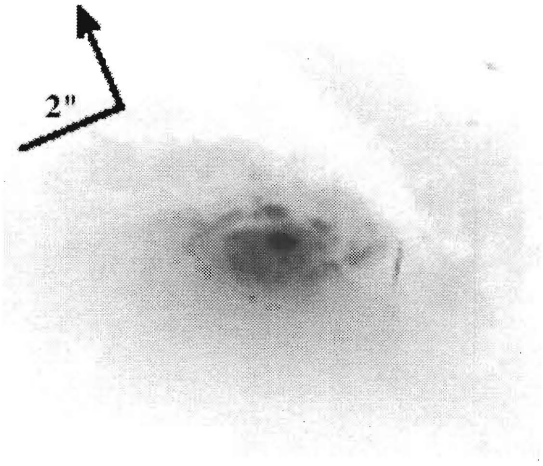

NGC 4968 (261 pc/")

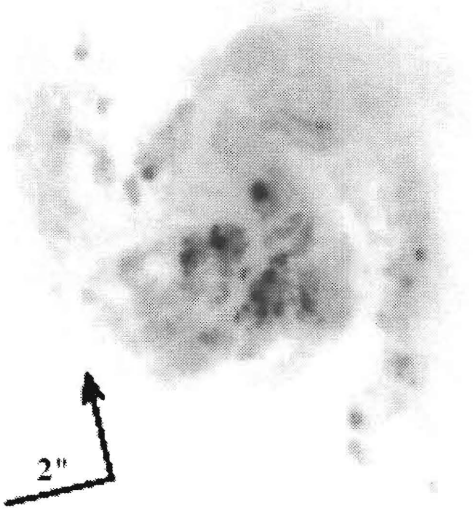

NGC 5135 (377 pc/")

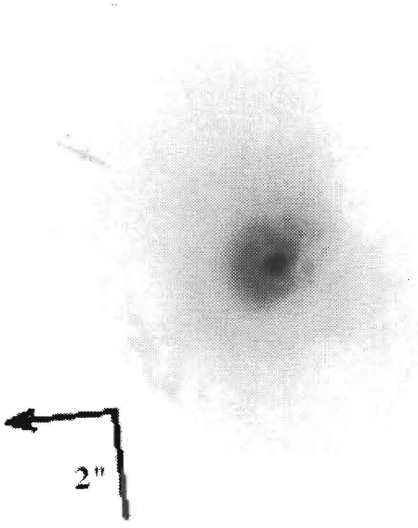

NGC 5347 (232 pc/")

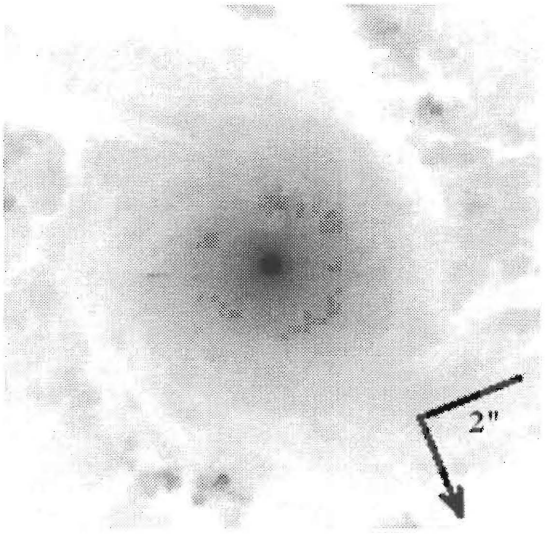

NGC 5427 (261 pc/")

Sy 2

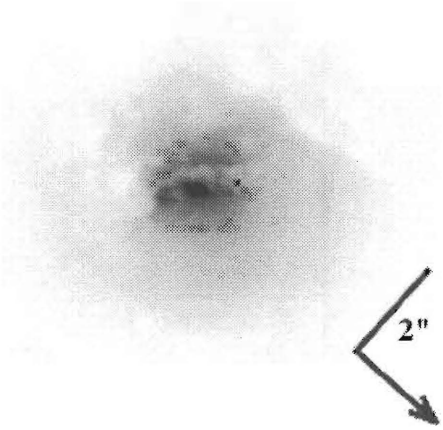

NGC 5929 (232 pc/")

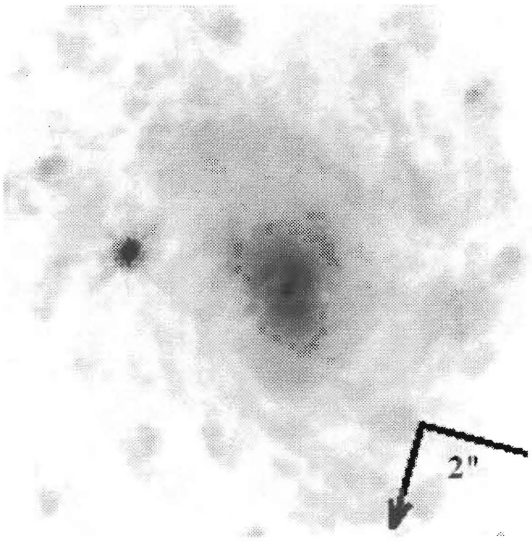

NGC 5953 (203 pc/")

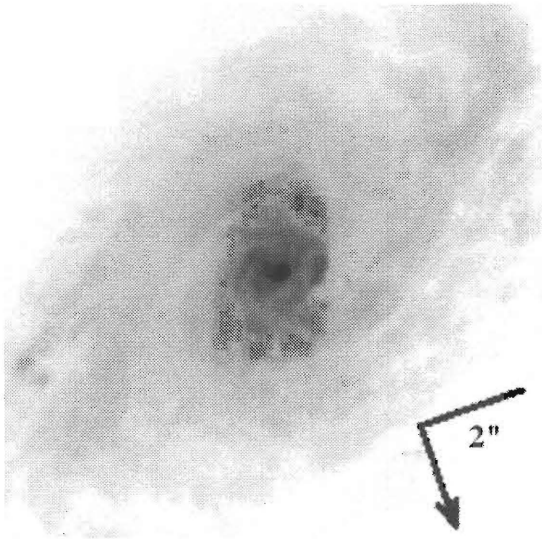

NGC 5995 (726 pc/")

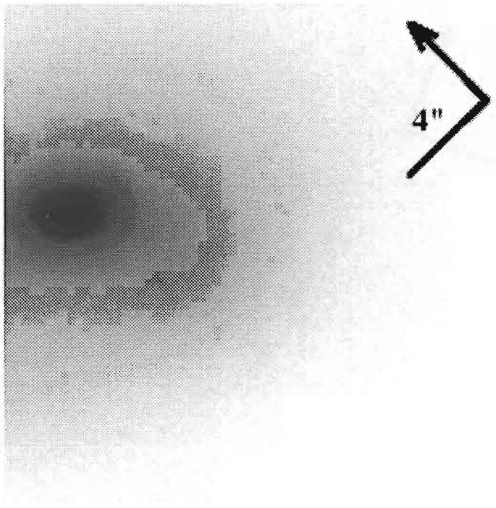

NGC 6211* (580 pc/")

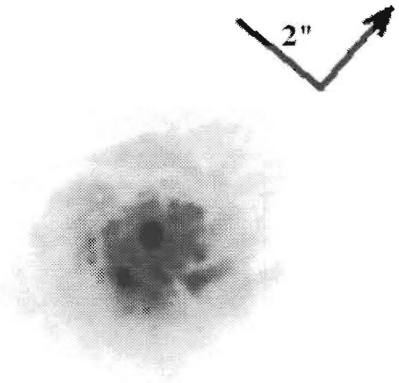

NGC 6217 (145 pc/")

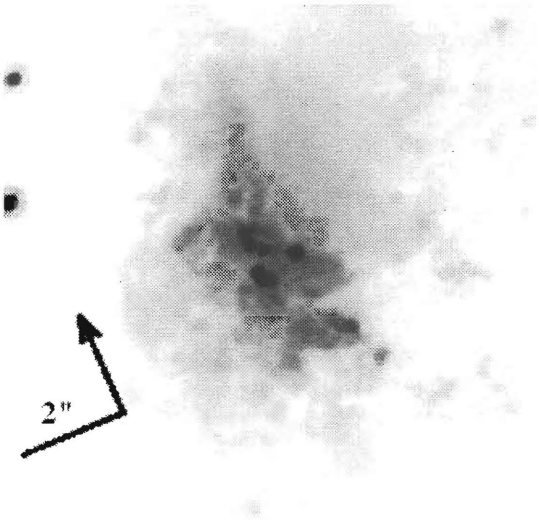

NGC 6221 (116 pc/")

Sy 2

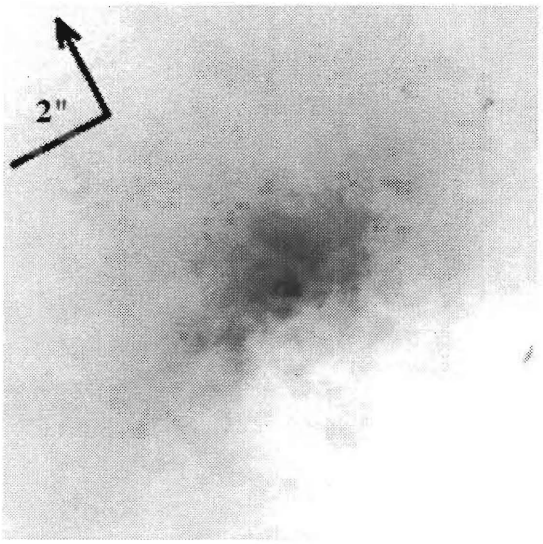

NGC 6300 (87 pc/")

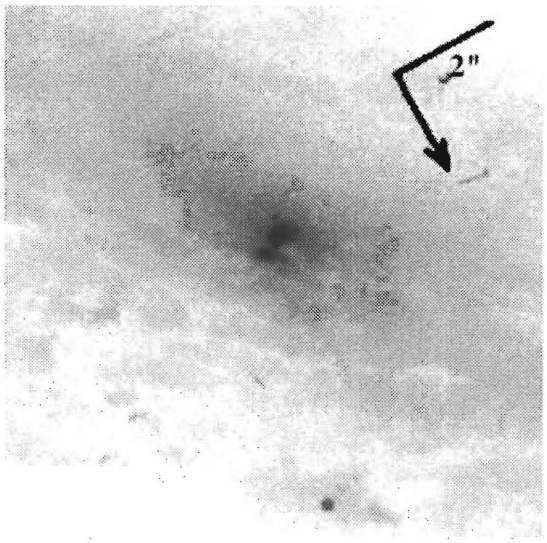

NGC 6393 (813 pc/")

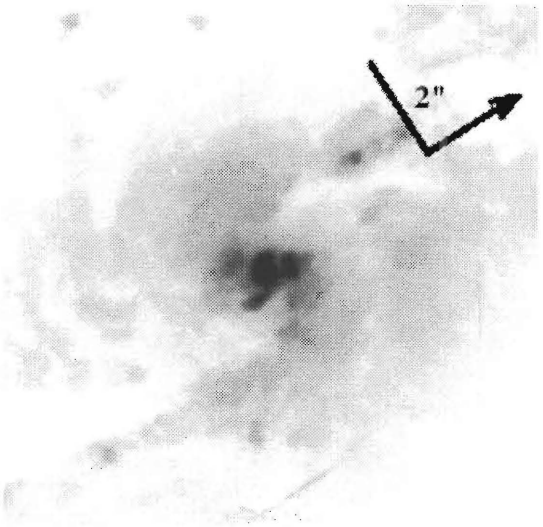

NGC 7130 (464 pc/")

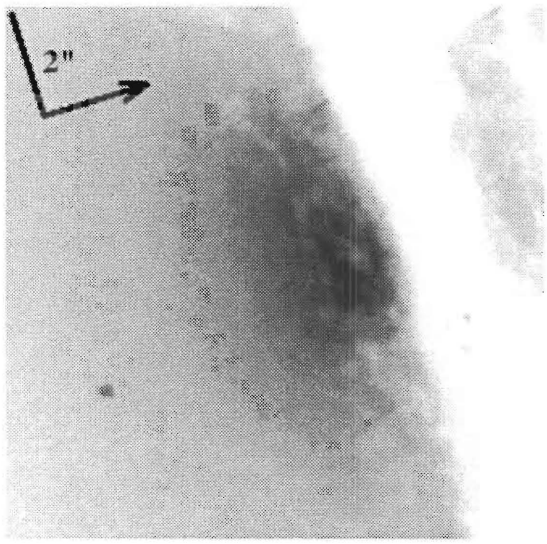

NGC 7172 (232 pc/")

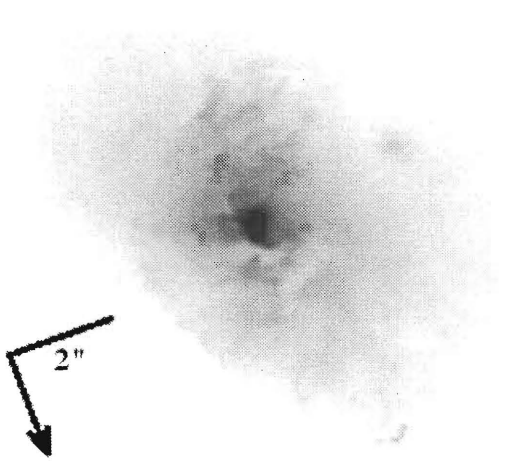

NGC 7212 (755 pc/")

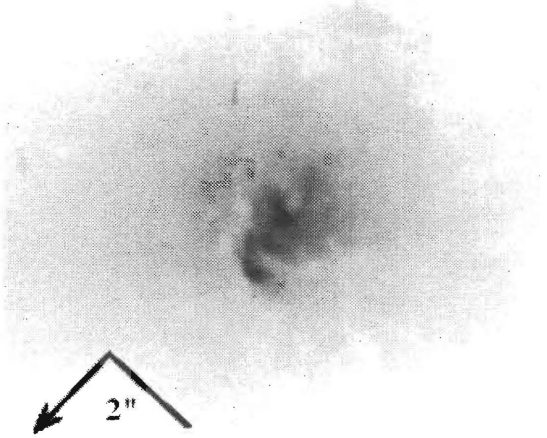

NGC 7319 (638 pc/")

Sy 2

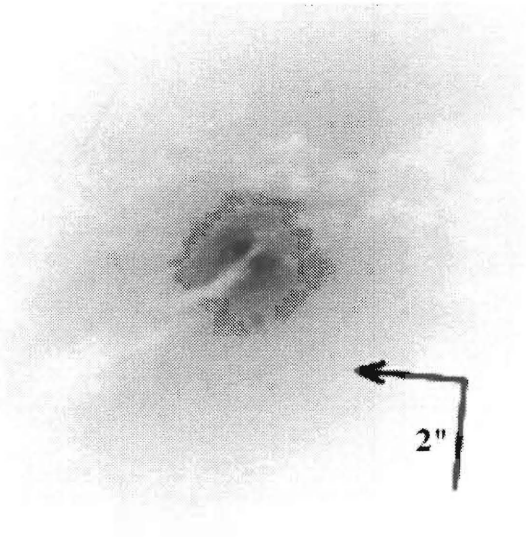

NGC 7410 (174 pc/")

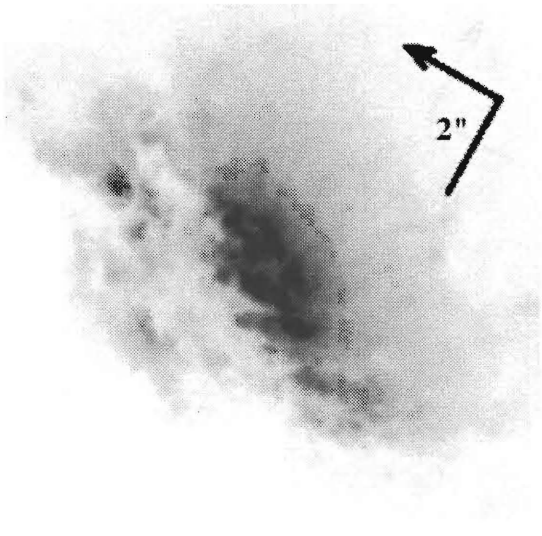

NGC 7582 (145 pc/")

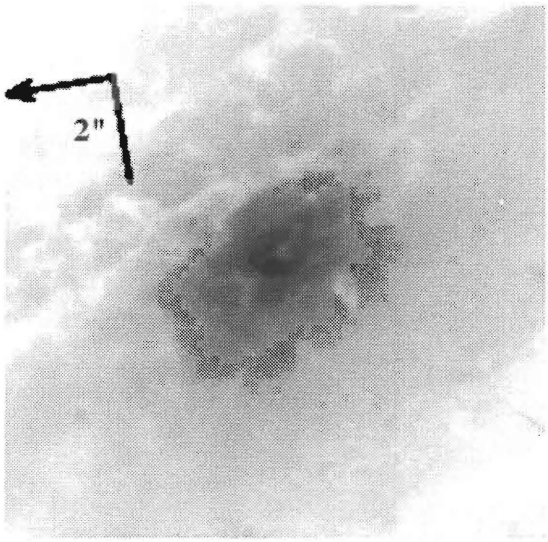

NGC 7590 (145 pc/")

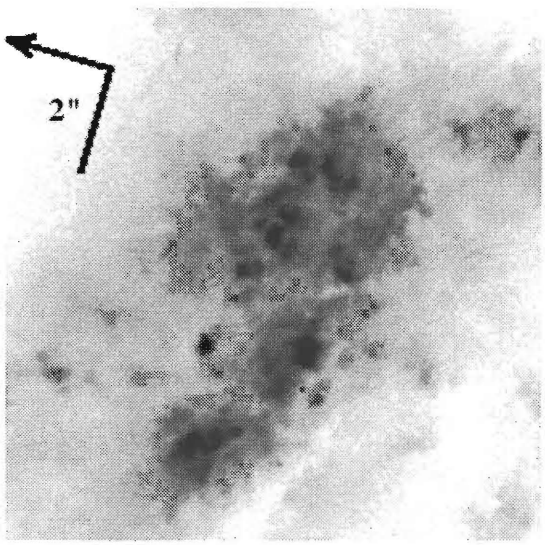

NGC 7592 (696 pc/")

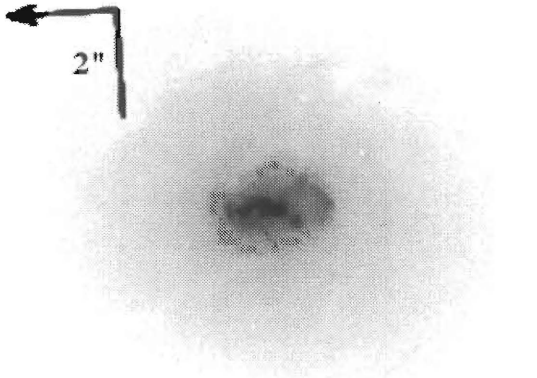

NGC 7682 (495 pc/")

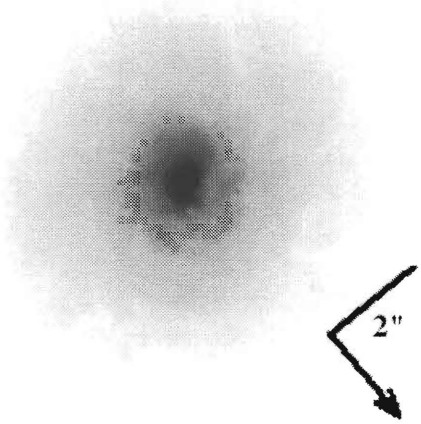

NGC 7743 (204 pc/")

Sy 2

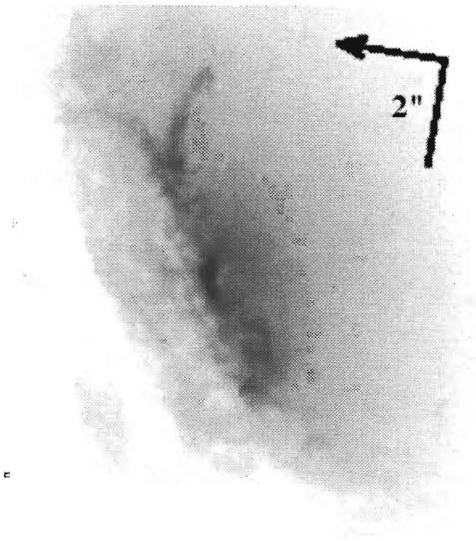

PKS 2048-572 (319 pc/")

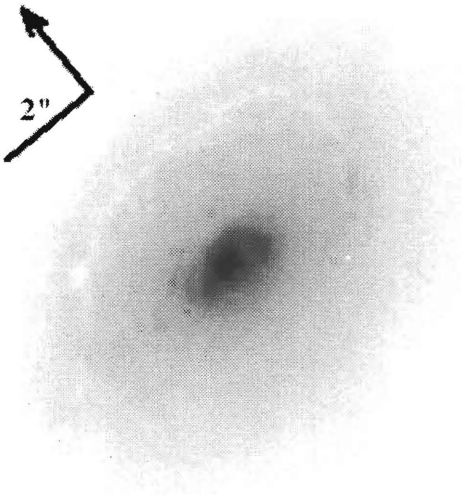

PKS 2158-380 (960 pc/")

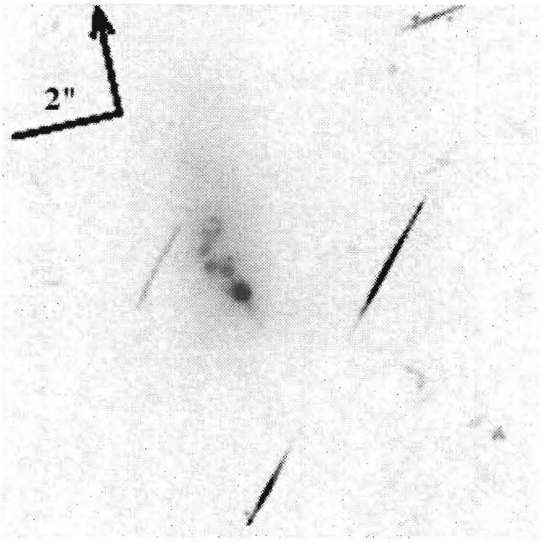

Q 1234+0848 (813 pc/")

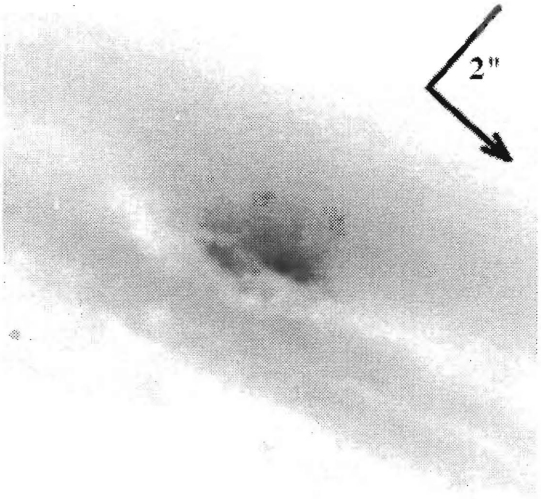

UGC 3255 (553 pc/")

UGC 4332* (524 pc/")

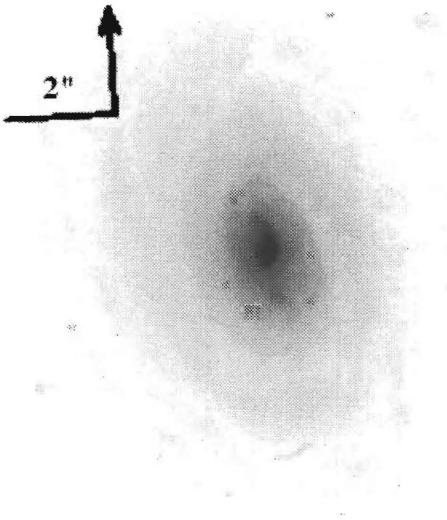

UGC 6100 (844 pc/")

Sy 2

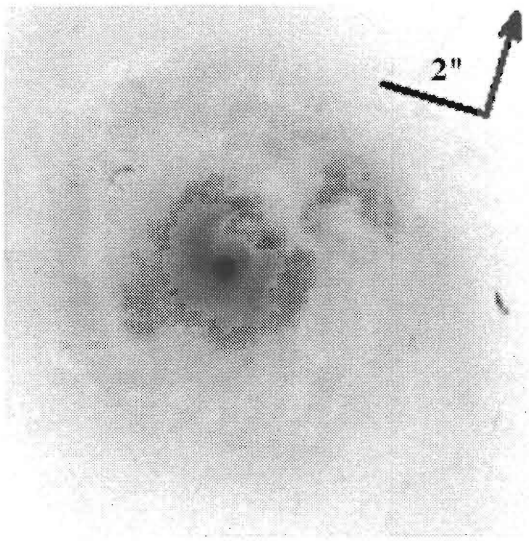

UM 105 (873 pc/")

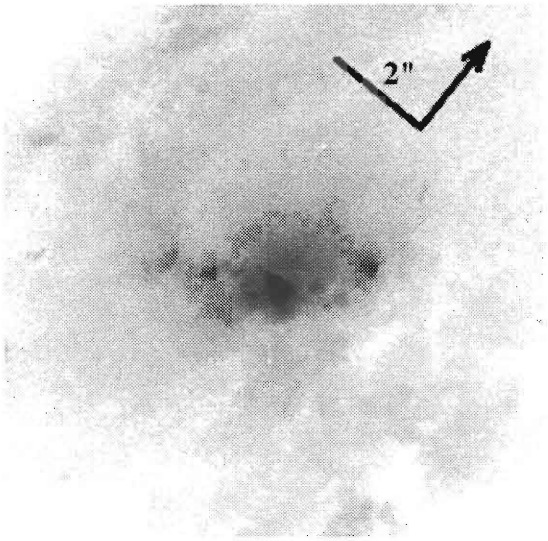

UM 319 (464 pc/")

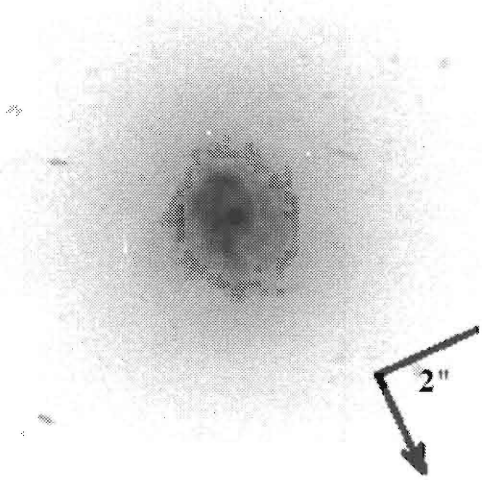

UM 625 (726 pc/")

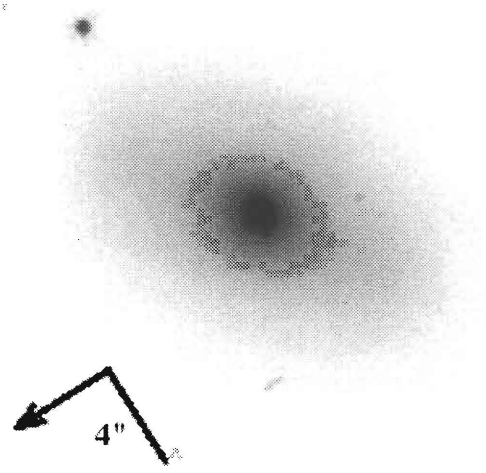

WAS 2* (960 pc/")

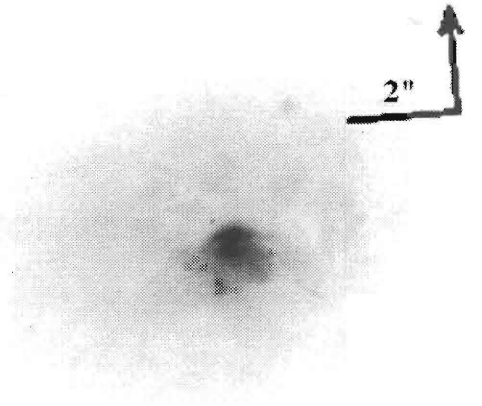

ZW 1408+137 (pc/")

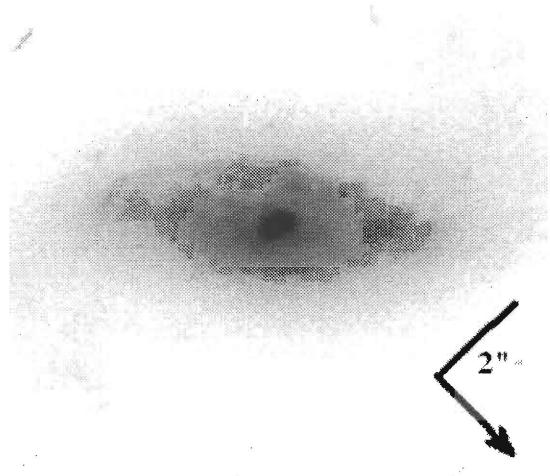

ZW 1541+286 (pc/")

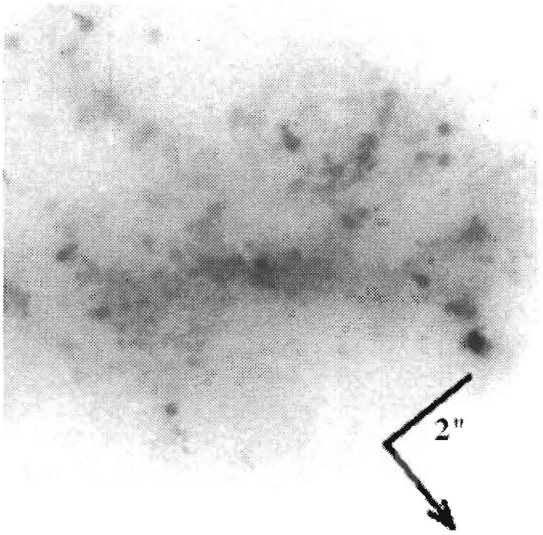

ESO 185-IG13 (551 pc/")

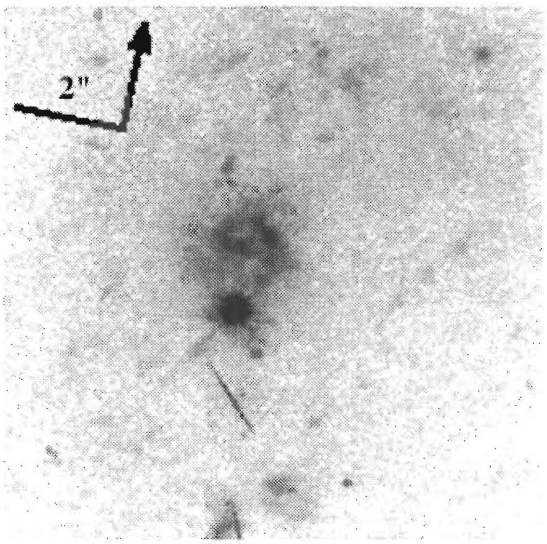

ESO 325-IG41 (174 pc/")

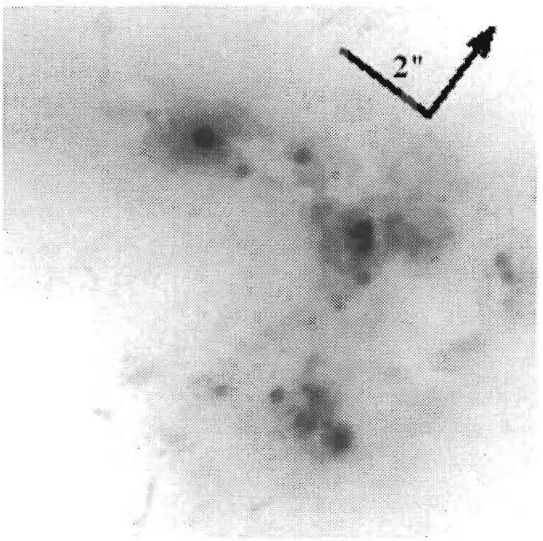

ESO 350-IG38 (580 pc/")

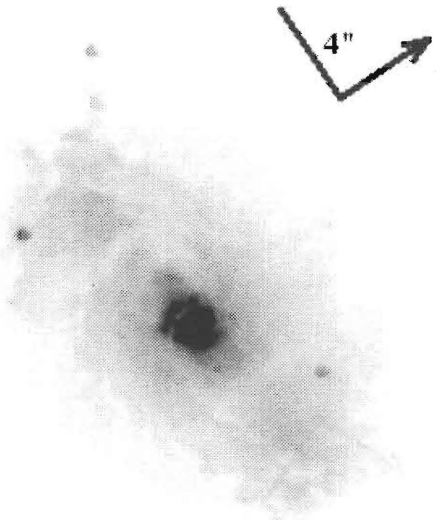

F 280° (290 pc/")

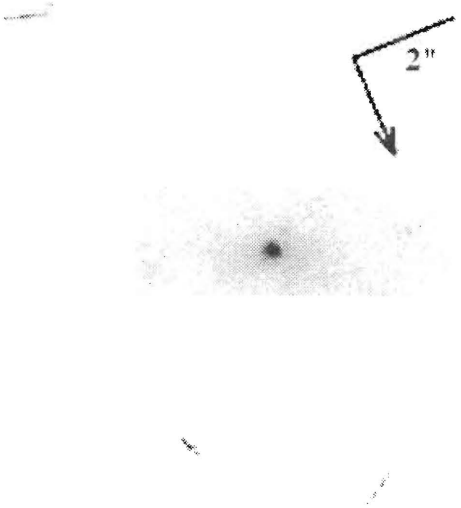

G 1307-1608 (929 pc/")

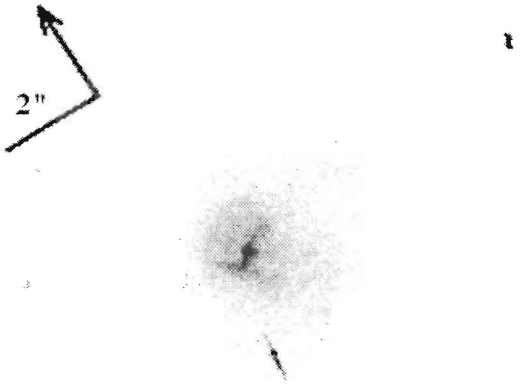

G 1314-1532 (377 pc/")

HII

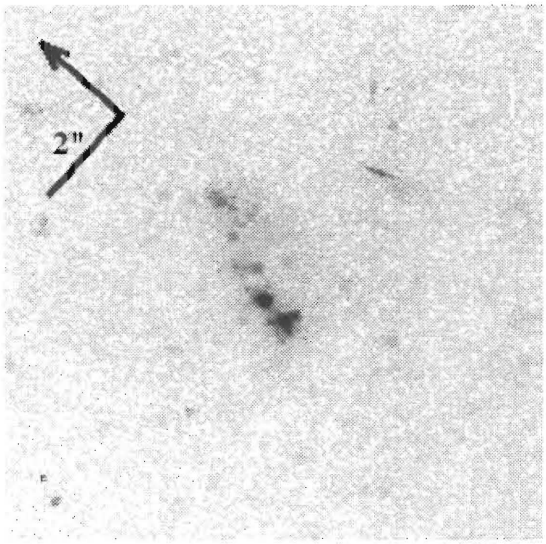

IC 3576 (87 pc/")

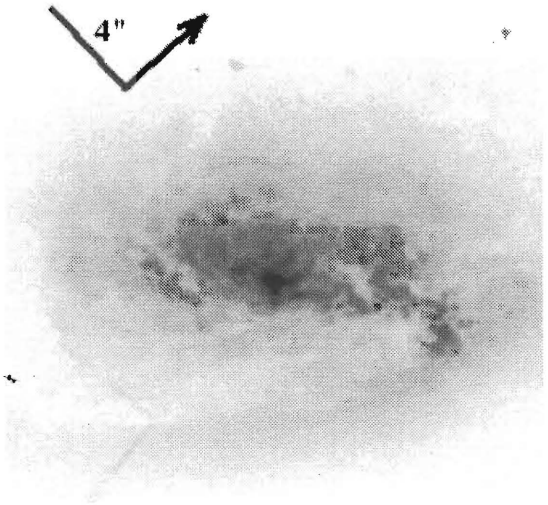

IC 4687* (495 pc/")

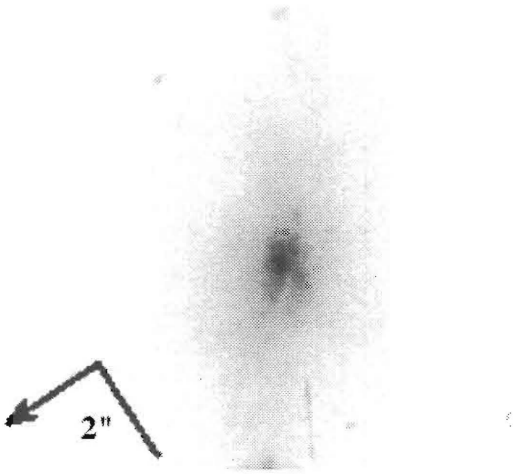

KUV 13000+29 (580 pc/")

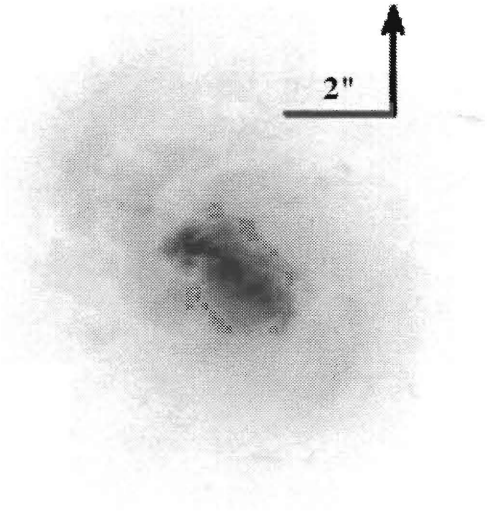

MRK 25 (290 pc/")

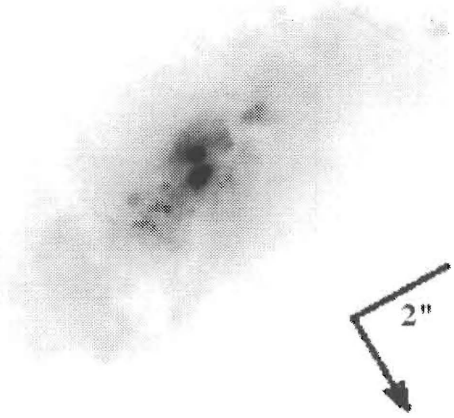

MRK 52 (203 pc/")

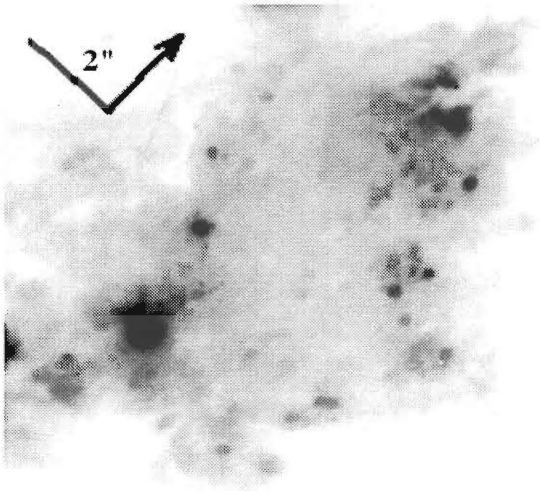

MRK 171 (290 pc/")

HII

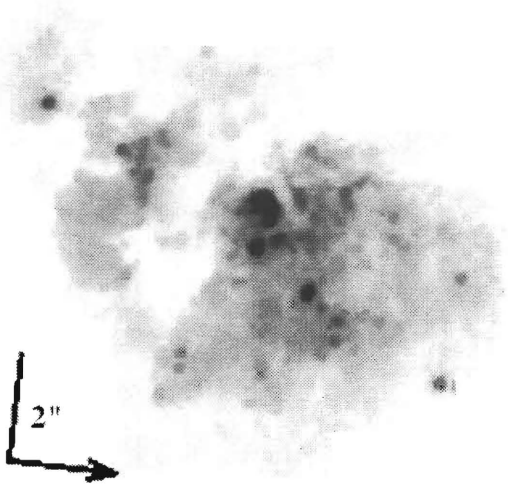

MRK 201 (232 pc/")

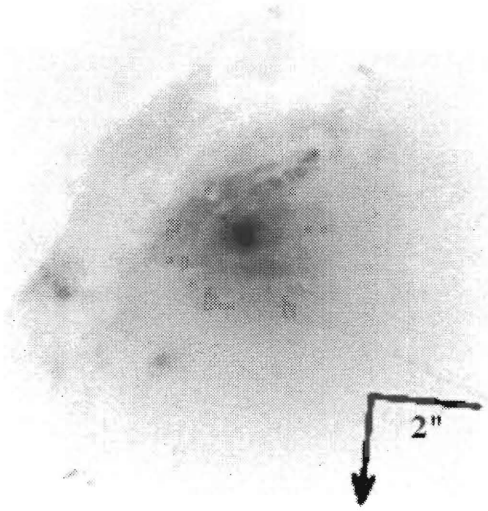

MRK 298 (987 pc/")

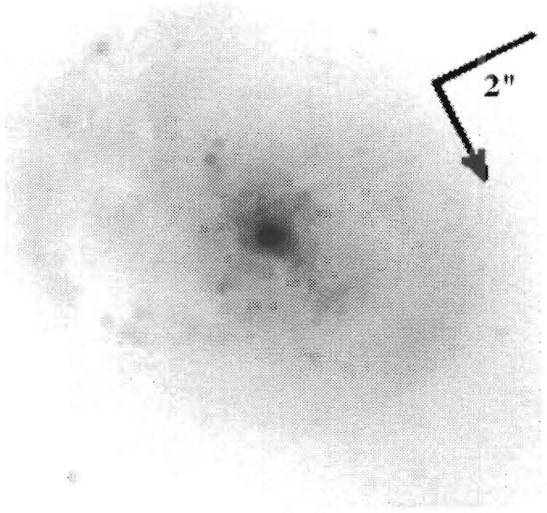

MRK 308 (696 pc/")

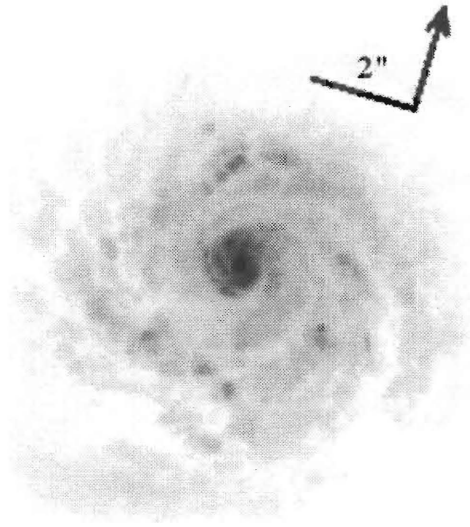

MRK 567 (957 pc/")

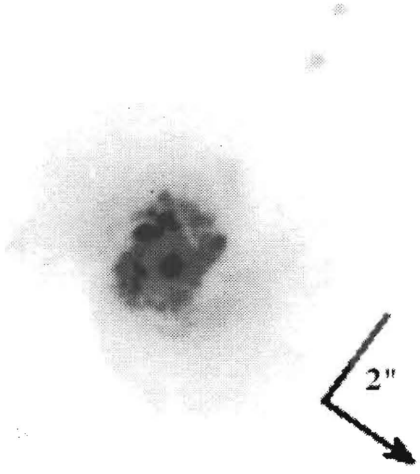

MRK 703 (377 pc/")

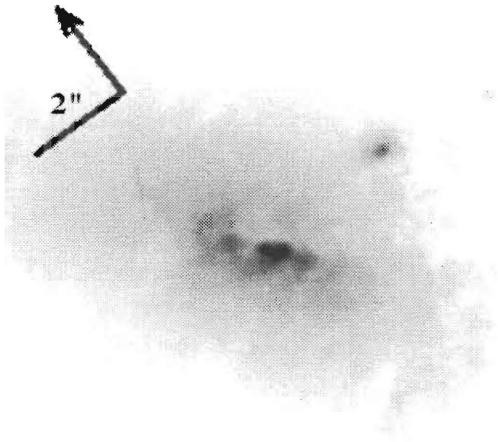

MRK 759 (174 pc/")

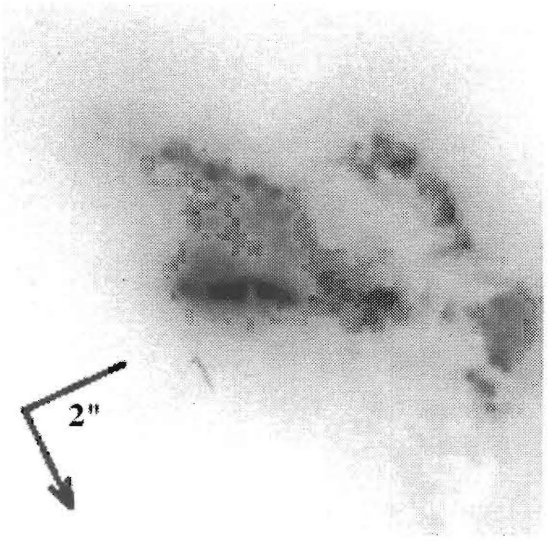

MRK 789 (929 pc/")

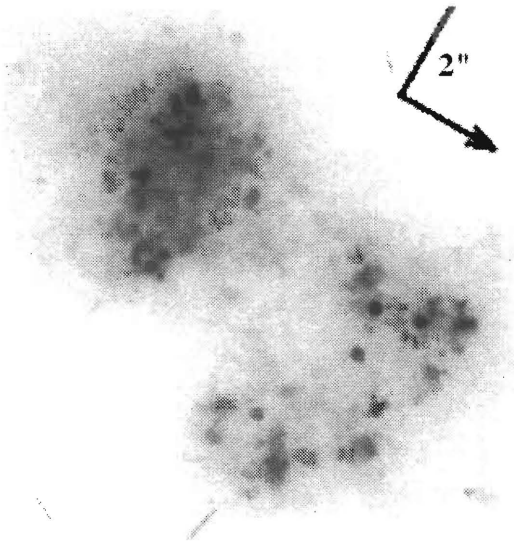

MRK 930 (551 pc/")

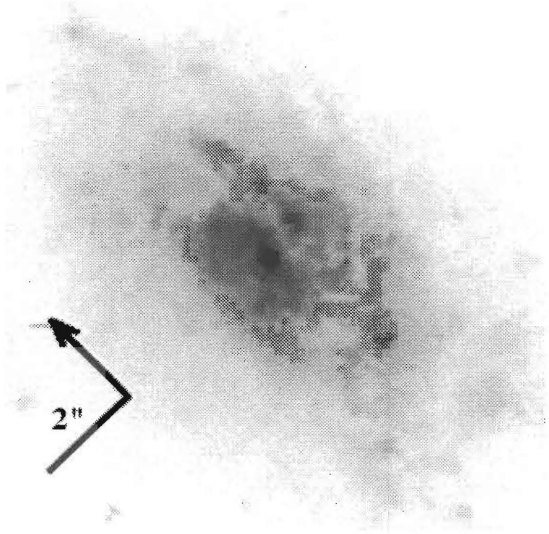

MRK 1087 (813 pc/")

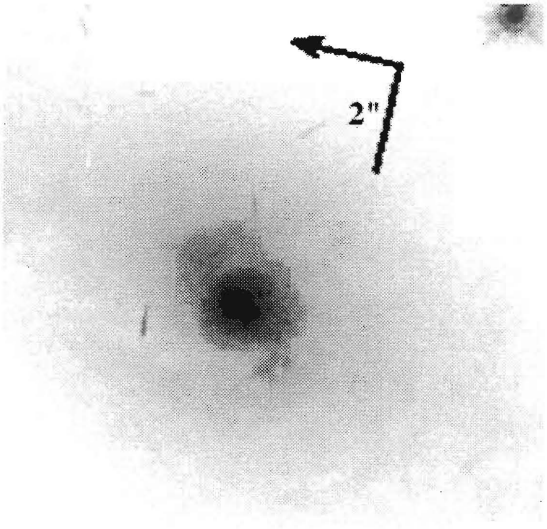

MRK 1133 (696 pc/")

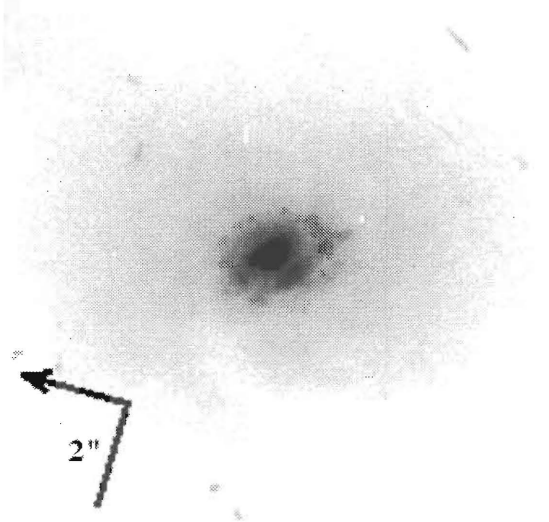

MRK 1149 (609 pc/")

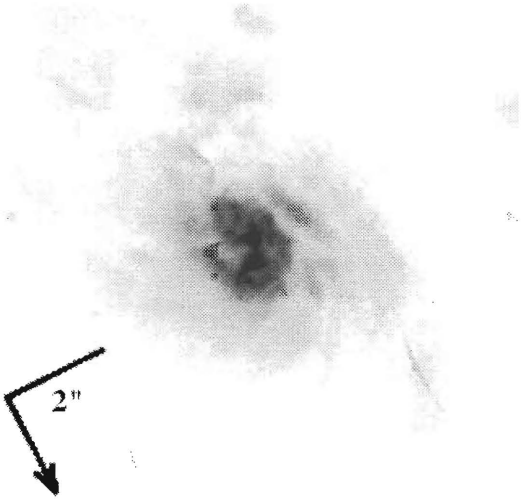

MRK 1261 (755 pc/")

HII

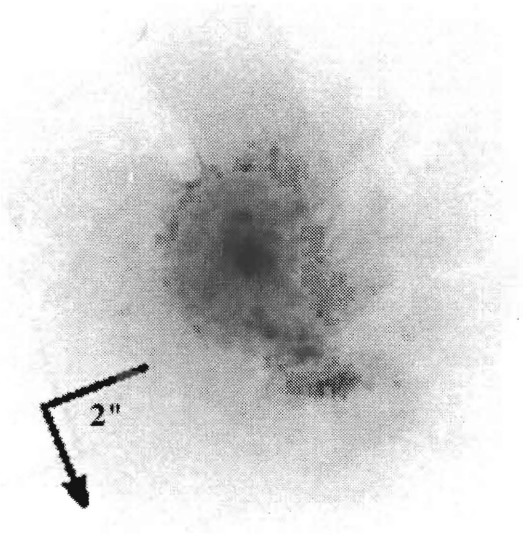

MRK 1308 (116 pc/")

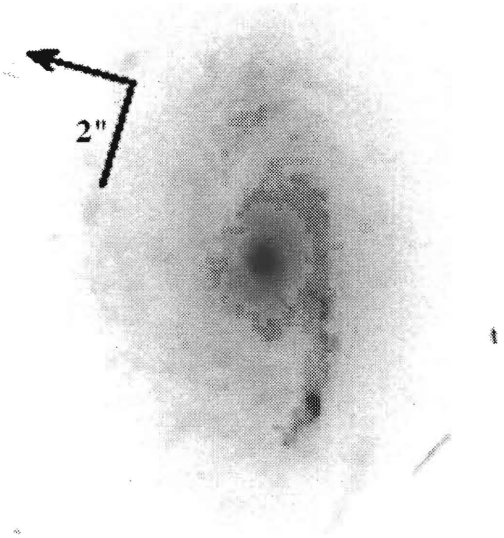

MRK 1408 (987 pc/")

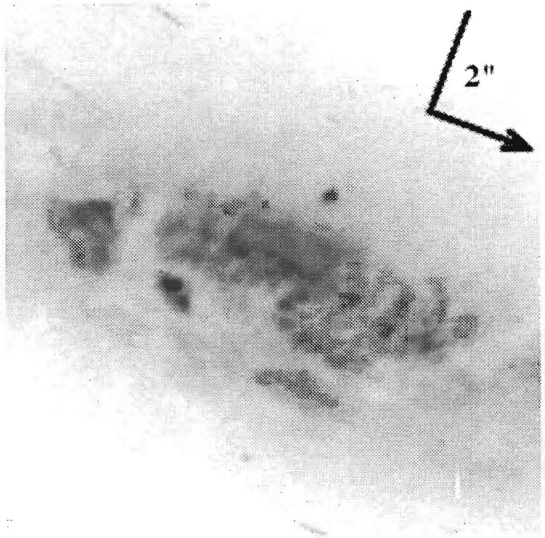

MRK 1414 (406 pc/")

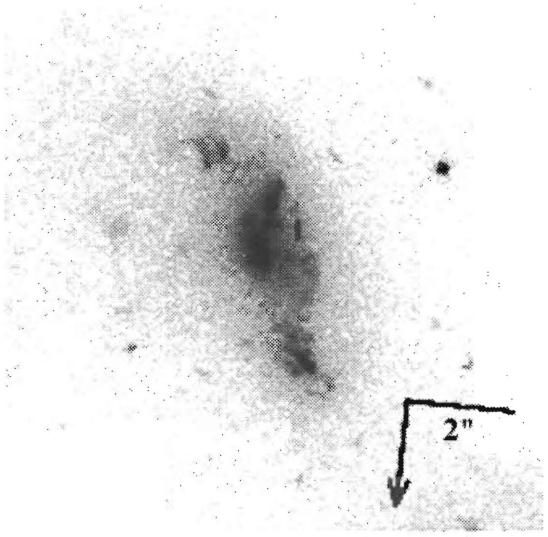

MRK 1459 (784 pc/")

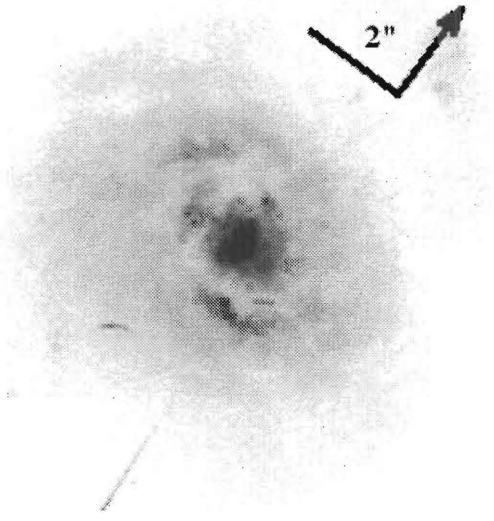

MRK 1490 (755 pc/")

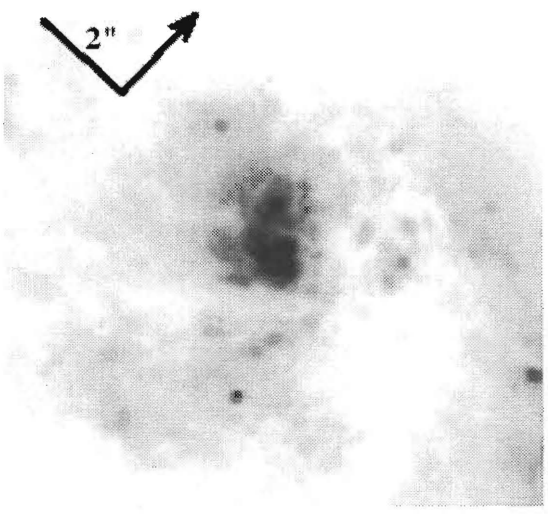

NGC 1614 (435 pc/")

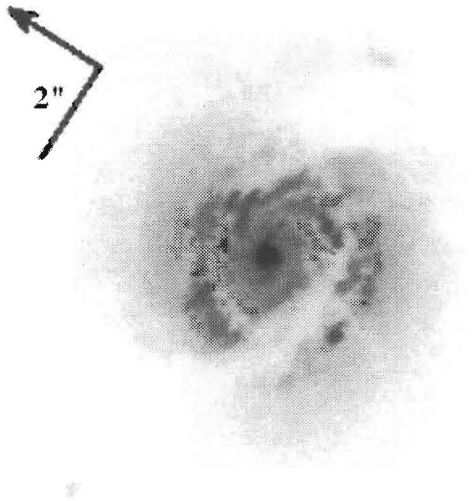

NGC 2377 (203 pc/")

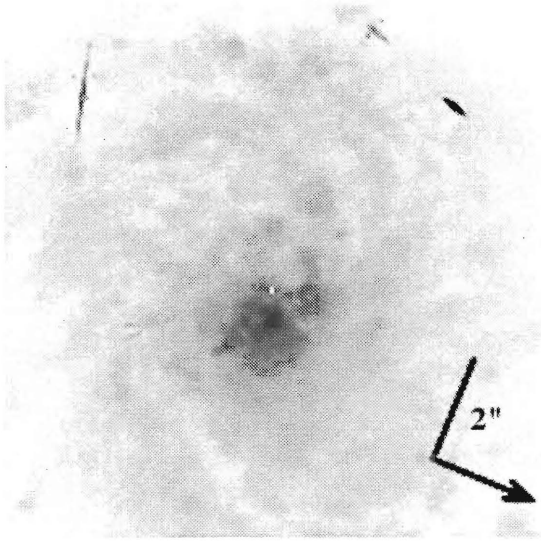

NGC 2989 (377 pc/")

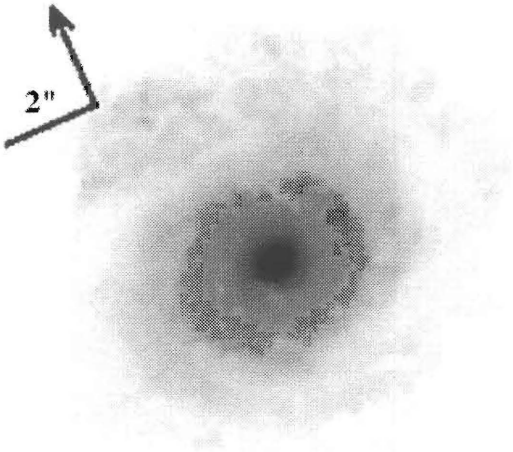

NGC 3032 (145 pc/")

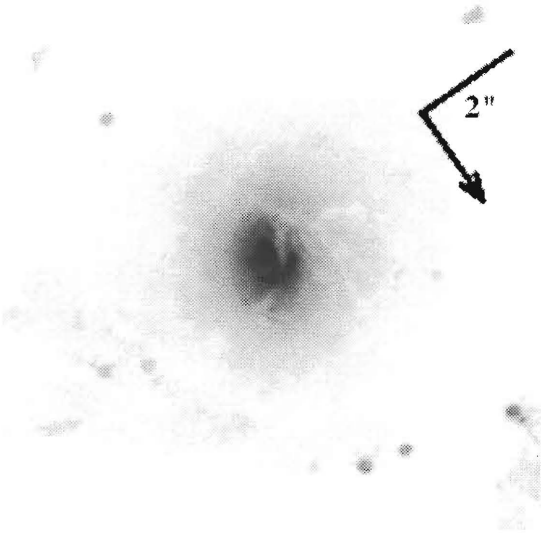

NGC 3310 (87 pc/")

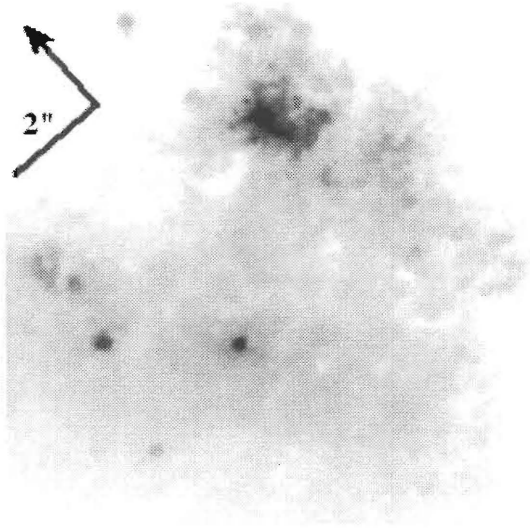

NGC 3353 (87 pc/")

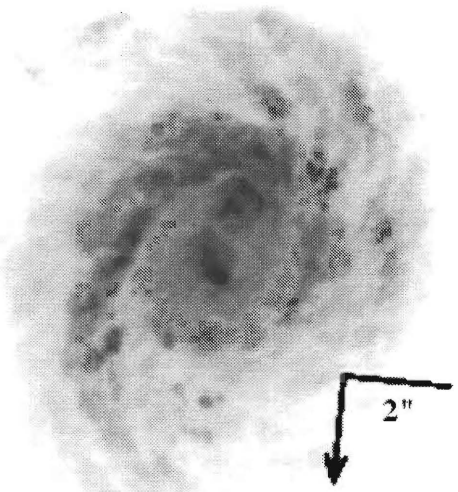

NGC 3504 (145 pc/")

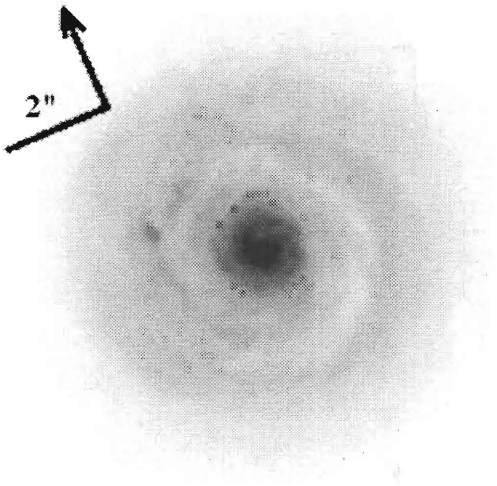

NGC 4990 (290 pc/")

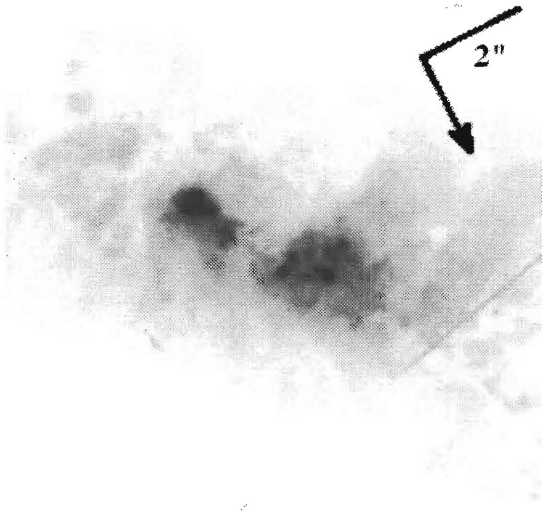

NGC 5597 (232 pc/")

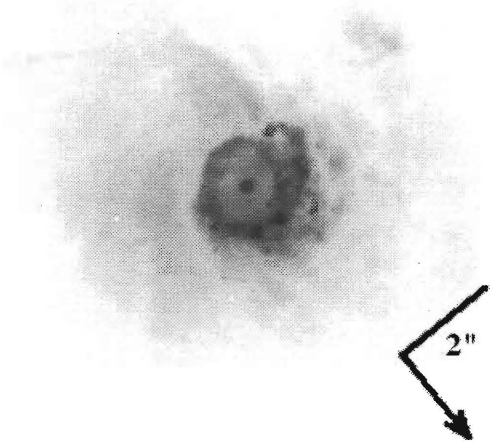

NGC 5757 (232 pc/")

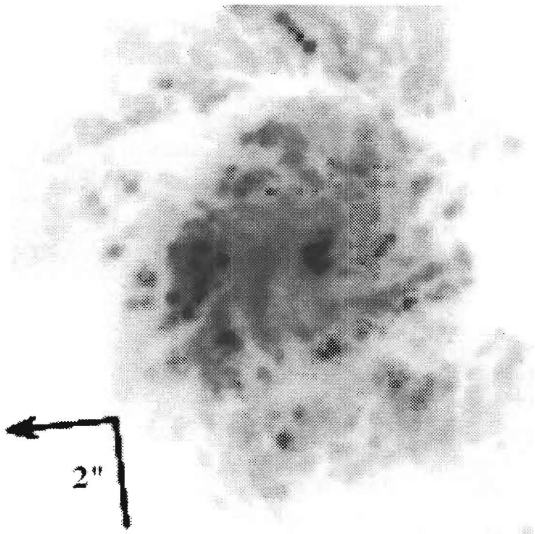

NGC 7552 (145 pc/")

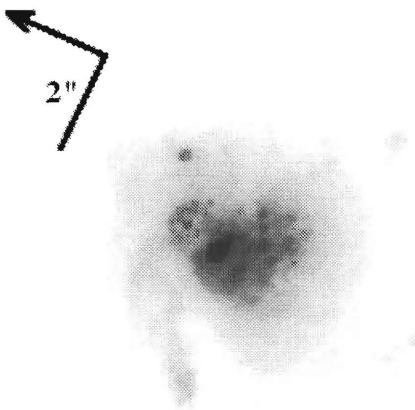

NGC 7714 (261 pc/")

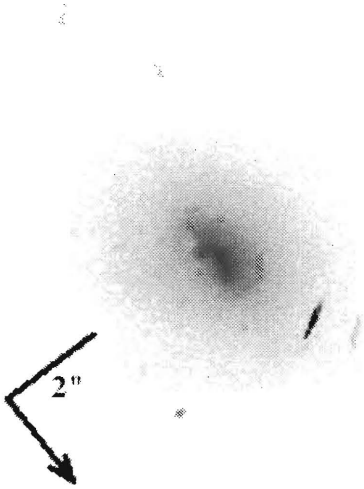

Q 1209-1105 (464 pc/")

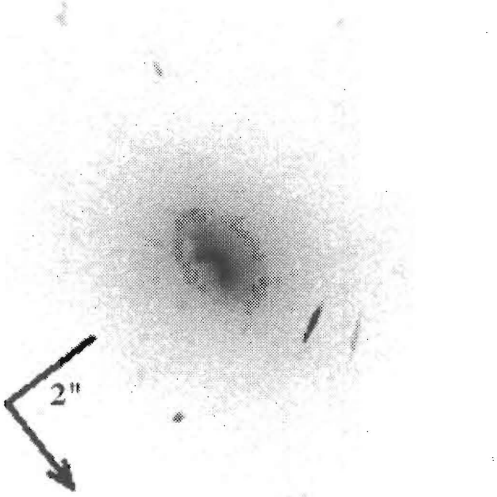

Q 1209-1105 (464 pc/")

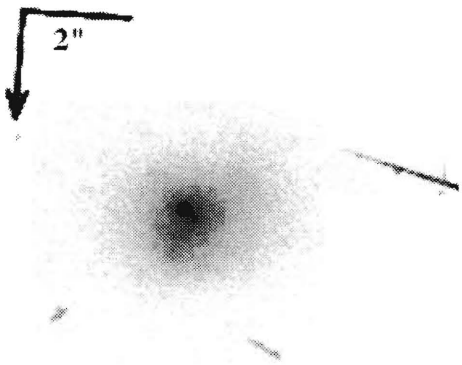

Q 1241+1624 (755 pc/")

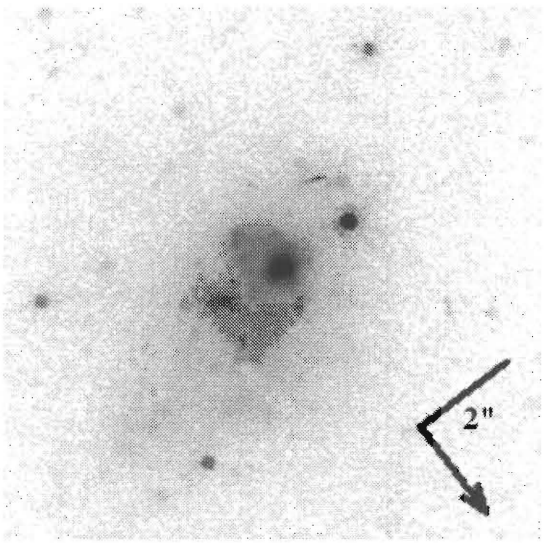

SZ 80 (755 pc/")

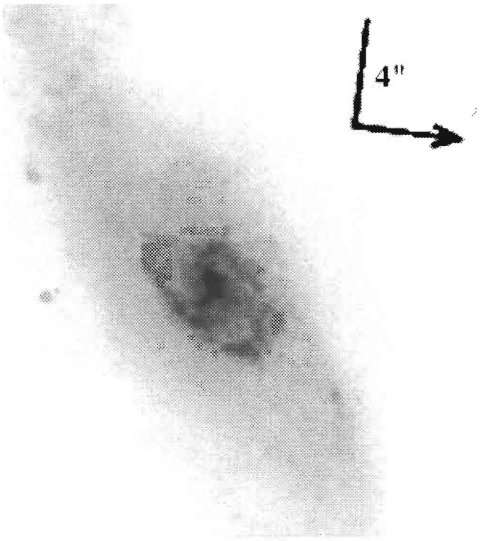

UGC 8929* (785 pc/")

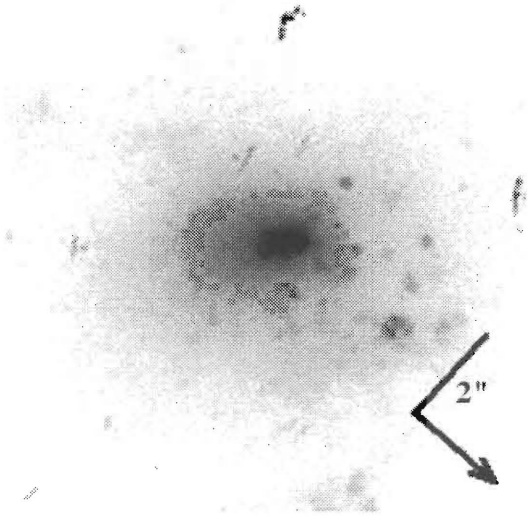

WAS 96 (987 pc/")

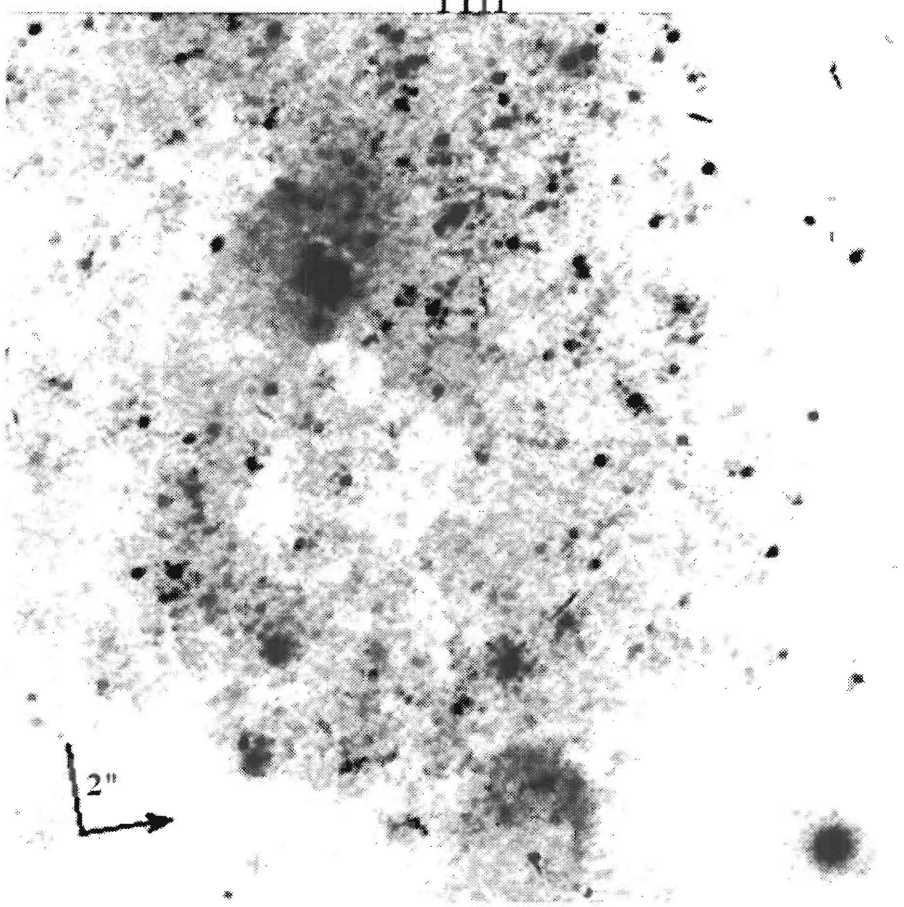

NGC 625 (29 pc/")

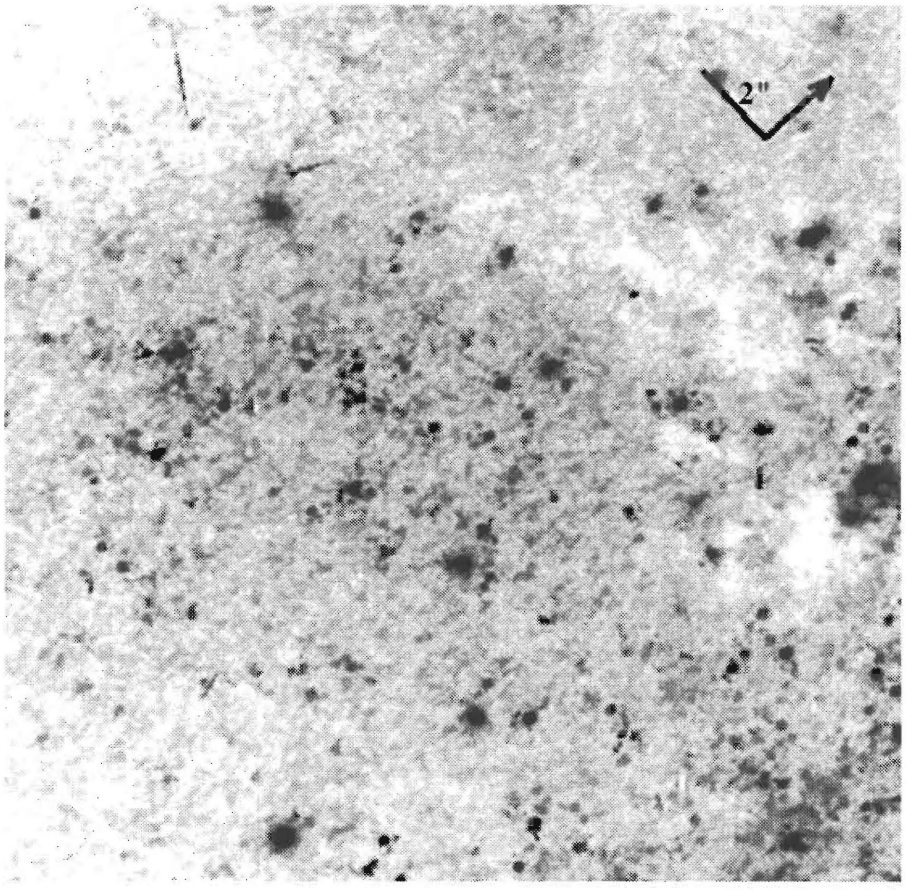

NGC 3738 (29 pc/")

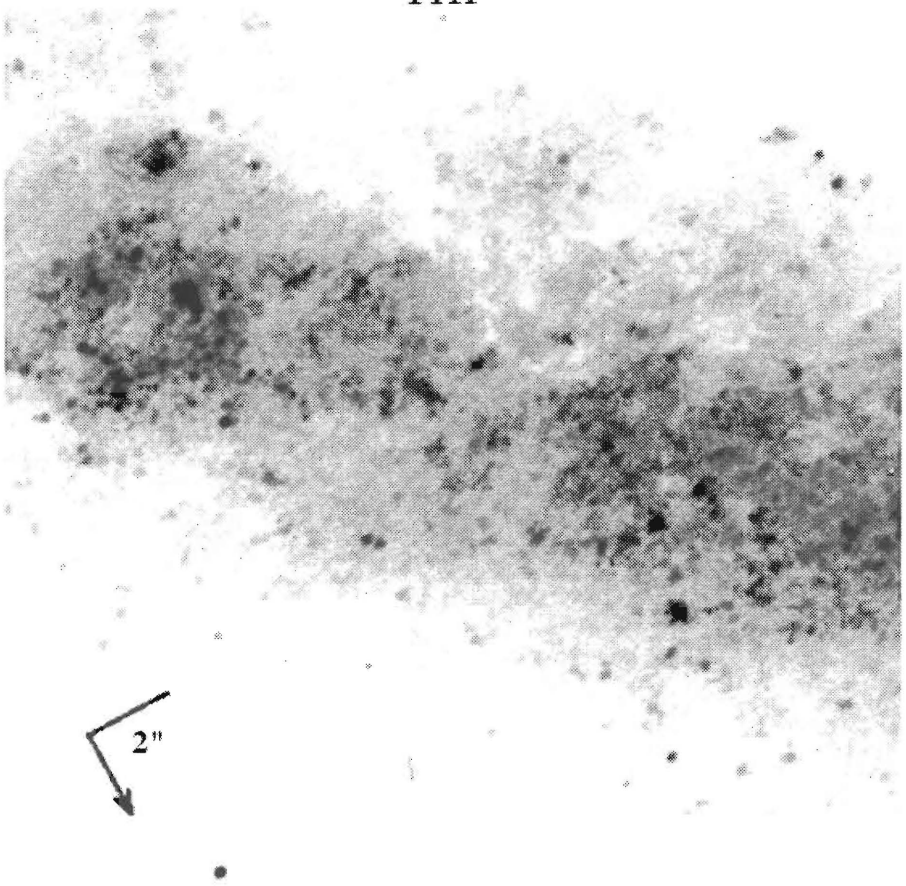

NGC 4700 (116 pc/")

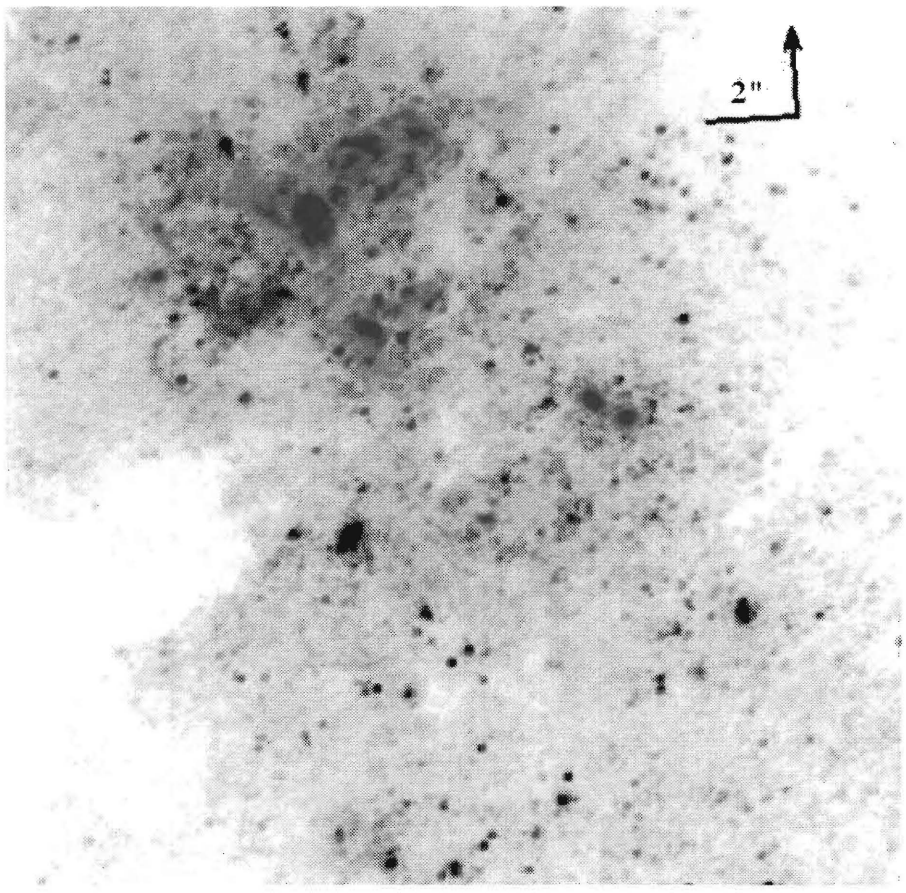

NGC 5253 (29 pc/")

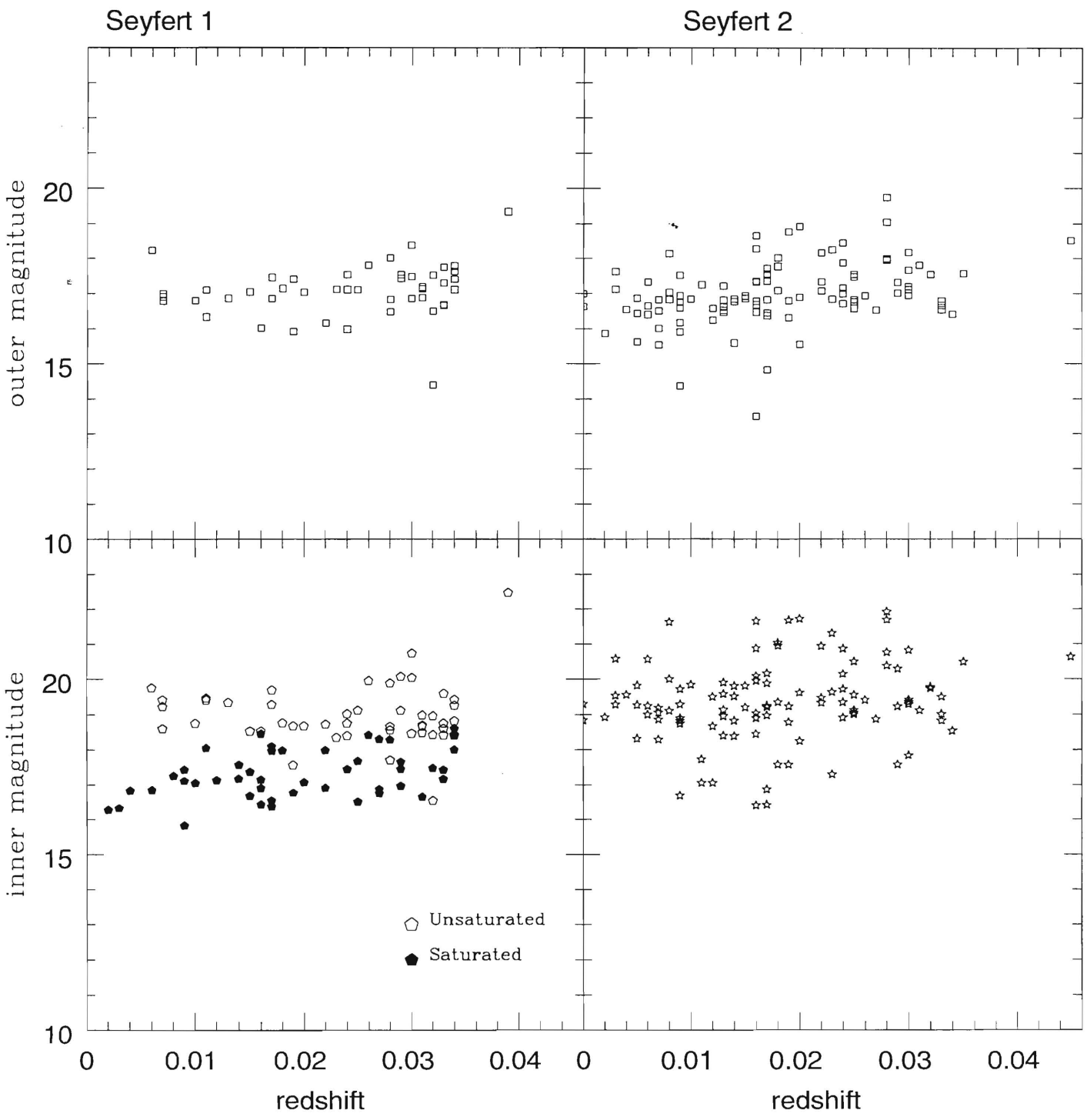
Seyfert 1
Seyfert 2
outer magnitude
inner magnitude
20
15
10
0
0.01
0.02
0.03
0.04
redshift
Unsaturated
Saturated

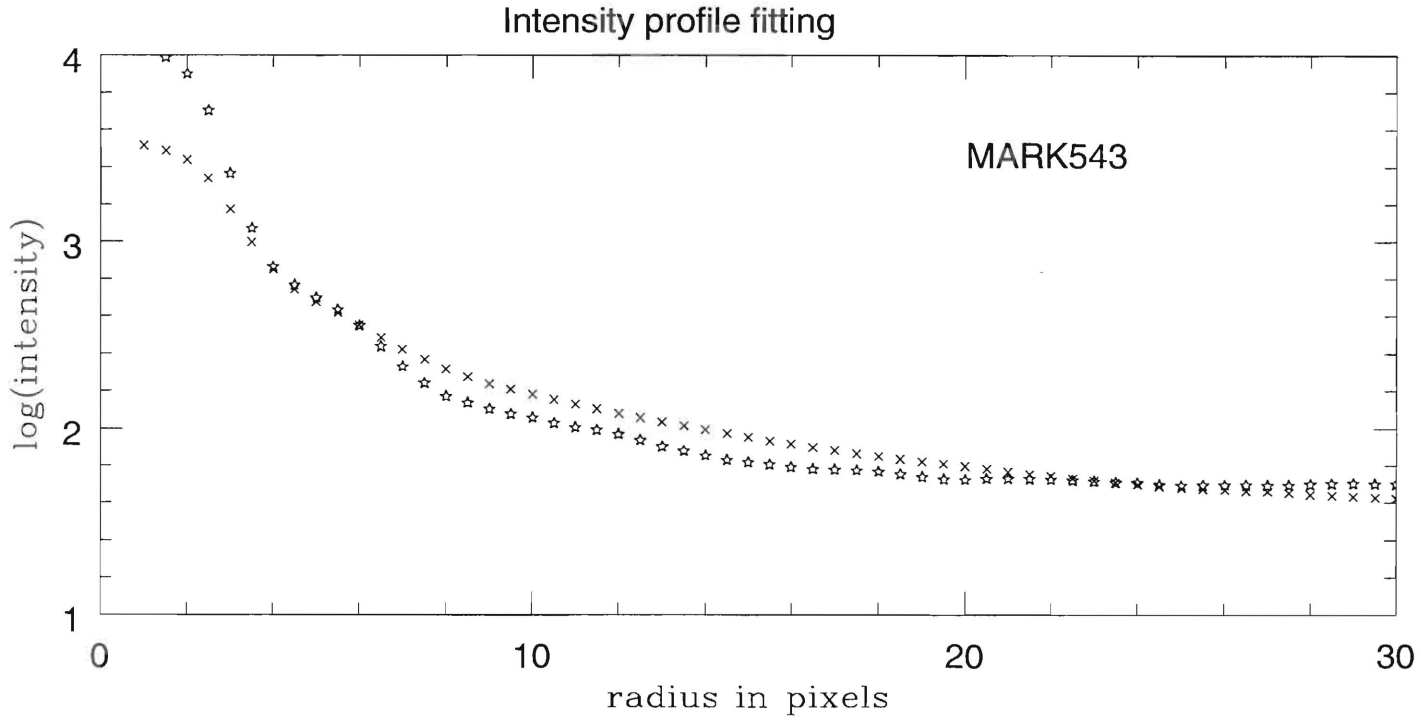
Intensity profile fitting
MARK543
log(intensity)
radius in pixels
0
10
20
30
1
2
3
4

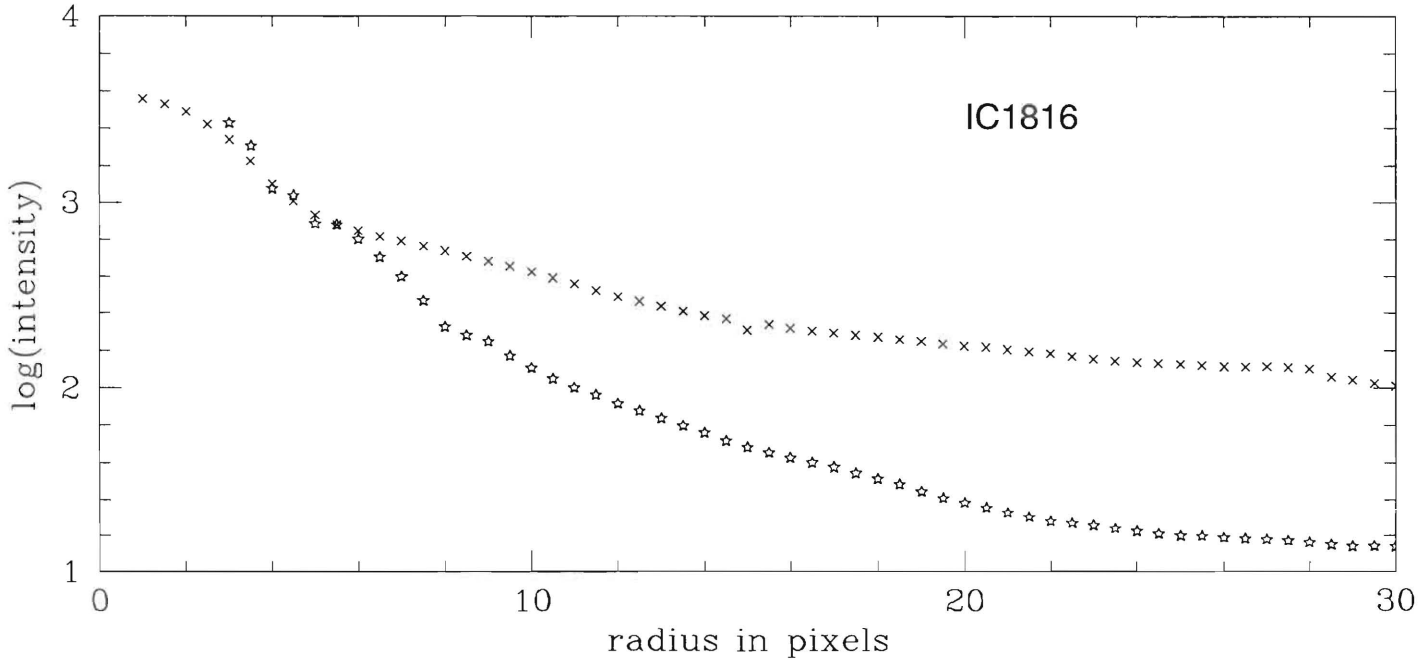
IC1816
log(intensity)
radius in pixels
0
10
20
30
1
2
3
4

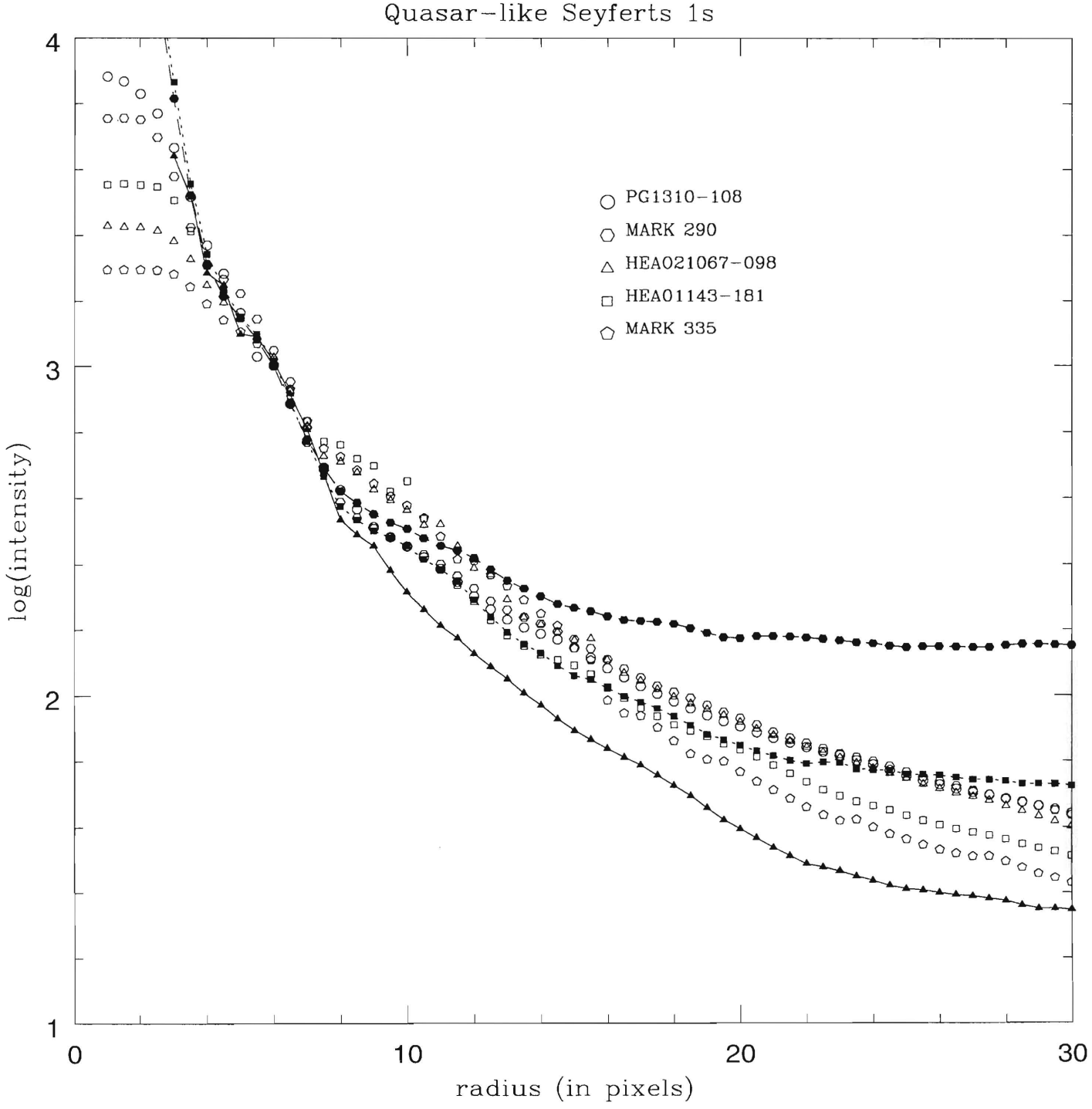
Quasar-like Seyferts 1s
PG1310-108
MARK 290
HEA021067-098
HEA01143-181
MARK 335
log(intensity)
radius (in pixels)
4
3
2
1
0
10
20
30

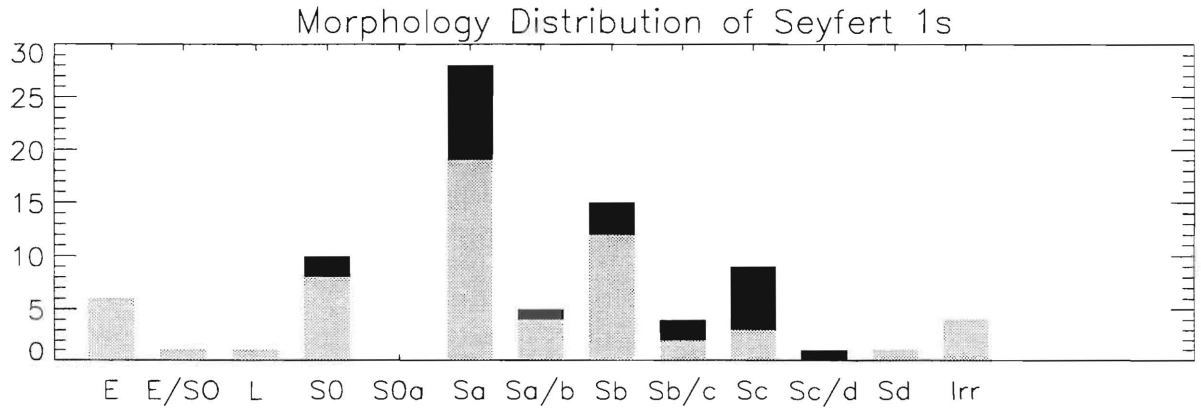
Morphology Distribution of Seyfert 1s
30
25
20
15
10
5
0
E
E/SO
L
S0
S0a
Sa
Sa/b
Sb
Sb/c
Sc
Sc/d
Sd
Irr

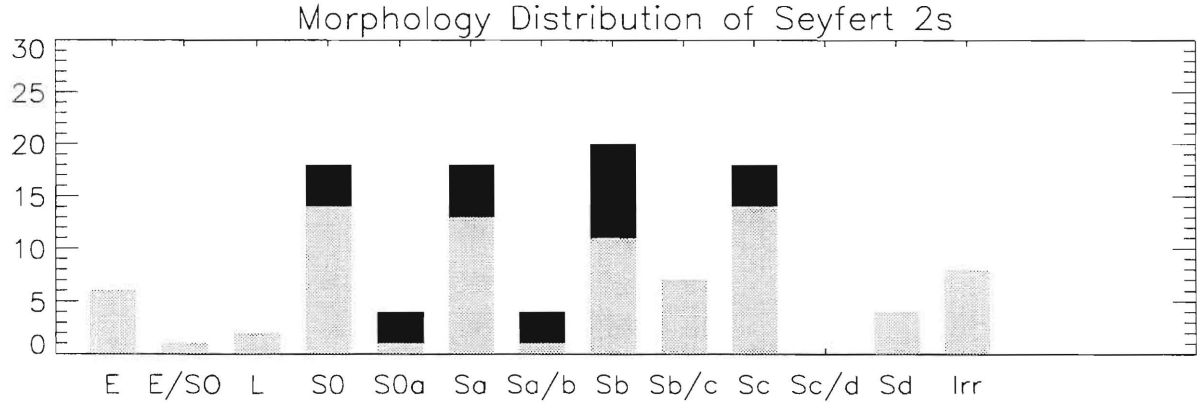
Morphology Distribution of Seyfert 2s
30
25
20
15
10
5
0
E
E/SO
L
S0
S0a
Sa
Sa/b
Sb
Sb/c
Sc
Sc/d
Sd
Irr

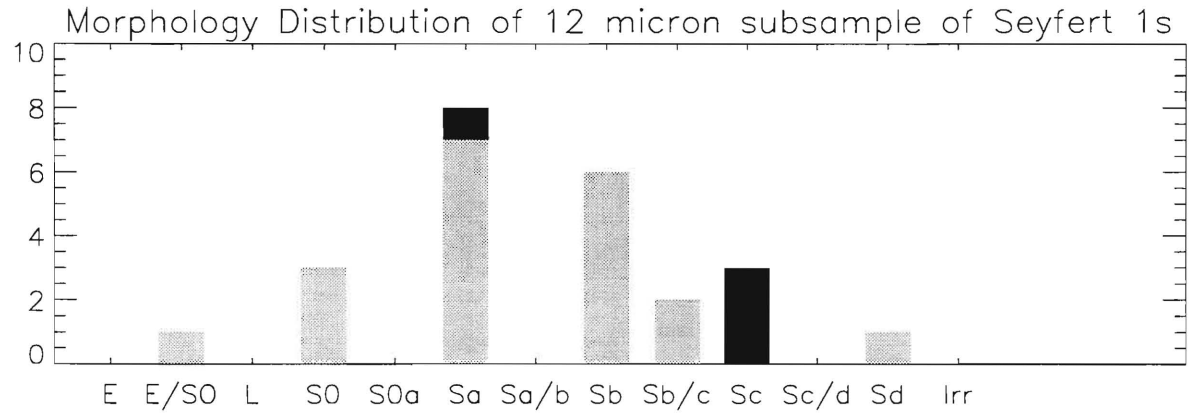
Morphology Distribution of 12 micron subsample of Seyfert 1s
10
8
6
4
2
0
E
E/SO
L
SO
SOa
Sa
Sa/b
Sb
Sb/c
Sc
Sc/d
Sd
Irr

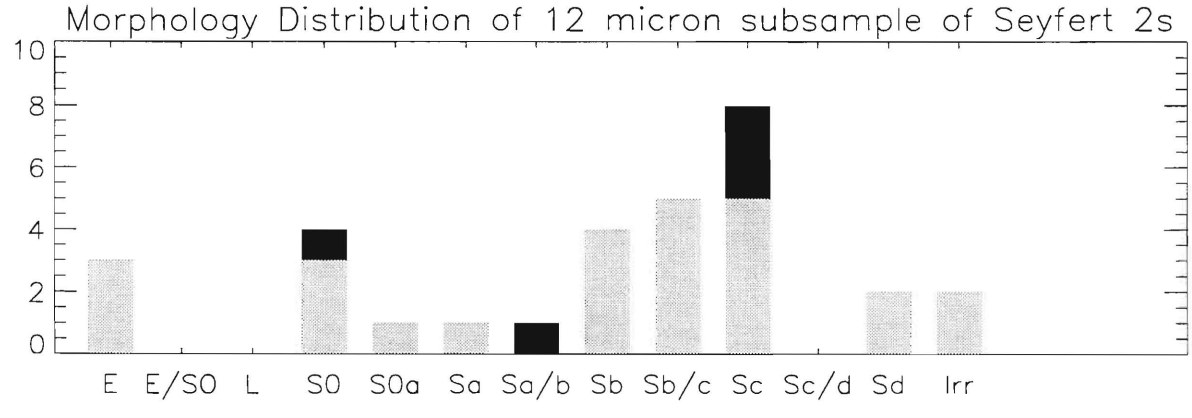
Morphology Distribution of 12 micron subsample of Seyfert 2s
10
8
6
4
2
0
E
E/SO
L
SO
SOa
Sa
Sa/b
Sb
Sb/c
Sc
Sc/d
Sd
Irr

Accreting Torus Model (ATM)

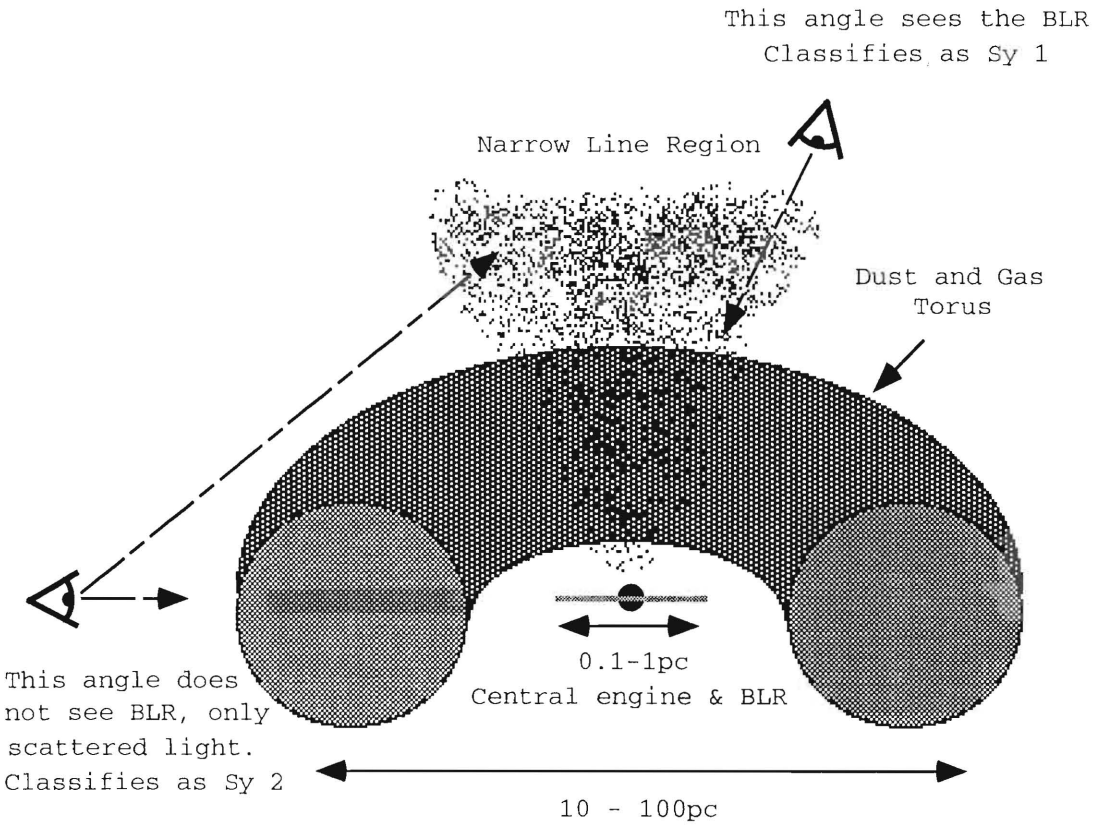

Galactic Dust Model (GDM)